A New Approach to Modelling the Dynamics of Cardiac Action Potentials

GRAHAM DUCKETT

Thesis submitted for the degree of Doctor of Philosophy

Mathematics Institute, University of Warwick

July 1998

Contents

Acknowledgements

Firstly, I would like to thank my supervisor Dr. Dwight Barkley for introducing me to this interesting subject, and for his continuing help, encouragement and direction throughout my research.

I am especially grateful to my parents for their support throughout my study, both on a personal and financial level.

Finally, I would like to thank all my good friends and colleagues, both here at Warwick and elsewhere, for their friendship and help over the last few years.

This research has been supported financially by the Engineering and Physical Sciences Research Council supplemented by income from the supervision system at Warwick.

Declaration

The material in this thesis is, to the best of my knowledge, original except where otherwise stated.

Particular attention should be drawn to Chapter 2, which contains background information taken from various sources as detailed in the bibliography, and the initial part of Chapter 3, which is based on work previously published.

Summary

This thesis is concerned with the development of a new approach to the modelling of cardiac action potentials. Electrophysiological models of the heart have become very accurate in recent years giving rise to extremely complicated systems of differential equations. Although describing the behaviour of cardiac cells well, the models are computationally demanding for numerical simulations and are very difficult to analyse from a mathematical (dynamical-systems) viewpoint. Simplified mathematical models that capture the underlying dynamics to a certain extent are therefore frequently used. However, from a physiological viewpoint these equations are unrealistic and often fail to reproduce important quantitative properties of the tissue. In this thesis we introduce a different approach to the mathematical modelling of cardiac action potentials with the aim of gaining a clearer insight into the origin of the dynamics of electrophysiological models.

Chapter 1 contains an introduction to the research and outlines the main aims of the work. In Chapter 2 various background material is introduced. This includes some basic electrophysiology, ideas currently used in mathematical modelling of excitable media, and details of models previously developed for the study of cardiac tissue. In Chapter 3, following a detailed analysis of an early physiological model, we develop a mathematical model based on the currents involved. This model reproduces, to good accuracy, action potentials of heart tissue and we discuss the essential ideas behind the dynamics. In Chapter 4 the mathematical model developed in the previous chapter is analysed in more detail and simpler equations using similar ideas are introduced. Various types of action potentials of varying behaviours are studied. In Chapter 5 we investigate some spatial simulations of the new mathematical models. We principally concentrate on one-dimensional studies but towards the end of the chapter we look at some two-dimensional simulations. Finally, in Chapter 6, we discuss our conclusions and some possible ideas for further related work. Details of our methods of numerical simulation are included in Appendix A.

Chapter 1

Introduction

A healthy human heart beats at a fairly regular rate of about once a second for an average of around 75 years. Although the actual rate can vary from time to time and from person to person, the steady rhythmic pattern of the beating is essential for maintaining the normal circulation of blood. Any interruption, even for only a few minutes, can lead to circulatory failure and death. A healthy heart is therefore essential to life and the study of it is one of the most important applications of mathematical modelling in biology. Furthermore, with recent advances in computer technology and experimental techniques for studying heart tissue, and progress in nonlinear dynamics, research into the heart has generated keen contemporary interest and become increasingly more exact.

The isolated beating of the heart had been observed on many occasions, but it was not until 1628 that William Harvey discovered that the purpose of the heartbeat was to pump blood around the body. An account of this discovery may be found in [46]. However, even when the purpose of the heartbeat was understood, the actual mechanism of the initiation of the heartbeat remained a mystery until the late nineteenth century when knowledge of physics and chemistry became sufficiently advanced. To pump the blood around the body the muscles of the heart contract and expand at a regular rate. This muscular contraction is driven by an electrical wave originating at a specific region of the heart and propagating through the cardiac tissue. As the wave spreads through the tissue, muscular contraction is triggered in the cells. Each normal heartbeat involves only one electrical impulse or action

potential in each cardiac muscle cell. In order to study the mechanism of the heart it is necessary to have an understanding of the electrical processes that drive it.

The electrical currents generated during the beating of the heart can be detected at points a long distance away from the heart itself and may even be measured at the surface of the body. The waves recorded at the surface of the body are known as electrocardiograms (ECGs). Although these surface measurements are useful for diagnostic purposes and give information about certain events occurring in the heart, the signals do not currently provide sufficient information about the underlying electrical mechanism. In order to achieve this it is necessary to record directly from the heart itself, a requirement that has led to increasingly sophisticated experimental techniques for analysing cardiac tissue being developed over the last fifty years or so. Two well known examples of these methods are the voltage clamp and the patch clamp techniques. These have enabled a detailed analysis of electrical properties of the heart to be carried out at the cellular level.

Probably the most famous example of this type is the Nobel prize winning work on the squid giant axon conducted by Hodgkin and Huxley in the early 1950s [3]. The experiments carried out enabled them to separate the membrane current into sodium and potassium components and to construct a mathematical model describing the way in which these currents vary with membrane potential and time. Most of the ideas for modelling of cell membranes came from this work and shall be discussed later. The voltage clamp technique developed by Hodgkin and Huxley to analyse the squid membrane was later extended to the membrane of heart cells enabling simple models of the electrical activity in cardiac tissue to be constructed. One of the first cardiac models was that of Noble [6] in 1962 which applied the approach of Hodgkin and Huxley to heart tissue, in particular the Purkinje Fibres.

With time the experimental techniques improved, notably with the patch clamp technique which made it possible to make measurements on individual ionic channels in a small patch of cell membrane. Models constructed from these measurements have become more and more accurate [8, 9, 12, 15, 20, 32, 36] giving rise to extremely complicated, high-order, stiff, systems of differential equations describing individual

cardiac cells.

The complexity of the resulting models makes it extremely difficult to understand the origins of the dynamics from a mathematical (dynamical-systems) viewpoint. They are also extremely computationally demanding for numerically simulating waves in extended media, especially in three spatial dimensions. These problems have led to simplified models being developed, the FitzHugh-Nagumo equations [4, 5] for excitable media being the most famous. These equations, which are in fact a simplification of the Hodgkin-Huxley equations, capture the main features of action potentials and have a simple phase space picture explaining the essential features of excitability; threshold, excitation and recovery. The FitzHugh-Nagumo model has therefore been used extensively over the last 30 years or so to simulate waves in generic excitable media and they have dominated the theoretical analysis and numerical simulation of cardiac tissue [19]. However, while the FitzHugh-Nagumo equations are useful for basic analysis and capture the gross features of excitation propagation, they are not realistic from a physiological viewpoint and fail to simulate several quantitative parameters of cardiac tissue such as the shape of the action potential and restitution properties of the tissue. There have been several attempts to improve the FitzHugh-Nagumo approach to quantitatively describe the shape of the action potential [10, 40] and in particular to match more closely the dispersion and restitution properties of actual excitable media using modified FitzHugh-Nagumo equations [23, 35, 40]. While this is a reasonable approach for many applications, it does not provide much insight into the origins of the dynamics of the electrophysiological models, nor do the improved models accurately capture the spike dynamics.

There is therefore a need to construct relatively simple but more physiologically realistic equations that one can use to gain further insight into the dynamical behaviour of cardiac action potentials. The aim of this work is to develop a simple model for an excitable system with the following properties:

1. The model contains only three variables corresponding directly to physiologically relevant variables; membrane potential, inward current and outward current.

2. The differential equations are expressed in terms of relatively simple polynomial functions of the dependent variables.

3. The dynamics of the model match in great detail the dynamics of electrophysiological models and for the correct mathematical reasons.

Chapter 2

Electrophysiology and Mathematical Modelling of the Heart

We begin by introducing some basic ideas from electrophysiology and electrocardiology. This will illustrate how the mammalian heart works both in terms of the physical system (the contraction of muscles, the movement of blood etc.) and the electrical system (the voltage wave that causes muscular contraction and the ionic currents involved).

2.1 Electrophysiology

2.1.1 Anatomy of the Heart

First of all some basic ideas from anatomy shall be introduced. Figure 2.1 shows a diagrammatical representation of the mammalian heart which is composed of four main chambers; the left and right atria and the left and right ventricles.

The left and right atria are the smaller two of the four chambers and they receive blood returning from circulation and pass it on to the larger, and thicker walled,

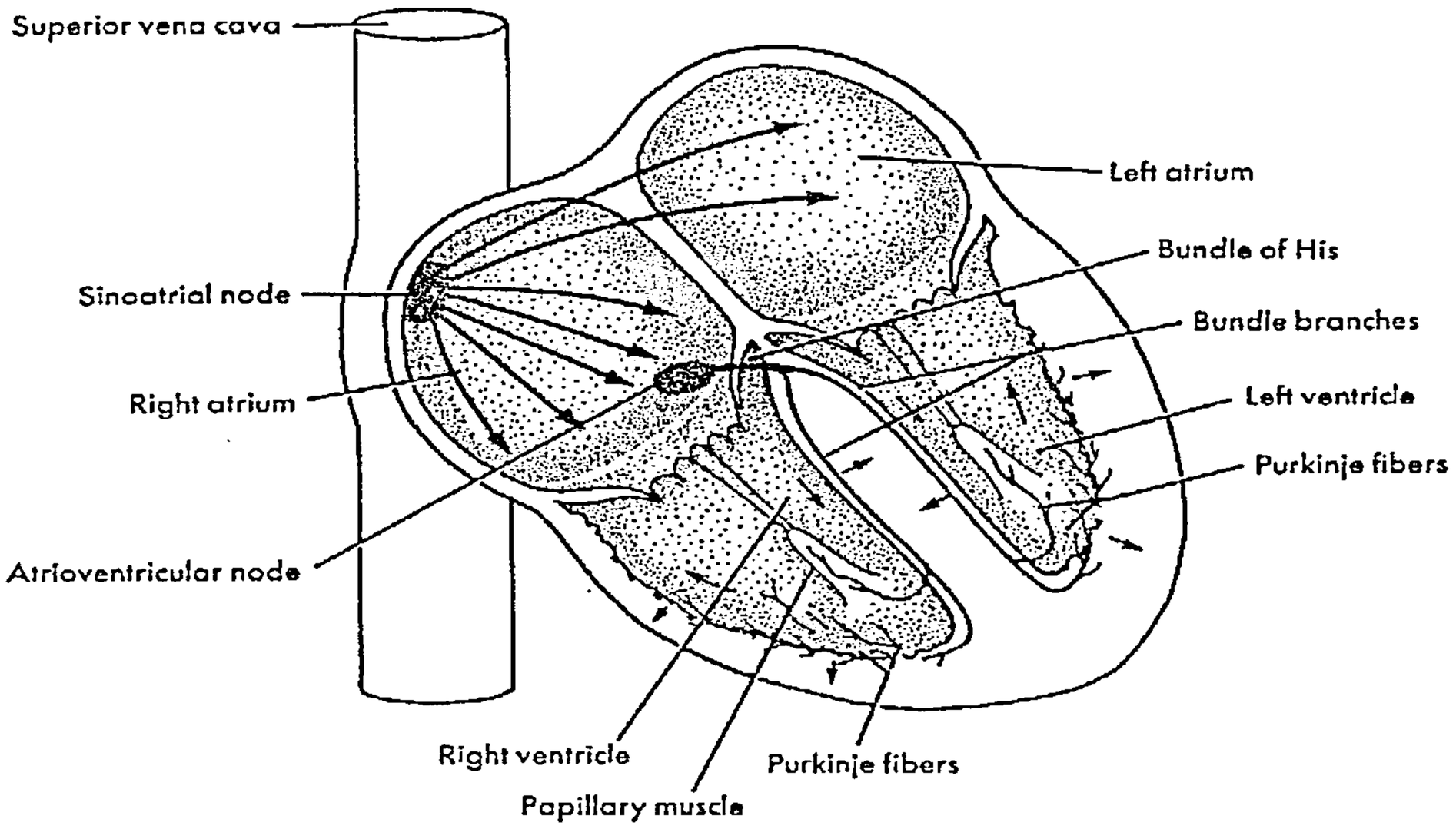

Figure 2.1: Schematic representation of the conduction system of the heart. Taken from [57] with permission.

ventricles. It is the ventricles that are responsible for pumping blood out into the two main arteries.

Deoxygenated blood from the right ventricle is pumped into the pulmonary artery that supplies the lung circulation. Oxygenated blood returning from pulmonary circulation enters the left atrium, is passed through to the left ventricle, and is pumped out into the aorta which supplies the systemic circulation (for all other tissues of the body). On returning from the systemic circulation blood enters the right atrium, is passed through to the right ventricle, and the blood cycle is complete.

In order for effective pumping of blood to the body it is important that the ventricles are filled with blood before ventricular contraction occurs. Therefore the contraction of the ventricles should be preceded by the contraction of the atria which eject blood into the ventricles. This is indeed the case. Each beat of the heart consists initially of the almost synchronous contraction of the two atria, causing the blood in them to be pumped through into the ventricles. After a delay of a few hundred milliseconds, this is followed by the nearly synchronous contraction of the two ventricles forcing

blood into the circulation.

These contractions of heart muscle tissue are driven by waves of electrical activity passing downwards through the heart initiating muscular contraction as they pass.

2.1.2 The Electrical Conduction System

The contraction of a cardiac cell occurs immediately after an electrical pulse has passed through it and hence the electrical activity should first pass through the atria and then on to the ventricles. The timing of this is achieved by specialised conducting tissues in the heart as illustrated in figure 2.1.

Electrical activity for each heartbeat is triggered by the sinoatrial (SA) node which is located near the junction between the right atrium and the superior vena cava. The SA node has a specialised pacemaker (or autorhythmic) mechanism and spontaneously generates electrical activity. Other parts of the heart also possess pacemaker mechanisms but the rate of beating in the SA node is higher and thus sets the pace of the heart as a whole. If the normal pattern of beating is disrupted, for example in a diseased heart, then other pacemaker sites, such as the Purkinje Fibres, can take over. The majority of normal cardiac tissue (atrial and ventricular muscle) does not exhibit pacemaker activity although it is excitable. That is, if the tissue is perturbed by an electrical pulse, above a threshold in both amplitude and duration, a large amplitude wave known as an action potential (see below) will occur. Perturbations below the threshold will just give rise to a small amplitude response and a quick return to the rest state.

The electrical excitation generated in the SA node spreads throughout the right atrium and a specialised conducting fibre known as Bachmann's bundle conducts the impulse directly to the left atrium. As the impulse passes across the atria excitation of the tissue occurs leading to the synchronous atrial muscular contraction and the ejection of blood into the ventricles.

Electrical activity in the atria does not pass through the walls between the atria and ventricles directly but travels through the atrioventricular (AV) node. The AV node

contains the same cell types as the SA node and is a small strip of tissue connecting the atria and ventricles. Conduction of the electrical impulse travels through the AV node relatively slowly to ensure that there is a significant delay between the excitation of the atria and that of the ventricles. Malfunction of this region can lead to the atria contracting without contraction of the ventricles or the contraction of the ventricles at a different rate set by pacemaker mechanisms in the conducting fibres beyond the AV node.

In a normally functioning heart, the upper portion of the fibres beyond the AV node, known as the Bundle of His, rapidly conduct the electrical impulse down through the Purkinje fibres which branch out into a tree-like structure to the surface of the ventricles. The rapid conduction along the Purkinje fibres ensures that the ventricles are excited, and hence contract, almost synchronously thus forcing the blood into the arteries at high pressure rather than just shifting it between different parts of the ventricles. Failure to achieve this synchronous excitation of the ventricles is a serious condition and occurs in ventricular fibrillation.

2.1.3 Cardiac Action Potentials

A cardiac action potential is the electrical wave that is triggered in the muscle cells as they are excited above their threshold value. The wave passes through the cardiac muscle causing contraction and thus the heartbeat.

Different regions of the heart are distinguishable anatomically and also distinguishable electrically. The actual waveform of the cardiac action potential will vary with the region of the heart. To investigate the electrical behaviour of a single cardiac cell, microelectrodes can be inserted into its interior enabling potential changes to be recorded. Two main types of action potentials are observed in the heart and they are known as the fast response and the slow response. Examples of these two types of behaviour are shown in figure 2.2.

The fast response is found to occur in normal myocardial fibres in the atria and ventricles and also in the Purkinje fibres. The slow response is found in the SA

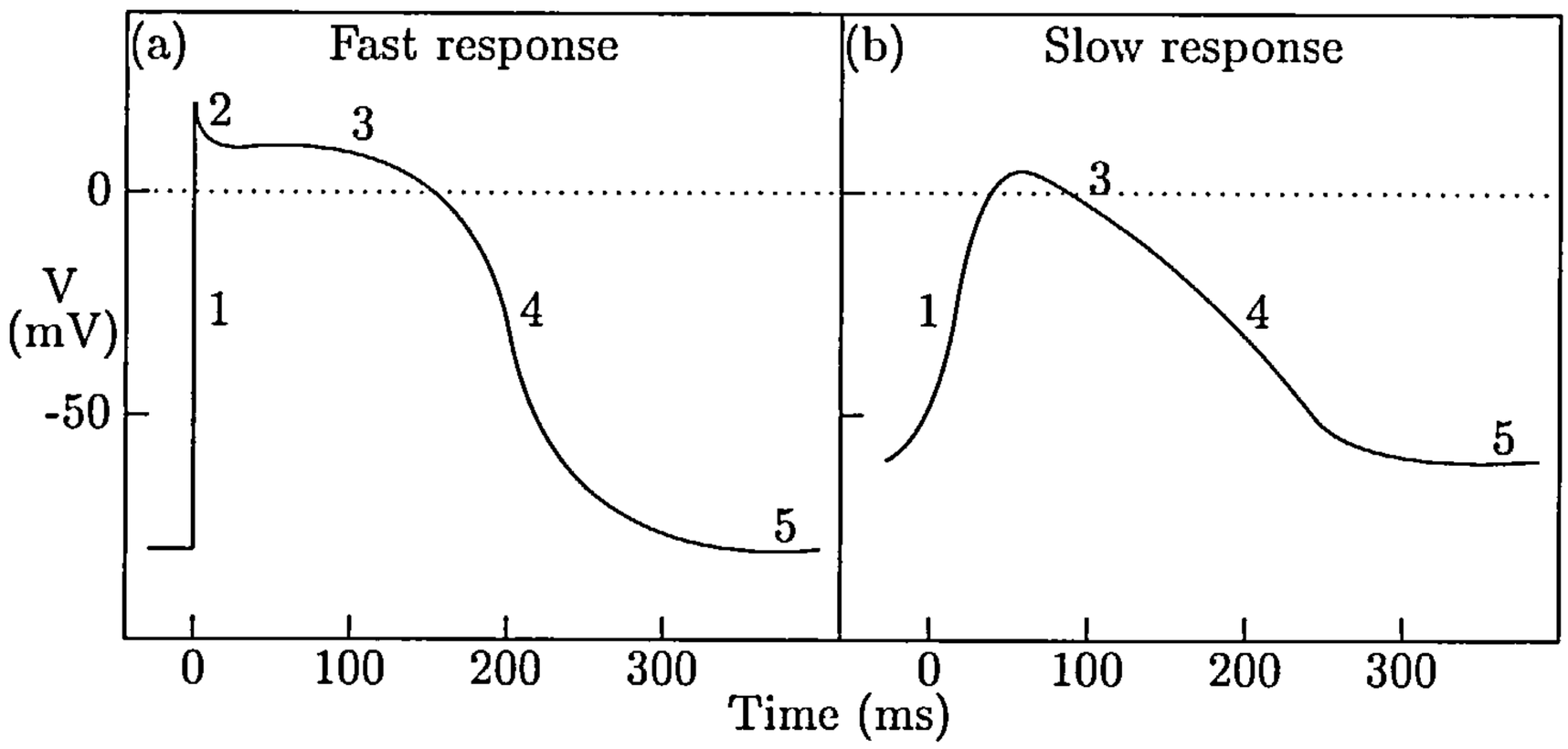

Figure 2.2: Changes in transmembrane potential for (a) the fast response and (b) the slow response. There are a few distinct regions or phases of an action potential; (1) the rapid upstroke (depolarisation), (2) a brief period of recovery, (3) the plateau, (4) the recovery (repolarisation), and (5) the resting state.

node, the natural pacemaker region of the heart, and in the AV node, the specialised tissue involved in conducting the cardiac impulse from the atria to the ventricles.

Transmembrane potential, usually referred to simply as potential, is taken to be the difference between the potential inside the cell and the potential outside. Note that when a cell is in its resting state the potential of the interior of a cell is more negative than that outside in the surrounding region. This is characteristic of most cells within the body.

It can be seen from figure 2.2 that the fast and slow responses differ in numerous ways. The resting potential in heart tissue characterised by the fast response is more negative than in that characterised by the slow response. In fact by gradually shifting the resting membrane potential from its normal level of about $-90mV$ to a value of about $-60mV$ fast response action potentials can be converted to those of a slow response. The amplitude of the action potential, the speed of the upstroke, and the extent of the overshoot in the fast response are also greater than in the slow response. The amplitude and steepness of the upstroke are important factors in the velocity of propagation and hence in cardiac tissue characterised by the slow response

the conduction velocity is much slower than in tissues displaying the fast response. The difference between the fast response in the atria and that in the ventricles is that the plateau phase in a ventricle action potential is of greater duration. The fast response in the Purkinje fibres is typically similar to that in the ventricles although the upstroke is extremely sharp giving rise to quick conduction velocities and a large overshoot.

Phase 5 of the action potential (see figure 2.2) reflects whether the cell possesses the property of autorhythmicity or not. If the voltage gradually slopes upwards throughout this phase another action potential will be initiated and the behaviour will be that of a pacemaker. However, if this phase is flat then the voltage will remain at the resting state and will not exhibit autorhythmicity.

2.1.4 Ionic Channels and Currents

The action potentials discussed in the previous section are generated by the flow of ions between the inside and outside of each individual cardiac cell. This transfer of ions involves specialised ionic channels connecting the inside of a cell to the surrounding medium. The principal ions involved for cardiac tissue are sodium, Na^+, potassium, K^+, and calcium, Ca^{2+}, although other ions such as chlorine, Cl^-, are present in smaller quantities. The ionic channels are highly ion specific so for example a channel that permits sodium ion transfer is not permeable to the transfer of potassium or calcium ions. For a particular ion type there is more than one channel and depending on the point of the action potential different channels will be open or closed to the transfer of that ion. Investigation of the ionic channels has been helped greatly by experimental techniques such as the patch clamp technique. These methods have led to the discovery of more and more channels and also enabled the investigation of the behaviour of an individual channel as an action potential passes through the cell.

Figure 2.3 gives a schematic representation of the ion transfer process throughout a fast response action potential. As the voltage of the cardiac cell is increased past some threshold value, the fast sodium channels are opened up and a fast influx of

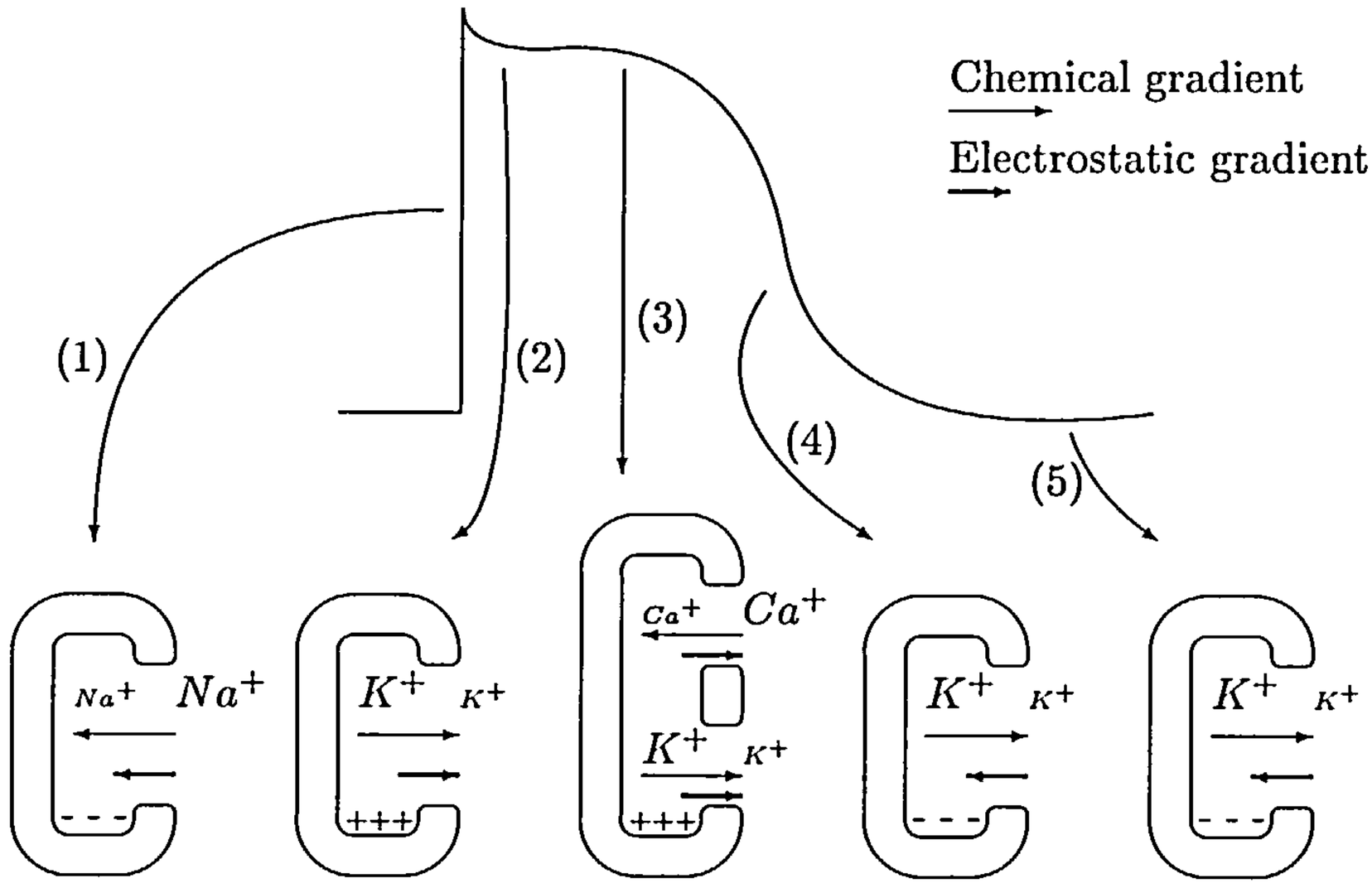

Figure 2.3: The principal ionic channels that generate an action potential (fast response). The direction of the chemical and electrostatic gradients is illustrated by arrows. The charge inside the cell is also shown by +'s or -'s.

Na^+ ions occurs generating the upstroke (phase 1). (Note that in the slow response the upstroke is mainly due to calcium ions). This influx continues until the voltage reaches a value of around 20mV and the sodium channels close. Immediately after the upstroke there is an efflux of K^+ ions through a specific potassium channel generating the brief period of repolarisation (phase 2). The plateau of the action potential is caused by a balance of an influx of Ca^{2+} ions through certain Ca^{2+} channels and the efflux of K^+ ions through K^+ channels (phase 3). The period of repolarisation occurs as a result of the efflux of K^+ ions being favoured (phase 4) and this continues to a lesser extent throughout the return to equilibrium (phase 5).

After a cardiac action potential has passed, the concentration of ions inside and outside the cell will be different to the concentrations preceding the action potential. This concentration is restored to it's original value by ionic exchange pumps which are present in cardiac tissue. The three main electrogenic pumps are the Na^+–K^+ exchange pump which ensures that the sodium and potassium concentration gradients are maintained, the outward Na^+–Ca^{2+} exchange pump which pumps

sodium and calcium ions, and a direct outward Ca^{2+} pump.

The movement of ions between the inside and outside of each cardiac cell generates associated ionic currents. The main ionic currents are the sodium, potassium and calcium currents. The size and orientation of these currents (for the Beeler-Reuter model) is shown in figure 2.4. The Beeler-Reuter [9] model for ventricular tissue is

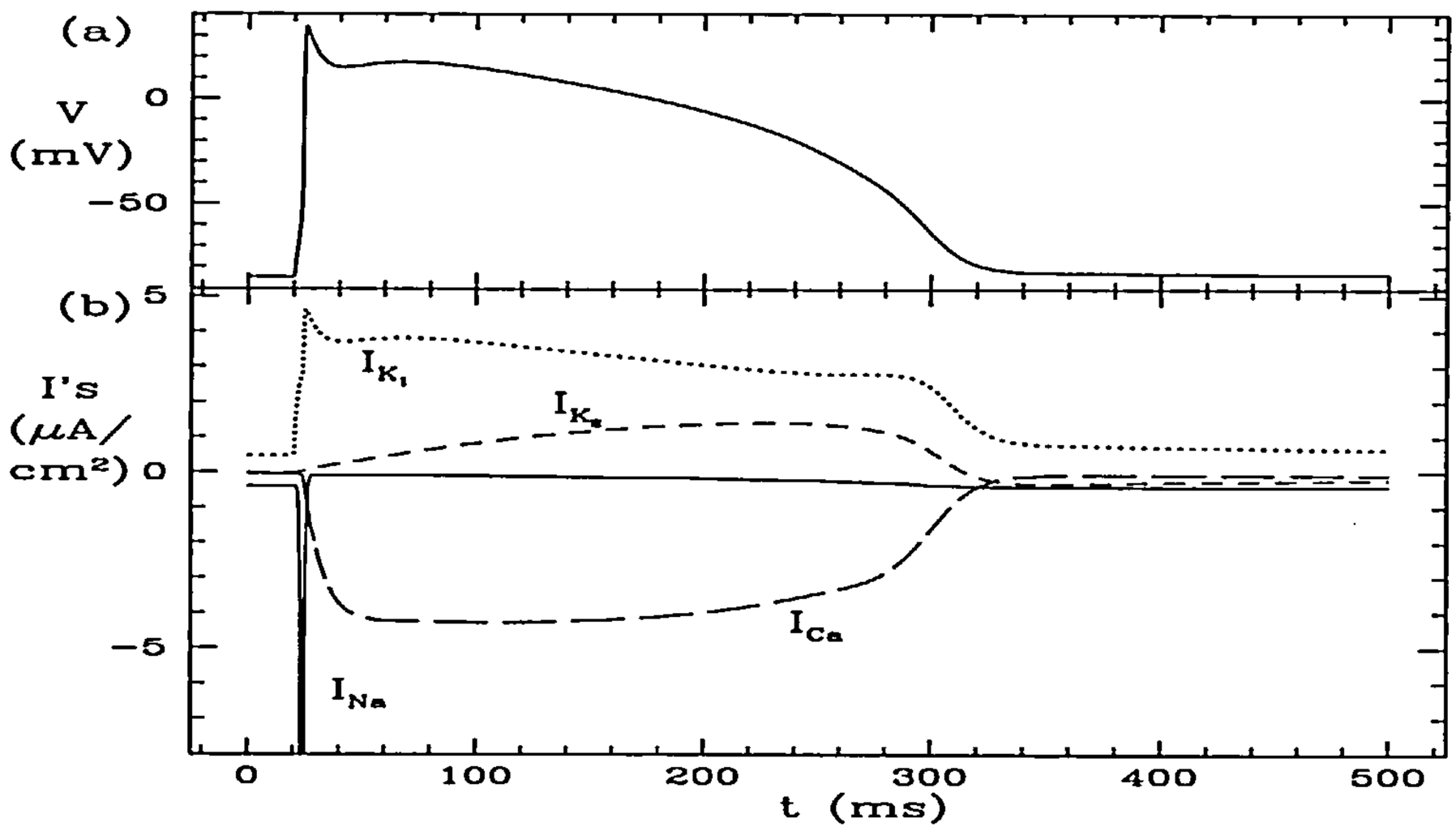

Figure 2.4: Example ionic currents generated by the flow of ions during an action potential. Both (a) the voltage and (b) the principal ionic currents are shown. Note that the I_{Na} current is truncated and reaches a value of around $-130\mu A/cm^2$. (From a simulation of the Beeler-Reuter model).

frequently used in cardiac electrophysiology and includes four main currents; a slow inward calcium current (I_{Ca}), an outward time and voltage dependent potassium current (I_{K_2}), an inwardly rectifying time-independent potassium current (I_{K_1}), and a fast inward sodium current (I_{Na}). Note that there are more refined models than the Beeler-Reuter model but the basic mechanisms are the same. It can be seen from figure 2.4 that the fast upstroke of the cardiac action potential is generated almost solely by the fast inward sodium current resulting from the fast influx of Na^+ ions. The plateau phase is then maintained by a balance of the slow inward

calcium current and the outward potassium currents. The plateau is terminated by the inactivation of the calcium current and the activation of the potassium current I_{K_2} and repolarisation occurs with all the currents returning to their rest values.

2.1.5 Relationship Between the Electrical System and the Physical System

The relationship between the electrical events occurring in heart tissue and the actual mechanical contraction is shown in figure 2.5. It can be seen that the peak force of contraction coincides with the completion of repolarisation and the duration of contraction is similar to the duration of the action potential. The duration of a

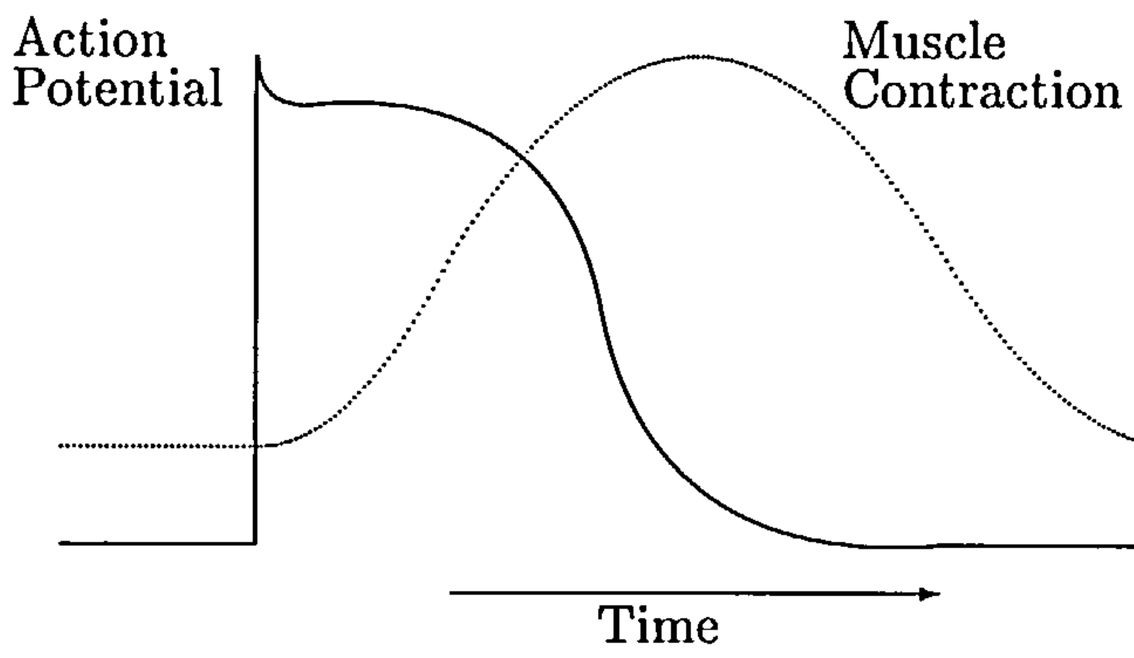

Figure 2.5: Relationship between the changes in transmembrane potential (solid) and the contraction of ventricular muscle (dotted).

cardiac action potential is extremely large compared to that in skeletal muscle where it is simply a trigger for mechanical activity. The fact that the action potential in the heart overlaps with the actual contraction of the tissue enables it to govern the duration and magnitude of the contraction as well as triggering it. It also means that the cells do not become excitable again until the action potential is terminated, a period known as the refractory period. Heart muscle can therefore not be re-excited until the previous contraction is largely over, an important factor in a muscle that acts as a pump.

2.2 Theory of Current Flow

We shall now discuss the theory of current flow in cell membranes [48, 57]. The ideas below result mainly from work by Hodgkin and Huxley [3] in which numerous voltage clamp studies on the giant axon of the squid were carried out. In a voltage clamp experiment, the voltage difference between the inside and outside of the membrane is fixed (clamped) at specified values. Starting from a steady state situation the potential is instantaneously changed to a new value and the changes in currents through the membrane are observed as a new steady state is achieved. The results of such experiments suggest that the ion-transfer process is a relatively simple one and Hodgkin and Huxley formulated nonlinear differential equations that describe the flow of ionic currents across the membrane. The main ideas from this formulation are outlined below.

2.2.1 Equilibrium Potentials

For each ionic channel in a cardiac cell there are two main forces acting on the ions travelling through it; the chemical force due to the concentration gradient of ions and the electrostatic force resulting from the intracellular potential. The potential at which these two forces balance each other out is called the equilibrium potential and is given by the Nernst equation

$$V = \frac{RT}{zF} \ln \left(\frac{[C]_o}{[C]_i} \right) \tag{2.1}$$

Here R is the gas constant, T is the absolute temperature, z is the valency the ion species involved, F is the Faraday constant, and $[C]_o$ and $[C]_i$ are the extracellular and intracellular ion concentrations respectively. When the membrane potential is at its equilibrium value there is no net flow of ions through the channel. On changing the membrane potential from its equilibrium value, ion flow will commence, the rate of which will be determined by the difference of the membrane potential and equilibrium potential, and the conductivity of the membrane. Therefore, the current

due to the flow of a potassium ion, for example, will be given by

$$I_K = g_K(V - V_K)$$

where I_K is the ionic current through the potassium channel, g_K is the membrane conductance to potassium ion, and V_K is its equilibrium potential. The conductance depends on both the number of conducting channels and the properties of individual channels.

2.2.2 Rectification

If all the conducting channels are open then one may expect the ionic channels to behave as simple ohmic conductors, i.e.

$$\bar{I}_K = \bar{g}_K(V - V_K)$$

where the conductance $\bar{g}_K$ is constant and $\bar{I}_K$ is the resulting current. Although this is true for squid nerve, two nonlinear types of behaviour have been observed in cardiac muscle membrane. These are shown in figure 2.6. The first case is known as

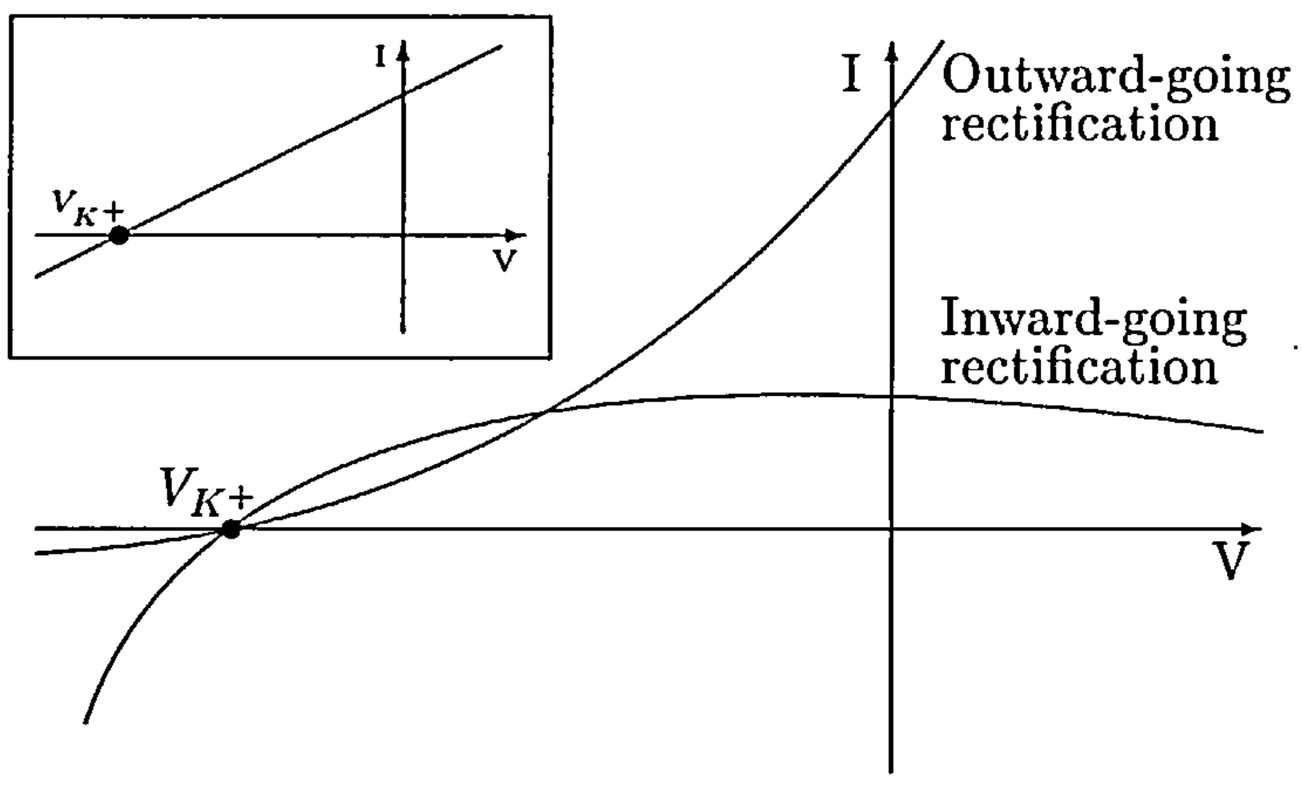

Figure 2.6: Outward-going and inward-going rectification for K^+ channels. The current–voltage diagram given by the (linear) Nernst equation (2.1) is also shown (inset).

outward-going rectification and the ionic channels conduct more easily as outward current is passed through them. (i.e. to positive changes in potential). The second

case is known as inward-going rectification and the channels conduct more easily as inward current is passed through them. (i.e. to negative changes in potential).

2.2.3 Gating Mechanisms

It is observed that ionic channels are both voltage dependent and time dependent. That is, as the membrane potential is increased, the ionic channels typically conduct more easily and this response is not instantaneous.

The kinetic scheme that allows the ionic channels to open and close, thus conducting ions or preventing their movement, is known as the gating mechanism. The concept was introduced by Hodgkin and Huxley and though not entirely correct, it is still used today for mathematical modelling.

The assumption is that each ionic channel is controlled by gates which may be either open or closed as shown in figure 2.7. If the fraction of gates which is open is x,

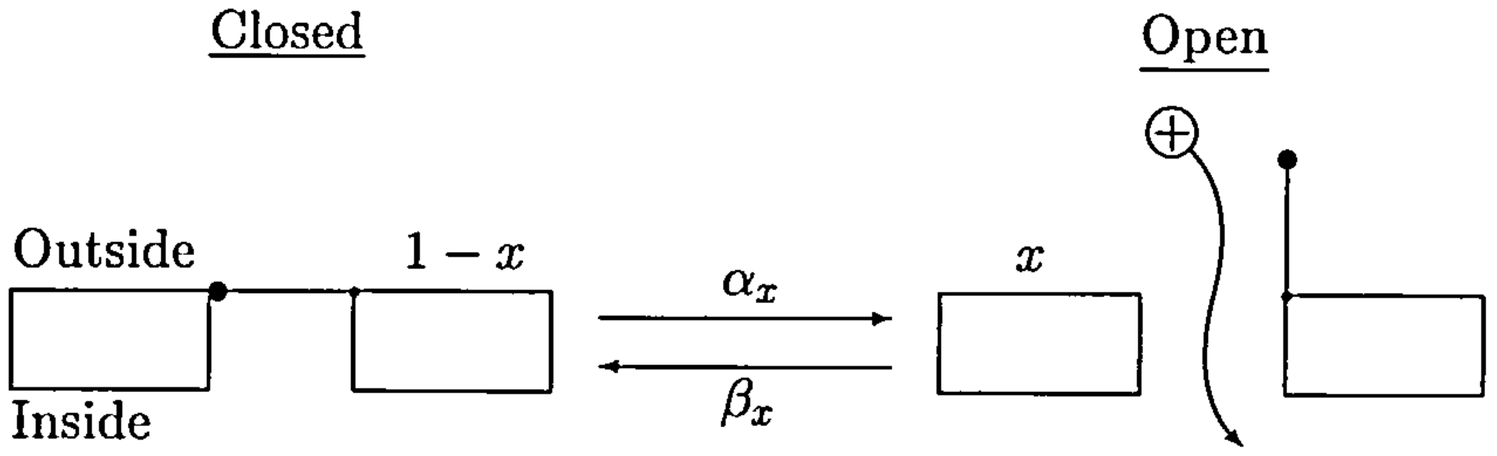

Figure 2.7: Schematic diagram illustrating the gating mechanism.

then the fraction which is closed is $1-x$. Note therefore that x will vary between 0 and 1. Also, if the rate at which gates open is α_x, and the rate at which gates close is β_x, then the overall rate of change in the fraction of open channels will be given by the following first-order differential equation.

$$\frac{dx}{dt} = \alpha_x(1-x) - \beta_x x \tag{2.2}$$

Both α_x and β_x are functions of voltage and as the membrane depolarises α_x increases opening more channels. Similarly β_x decreases closing less channels. The

steady state value x_∞ occurs when $\frac{dx}{dt} = 0$. Therefore

$$x_\infty = \frac{\alpha_x}{\alpha_x + \beta_x}$$

The graph of x_∞ is a sigmoidal function of voltage and is often referred to as the activation curve. Equation (2.2) may be rewritten as

$$\frac{dx}{dt} = \frac{x_\infty - x}{\tau_x}$$

where $\tau_x = 1/(\alpha_x + \beta_x)$. Assuming that the potential is constant we can solve this equation as follows.

$$\begin{aligned}
\frac{1}{\tau_x}\int_0^t dt &= -\int_{x_0}^{x} \frac{1}{x - x_\infty} dx \\
\Rightarrow \frac{t}{\tau_x} &= -\left[\ln|x - x_\infty|\right]_{x_0}^{x} \\
&= \ln|x_0 - x_\infty| - \ln|x - x_\infty| \\
\Rightarrow e^{\frac{t}{\tau_x}} &= \frac{x_0 - x_\infty}{x - x_\infty} \\
\Rightarrow x &= x_\infty - (x_\infty - x_0)\exp^{-\frac{t}{\tau_x}}
\end{aligned}$$

where x_0 is the value of x at time $t = 0$. Therefore, on instantaneously changing the voltage, x will change following an exponential time course with time constant τ_x to the value x_∞.

The current carried by a particular ionic channel, I_x, will be given by

$$I_x = x\overline{I}_x$$

where $\overline{I}_x$ is the maximum current when all the gates are open.

From experimental results it was observed by Hodgkin and Huxley that the initial increase of the potassium current followed a sigmoidal time course and not an exponential one. This phenomenon could be explained by assuming that each ionic channel is operated by more than one gating mechanism. Therefore, if the channel is to be fully conducting all the gates need to be open. The probability that the channel will conduct is thus x^γ where γ is the number of gates involved.

It was also observed that following the initial increase of the sodium current on depolarisation, it then decays exponentially. This behaviour is known as inactivation and may be accounted for by supposing that one of the gates moves in the opposite direction and more slowly than the others. This gate therefore closes on depolarisation of the membrane.

The general form of the gating mechanism for any particular channel will be

$$I_x = x_1^{\gamma_1} \dots x_n^{\gamma_n} \overline{I}_x$$

where x_i and γ_i, $(i = 1, \dots, n)$, are the gating variables and the number of gates involved respectively. Some of these gates will be activating and others inactivating and all the gate variables will be governed by an equation of the form of (2.2). In practice there are rarely more that three gating variables used for each ionic channel.

2.3 Hodgkin-Huxley Model

The ideas discussed in the previous section come from work done on squid nerve by Hodgkin and Huxley. This work won them the Nobel prize for Physiology and Medicine in 1963 and their model is now presented.

2.3.1 General Ideas

Current can be carried across the membrane in two ways; by the movement of ions down their respective electrochemical potential gradients or by charging the membrane capacity. Thus the total membrane current, I_m, is given by the sum of the ionic currents and the current flowing into the membrane capacity. The ionic current is split into components carried by sodium ions, potassium ions and other ions giving

$$I_m = C_m \frac{dV}{dt} + I_{Na} + I_K + I_l \tag{2.3}$$

where C_m is the membrane capacity in $\mu F/cm^2$ ($C_m = 1\mu F/cm^2$ was used by Hodgkin and Huxley for squid nerve), V is the membrane potential in mV, t is the

time in ms, and I_{Na} and I_K are the sodium and potassium ionic currents in $\mu A/cm^2$ respectively. I_l is a small leakage current made up by chloride and other ions.

N.B. Here, and in what follows, $V = E_m - E_r$, where E_r is the resting potential of the squid nerve and E_m is the membrane potential expressed in the form inside potential minus the outside potential. V was used by Hodgkin and Huxley so that the membrane at rest was given a value of zero. Also note that V has a sign such that the action potential is a negative variation in V.

As discussed in the previous section, Hodgkin and Huxley showed that the ionic currents through the membrane can be expressed as product of the relevant conductance and the electrical potential difference for the ion. This potential difference is equal to the difference between the membrane potential and the equilibrium potential (given by the Nernst equation) for the relevant ionic channel. The currents are therefore given by

$$\begin{aligned} I_{Na} &= g_{Na}(V - V_{Na}) \\ I_K &= g_K(V - V_K) \\ I_l &= g_l(V - V_l) \end{aligned}$$

where g_{Na}, g_K and g_l are the sodium, potassium and leakage conductances respectively in $m\ mho/cm^2$. V_{Na}, V_K and V_l are the equilibrium potentials in mV.

2.3.2 The Ionic Conductances

The sodium and potassium conductances, g_{Na} and g_K, are seen to vary with time and membrane potential whereas the membrane capacitance, C_m, the equilibrium potentials, V_{Na}, V_K and V_l, and the leak conductance, g_l, can be taken as constant. g_{Na} and g_K can be described by a gating mechanism.

When the membrane is depolarised, it is observed experimentally that both the sodium and potassium conductances increase with a delay but on repolarisation, decrease without a delay. As mentioned in the previous section, it is therefore useful to describe the conductances as a power of a (gating) variable which satisfies a first order differential equation. If a fourth power is used the rise of the conductance is

then described by a term of form $(1 - e^{-t})^4$, and the fall by a term of form e^{-4t}, which incorporate the observed experimental delay in the rise of conductance and the simple exponential fall in conductance. A fourth power is used for the potassium current, as given above, and a third power is used for sodium together with an inactivation term.

The Potassium Conductance

The potassium conductance, g_K, in the Hodgkin-Huxley model is given by

$$g_K = \overline{g}_K n^4 \tag{2.4}$$

where n satisfies the gating equation

$$\frac{dn}{dt} = \alpha_n(1-n) - \beta_n n \tag{2.5}$$

Here $\overline{g}_K = 36m\ mho/cm^2$ is a constant, n is a dimensionless gating variable varying between 0 and 1, and α_n and β_n are rate constants which vary with membrane potential but not with time.

Recall from earlier that equation (2.5) may be rewritten as

$$\frac{dn}{dt} = \frac{n_\infty - n}{\tau_n}$$

where $n_\infty = \alpha_n/(\alpha_n+\beta_n)$ and $\tau_n = 1/(\alpha_n+\beta_n)$, and that if we assume the potential is constant, the equation can be solved to give

$$n \;=\; n_\infty - (n_\infty - n_0)e^{-\frac{t}{\tau_n}}$$

where n_0 is the value of n at time $t = 0$. By eliminating n in equation (2.4), Hodgkin and Huxley compared the resulting equation for g_K with experimental results finding good agreement.

Rate Constants

The values of α_n and β_n were calculated experimentally via values of n_∞ and τ_n from the equations $\alpha_n = n_\infty/\tau_n$ and $\beta_n = (1-n_\infty)/\tau_n$. To find the functions $\alpha_n(V)$

and $\beta_n(V)$ curve fitting to all the experimental data was used and the following expressions were calculated.

$$\begin{aligned} \alpha_n &= 0.01(V+10)/(\exp[(V+10)/10]-1) \\ \beta_n &= \exp[V/80]/8 \end{aligned}$$

The Sodium Conductance

To describe the changes observed in the sodium conductance it is assumed that g_{Na} is determined by two variables, each obeying a first order gating equation. The sodium conductance is given by

$$g_{Na} = \bar{g}_{Na} m^3 h \tag{2.6}$$

where m and h satisfy the gating equations

$$\frac{dm}{dt} = \alpha_m(1-m) - \beta_m m \tag{2.7}$$

$$\frac{dh}{dt} = \alpha_h(1-h) - \beta_h h \tag{2.8}$$

respectively. Here $\bar{g}_{Na} = 120m\ mho/cm^2$ is a constant and the α's and β's are rate constants which are functions of voltage but not time. m is the activation variable and h is the inactivation variable and equations (2.7) and (2.8) can be solved to give

$$m = m_\infty - (m_\infty - m_0)e^{-\frac{t}{\tau_m}} \tag{2.9}$$

$$h = h_\infty - (h_\infty - h_0)e^{-\frac{t}{\tau_h}} \tag{2.10}$$

where m_∞, τ_m, m_0, h_∞, τ_h and h_0 are analogous to n_∞, τ_n and n_0 mentioned previously. Equations (2.6), (2.9) and (2.10) can be combined to give an equation for g_{Na} which gives good agreement with experimental data.

Rate Constants

As in the case of α_n and β_n, α_m and β_m were calculated from experimental data using $\alpha_m = m_\infty/\tau_m$ and $\beta_m = (1-m_\infty)/\tau_m$. Using curve fitting to the experimental data, the following functions for α_m and β_m in terms of voltage were obtained.

$$\begin{aligned} \alpha_m &= 0.1(V+25)/(\exp[(V+25)/10]-1) \\ \beta_m &= 4\exp[V/18] \end{aligned}$$

Similarly

$$\begin{aligned} \alpha_h &= 0.07\exp[V/20] \\ \beta_h &= 1/(\exp[(V+30)/10]+1) \end{aligned}$$

2.3.3 Final Equations

Combining the above equations for ionic conductances gives the following equation for the change in membrane voltage, V,

$$\begin{aligned} I_m &= C_m\frac{dV}{dt} + \overline{g}_K n^4(V-V_K) \\ &\quad + \overline{g}_{Na}m^3h(V-V_{Na}) + \overline{g}_l(V-V_l) \end{aligned} \tag{2.11}$$

together with (2.5), (2.7) and (2.8),

$$\begin{aligned} \frac{dn}{dt} &= \alpha_n(1-n) - \beta_n n \\ \frac{dm}{dt} &= \alpha_m(1-m) - \beta_m m \\ \frac{dh}{dt} &= \alpha_h(1-h) - \beta_h h \end{aligned}$$

Here the α's and β's are functions of the instantaneous membrane potential only and are given above. C_m, $\overline{g}_K$, $\overline{g}_{Na}$, $\overline{g}_l$, V_K, V_{Na} and V_l are all constants.

2.3.4 Simulation

If the nerve axon is voltage clamped then there is no current along the axis of the axon and the net membrane current I_m must therefore be zero (except during a stimulus). If the stimulus is of a short duration then the form of the action potential will be given by solving equation (2.11) with $I_m = 0$, $V = V_0$, its initial value, and m, h, n having their steady-state values. The results from such a simulation are shown in figure 2.8. The resulting action potential can be seen to have a duration of around $3ms$ (which is short compared to cardiac action potentials) and bears resemblance to the slow type response mentioned earlier. Short action potential durations are typical of nerve impulses where they act solely as a trigger for mechanical activity.

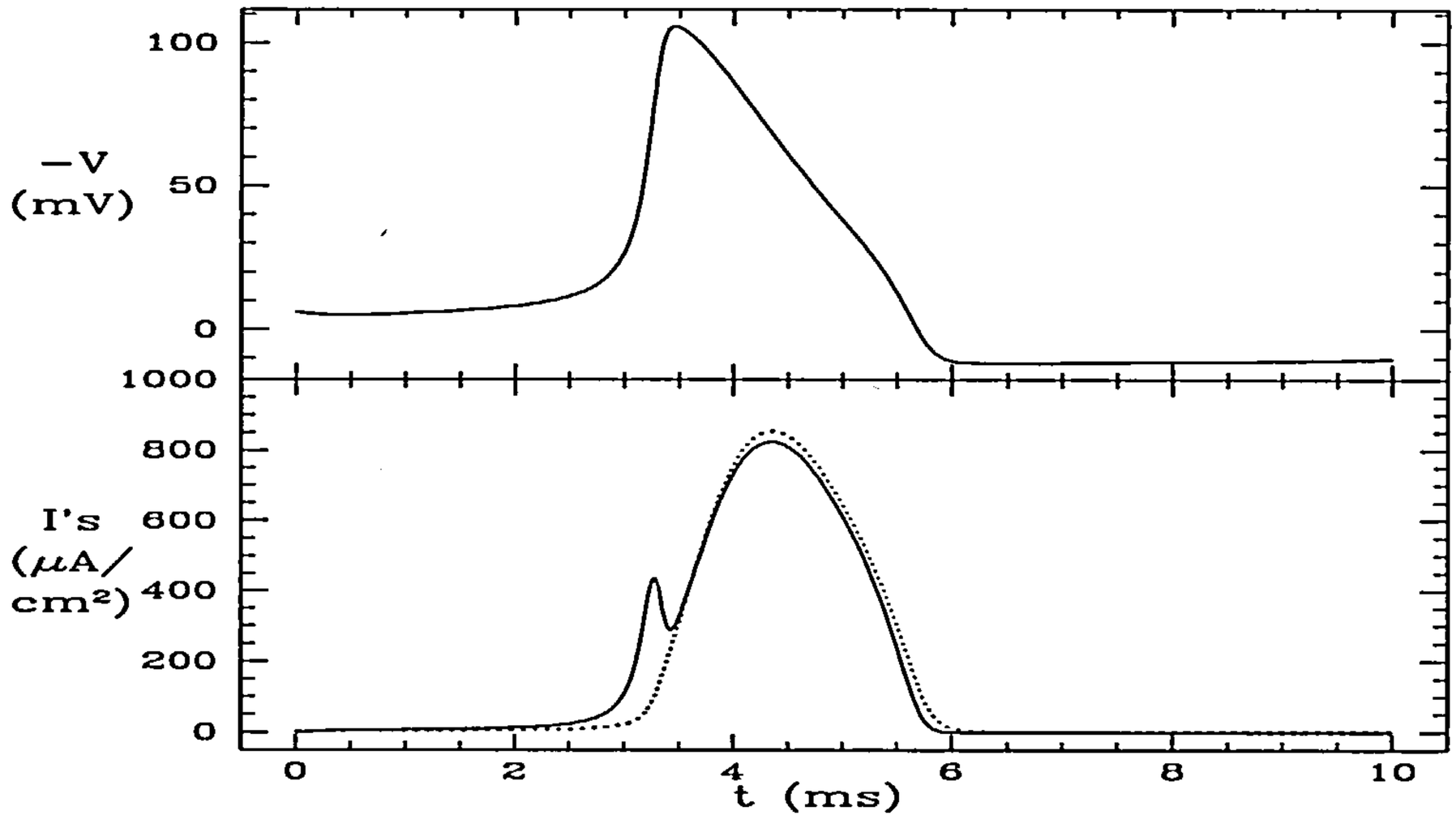

Figure 2.8: Simulation of the Hodgkin-Huxley equations. The top figure shows the variation of (negative) voltage with time. The bottom figure shows the variation of the currents I_{Na} (solid) and $-I_K$ (dotted).

2.4 Noble Model

We shall now outline one of the first models of cardiac tissue that was based on the Hodgkin-Huxley approach, namely the 1962 Noble model [6] of the Purkinje fibres of the heart.

One of the major differences between Purkinje fibres of the heart and squid nerve, and hence between the Hodgkin-Huxley and Noble models, is that depolarisation decreases the potassium permeability of the membrane (inward-going rectification). Thus, to take account of this behaviour, the equations describing the potassium current have to be modified. The equations describing the sodium current, however, are very similar to those used by Hodgkin and Huxley. Also, the membrane capacity, C_m, is approximately 12 times larger than that in squid nerve and hence C_m is taken to be $12\mu F/cm^2$.

Finally, the convention used by Noble for the membrane potential is to adopt that

usually used in experimental work in this field and express it as the potential of the inside of the membrane with respect to the outside. i.e. E_m in the previous chapter. The resting potential is a negative quantity and the action potential is a positive variation so the membrane potential E_m here is related to V in the previous section by $E_m = E_r - V$. Note here however that rather than using the notation E_m we will continue to use V.

2.4.1 The Potassium Current

In order to describe the potassium current mathematically, it is assumed that the potassium ions may move through two types of channel in the membrane.

In the first of these channels the potassium conductance, g_{K1}, is assumed to be an instantaneous function of the membrane potential which falls when the membrane depolarises giving the inward-going rectification property. The equation used for g_{K1} is

$$g_{K1} = 1.2\exp[(-V - 90)/50] + 0.015\exp[(V + 90)/60]$$

In the second of these two channels the conductance g_{K2} slowly rises when the membrane depolarises. The equation used is the same as that used by Hodgkin and Huxley (equation 2.4) but with a couple of numerical alterations. The first of these is that the value of $\overline{g}_{K2}$ ($\overline{g}_K$ in equation (2.4)) is made much smaller so as not to offset the decrease in g_{K1} on depolarisation. i.e. $g_{K2} = 1.2n^4$. n here is the gating variable and obeys the standard gating equation (2.2). Also, the rate constants for potassium are divided by a factor of around 100 as the onset of this effect in Purkinje fibres is much slower.

$$\begin{aligned} \alpha_n &= \frac{0.0001(-V - 50)}{\exp[(-V - 50)/10] - 1} \\ \beta_n &= 0.002\exp[(-V - 90)/80] \end{aligned}$$

The potassium equilibrium potential, V_K, is set to $-100mV$ giving the following equation for the potassium current.

$$I_K = (g_{K1} + g_{K2})(V + 100)$$

The current–voltage relation for potassium, described by the above equations, corresponds well with experimental data over the range of potentials covered by the action potential.

2.4.2 The Sodium Current

The form of the sodium conductance is the same as that used by Hodgkin and Huxley and the main modifications in the equations are alterations to the rate constants.

The functions for α_h and β_h are shifted along the voltage axis to make the equilibrium value for h coincide with experimental data.

$$\begin{aligned} \alpha_h &= 0.17\exp[(-V-90)/20] \\ \beta_h &= \frac{1}{\exp[(-V-42)/10]+1} \end{aligned}$$

Obtaining equations for the rate constants for m was achieved by a somewhat arbitrary process due to difficulties in gathering experimental data.

$$\begin{aligned} \alpha_m &= \frac{0.1(-V-48)}{\exp[(-V-48)/15]-1} \\ \beta_m &= \frac{0.12(V+8)}{\exp[(V+8)/5]-1} \end{aligned}$$

Finally, a small component of g_{Na} is assumed to be independent of membrane potential and time so that $g_{Na} = \overline{g}_{Na} + \tilde{g}_{Na}$, where $\tilde{g}_{Na}$ is constant. The equilibrium potential of sodium, V_{Na}, is given the value $40mV$, $\overline{g}_{Na}$ is set at $400m\ mho/cm^2$ and $\tilde{g}_{Na}$ at 0.14. This gives

$$I_{Na} = (400m^3h + 0.14)(V-40)$$

2.4.3 Final Equations

The final equations used by Noble are as follows.

$$\begin{aligned} I_m &= C_m\frac{dV}{dt} + (g_{K1}(V) + 1.2n^4)(V+100) \\ &\quad + (400m^3h + 0.14)(V-40) + g_l(V-V_l) \qquad (2.12) \\ \frac{dn}{dt} &= \alpha_n(1-n) - \beta_n n \end{aligned}$$

$$\begin{aligned} \frac{dm}{dt} &= \alpha_m(1-m) - \beta_m m \\ \frac{dh}{dt} &= \alpha_h(1-h) - \beta_h h \end{aligned}$$

where $g_{K1}(V)$, and the α's and β's are as described above. C_m is constant and is equal to $12\mu F/cm^2$.

The original Noble equations are spontaneously oscillatory although their character can be changed to excitable by slightly lowering the value of $\tilde{g}_{Na}$ from its standard value of 0.14 to 0.132 (see [21]).

Simulations of the Noble equations are presented in the following chapter.

2.5 Recent Ionic Models

The model proposed by Noble in 1962, as described in the previous section, reproduced cardiac action potentials to a reasonable accuracy. Furthermore, the changes in the overall inward and outward currents produced by the model are fairly close to those obtained experimentally. However, around ten years later, following extensive experimental analysis of the ionic currents in cardiac membranes using the voltage clamp technique, it was found that the model is incorrect on an ionic basis. That is, the ionic components of the currents and the kinetics of the ionic channels obtained by experiment differ from those used in the model. It was found that a substantial part of the inward current during the plateau is carried by calcium ions (not part of the Noble 1962 model) and not sodium ions. Furthermore, the actual gating mechanism involved for calcium is completely different.

These discoveries were taken into account by Beeler and Reuter [9] in their 1977 model of ventricular myocardial fibres. The model they developed has 8 variables and 3 principle ionic currents; sodium, potassium and calcium (with the different gating mechanism). This model produces accurate action potentials and for the correct physical reasons.

In the years that followed, the experimental techniques for analysing heart tissue

became increasingly more sophisticated, especially with the development of the patch clamp technique. More and more ionic currents and pumps were discovered and their behaviour could be analysed. In the process, models describing the behaviour of cardiac tissue have become considerably more complex [8, 12, 15, 20, 32].

Modern models describing cardiac tissue are extremely accurate and unfortunately extremely complicated (for example the Earm and Noble model describing an atrial cell [15] (now 8 years old) has 17 kinetic variables describing 11 different currents). Models for different parts of the heart are being continually developed to incorporate new experimental observations and one of the best sources of recent equations is an intermittently updated computer program [61].

Note that cardiac models become even more complex when the physical geometry of the heart is taken into account.

2.6 FitzHugh-Nagumo Equations

As mentioned above, as more knowledge about the mechanisms of the ionic channels in the heart has been acquired, the complexity of the models has increased. The mathematical analysis of these ionic models is extremely difficult and any insight into the dynamical behaviour is hard, if not impossible, to obtain. It is therefore natural to look for simple models which convey important aspects of the dynamics, and various mathematical models have been proposed. By far the most famous and frequently used of these models is the FitzHugh-Nagumo [4, 5] model. The FitzHugh-Nagumo equations are essentially a caricature of the Hodgkin-Huxley equations for squid nerve. They were constructed in an attempt to simplify the four-variable system whilst retaining the essential phenomenological characteristics. The simplifications are somewhat drastic (essentially, the fast m variable is set to its equilibrium value and h is set to a constant value leaving the variables V and n) but the resulting equations, which consist of just two variables, still capture the key features of the full system. The (homogeneous) FitzHugh-Nagumo equations can be written in the

following form

$$\begin{aligned} \frac{dv}{dt} &= I - v(v-a)(v-1) - w \\ \frac{dw}{dt} &= \epsilon(v - \gamma w) \end{aligned}$$

Here, v and w are the dynamical variables (representing voltage and the gate variables respectively), and a $(0 < a < 1)$, ϵ $(\epsilon \ll 1)$, and γ, are parameters. I is the stimulus current injected into the cell. With the stimulus current $I = 0$, the nullclines for the above set of equations take the form of those shown in figure 2.9. These equations, like the real squid axon (which has a quiescent resting state), have

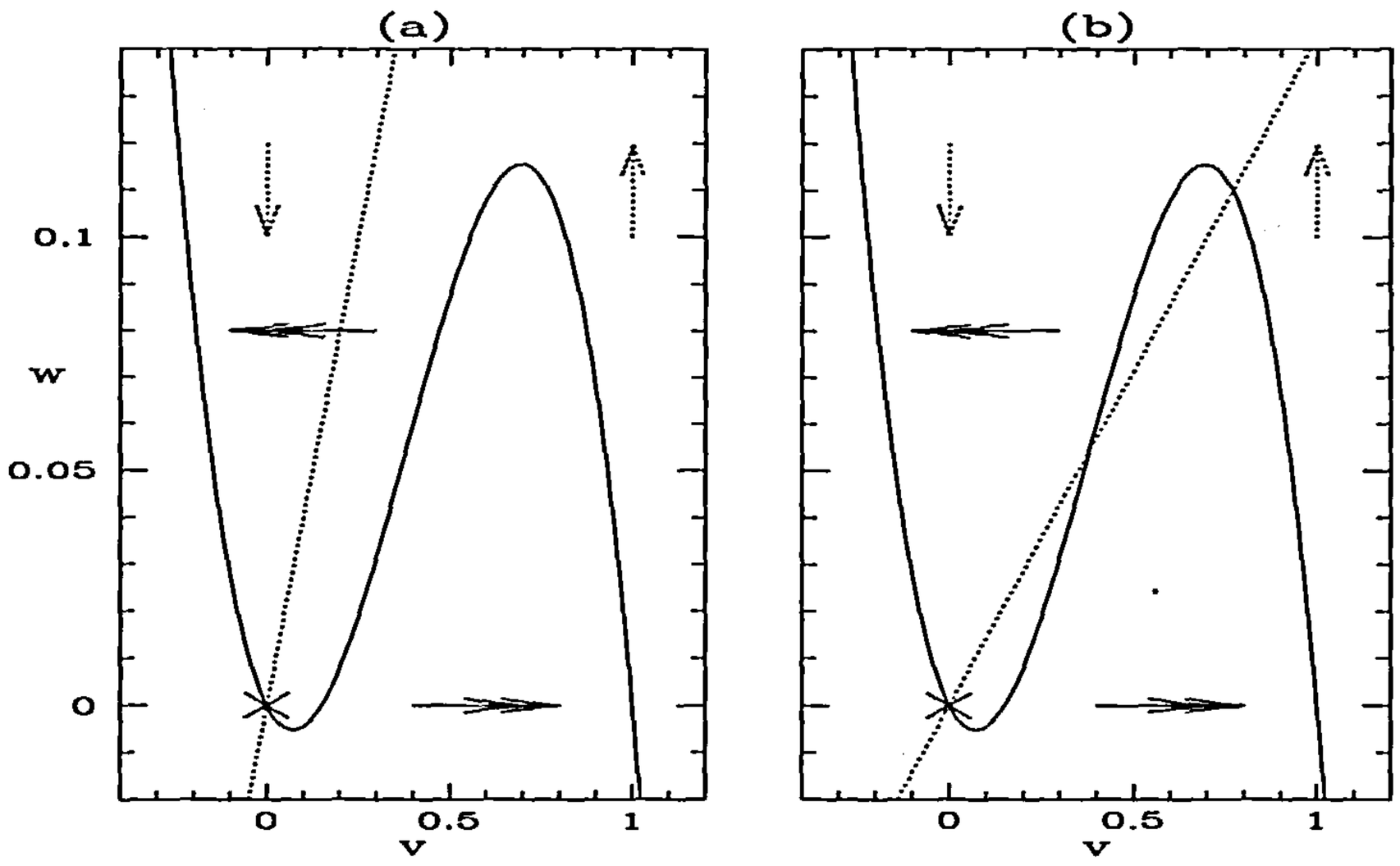

Figure 2.9: Nullclines for the FitzHugh-Nagumo equations with $I = 0$. Solid and dashed lines are used for v and w respectively. The arrows indicate the direction of the flow and the stable steady state at the origin is shown with a cross. Due to ϵ appearing in the $\dot{w}$ equation the rate of change of v will be larger. This is illustrated by the double arrows. Note that as the parameters vary there can be (a) one or (b) three steady states. We have used $a = 0.15$, $\epsilon = 0.002$ and $\gamma =$ (a) 2.5 and (b) 7.0.

a stable steady state at $(v, w) = (0, 0)$. Furthermore, the excitability characteristic can now clearly be seen from the nullcline structure of the equations. We shall concentrate on figure (a) with just one steady state. Applying a small stimulus current

(which has the effect of slightly raising the cubic nullcline) or perturbing/exciting v up to a value $v_0 < a$ will not produce an action potential and the trajectory will return to the stable steady state with v and w remaining small. However if v is excited to a value $v_0 > a$ (or a large stimulus current is applied) then the trajectory will follow a large amplitude detour before returning to the stable steady state. This gives rise to an action potential. Both these behaviours are shown in figure 2.10.

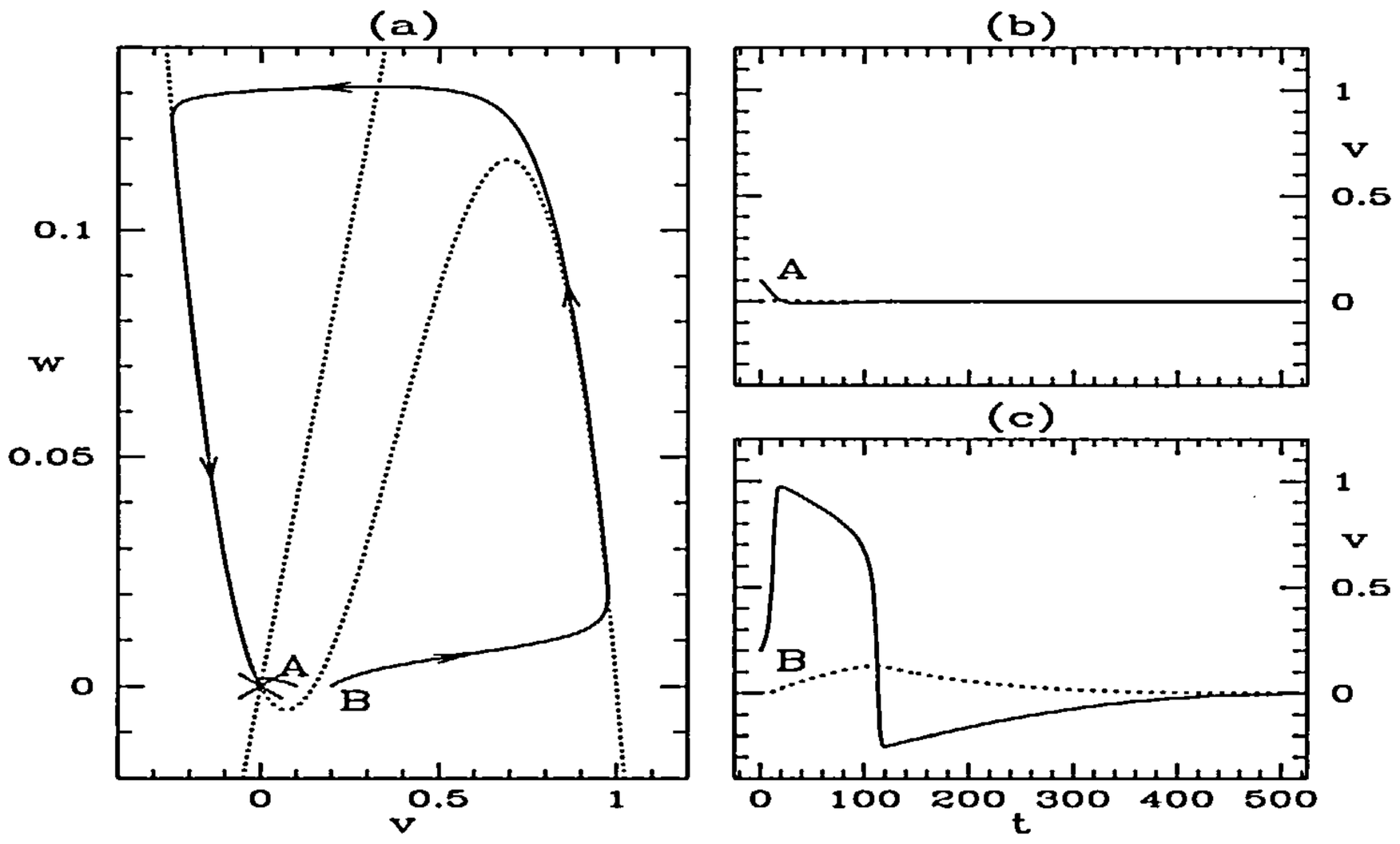

Figure 2.10: Trajectories for the FitzHugh-Nagumo equations. (a) The result of perturbing the initial value of v, v_0, to both a sub-threshold value A ($v_0 = 0.1$) and a super-threshold value B ($v_0 = 0.2$). As in figure 2.9, $a = 0.15$, $\epsilon = 0.002$ and $\gamma = 2.5$. (b) The time series of the sub-threshold trajectory and (c) the time series of the super-threshold trajectory showing both v (solid) and w (dotted).

It can be seen from this figure that the FitzHugh-Nagumo model gives rise to waves that capture the main features of an action potential. However it fails to simulate several quantitative characteristics of cardiac action potentials such the different time scales of depolarisation and repolarisation and the overshoot on the upstroke. Furthermore, although the structure of the phase plane is relatively simple, and it illustrates the excitability characteristic well, it does not give much of an insight

into the dynamics or phase plane structure of the physiological system.

Chapter 3

Modelling the Currents

The purpose of this chapter is to develop a new class of cardiac models based on a dynamical systems analysis of currents rather than on detailed physiological modelling of actual gate variables. Rather than concentrating on each individual ionic current (of which there are many), the philosophy will be to consider only the overall inward and outward currents.

The start of this chapter shall concentrate on the 1962 Noble model [6] and we shall present the first full analysis of this model from a phase plane, i.e. dynamical systems, viewpoint. We shall investigate the dynamics in terms of the inward and outward currents and therefore re-write the Noble model in terms of the currents involved and analyse the phase plane structure of the resulting equations. A few important properties will become evident and these will be briefly discussed.

Following the analysis of the Noble phase plane we shall introduce a new three variable model (voltage, inward and outward current) that is simple in form and that reproduces very accurately the Noble cardiac action potentials and currents. Again, the main ideas will be discussed and we will get a further insight into how the Noble equations generate action potentials.

Note that for the duration of this chapter and the next we shall only be concerned with single cell models, i.e. with no spatial dependence.

3.1 Noble Model

3.1.1 Initial Discussion

The 1962 Noble model is relatively simple (four dynamic variables) and considers only the sodium (inward) and potassium (outward) currents. As mentioned earlier, the ionic basis of the model is incorrect in the sense that it omits the calcium current responsible for the plateau of the action potential and more mechanistically accurate models exist. However, there are various reasons why it is useful to study the Noble model. Firstly, the actual cardiac action potentials generated by the model resemble closely those obtained experimentally in terms of their shape and duration. Furthermore, the overall inward and outward currents are also fairly accurate. The Noble model also displays some rate dependent changes in action potential duration which are important in cardiac tissue. Finally, due to the relative simplicity of the model, it is possible to analyse the dynamics in phase plane.

We first must convert the equations from the V, n, m and h variables to V, I_{Na} and I_K variables. To a good approximation, the fast gating variable m can be replaced by its equilibrium value $m_\infty(V)$. This does not alter the shape of the action potentials or currents to any great degree as can be seen from figure 3.1. The gate variable m is the activation variable for the sodium current which causes the upstroke. It is not surprising therefore that the main difference in a simulation with m set instantaneously to its equilibrium value occurs during the upstroke. The upstroke is in fact sharper (no time delay for m) and the sodium current reaches a higher value. The remainder of the action potential remains essentially the same. This reduces the Noble model to three variables (V, n and h). Note that in the FitzHugh-Nagumo model (where m is also set to it's infinity value), h is set to a constant. This is a drastic simplification as in reality h varies considerably.

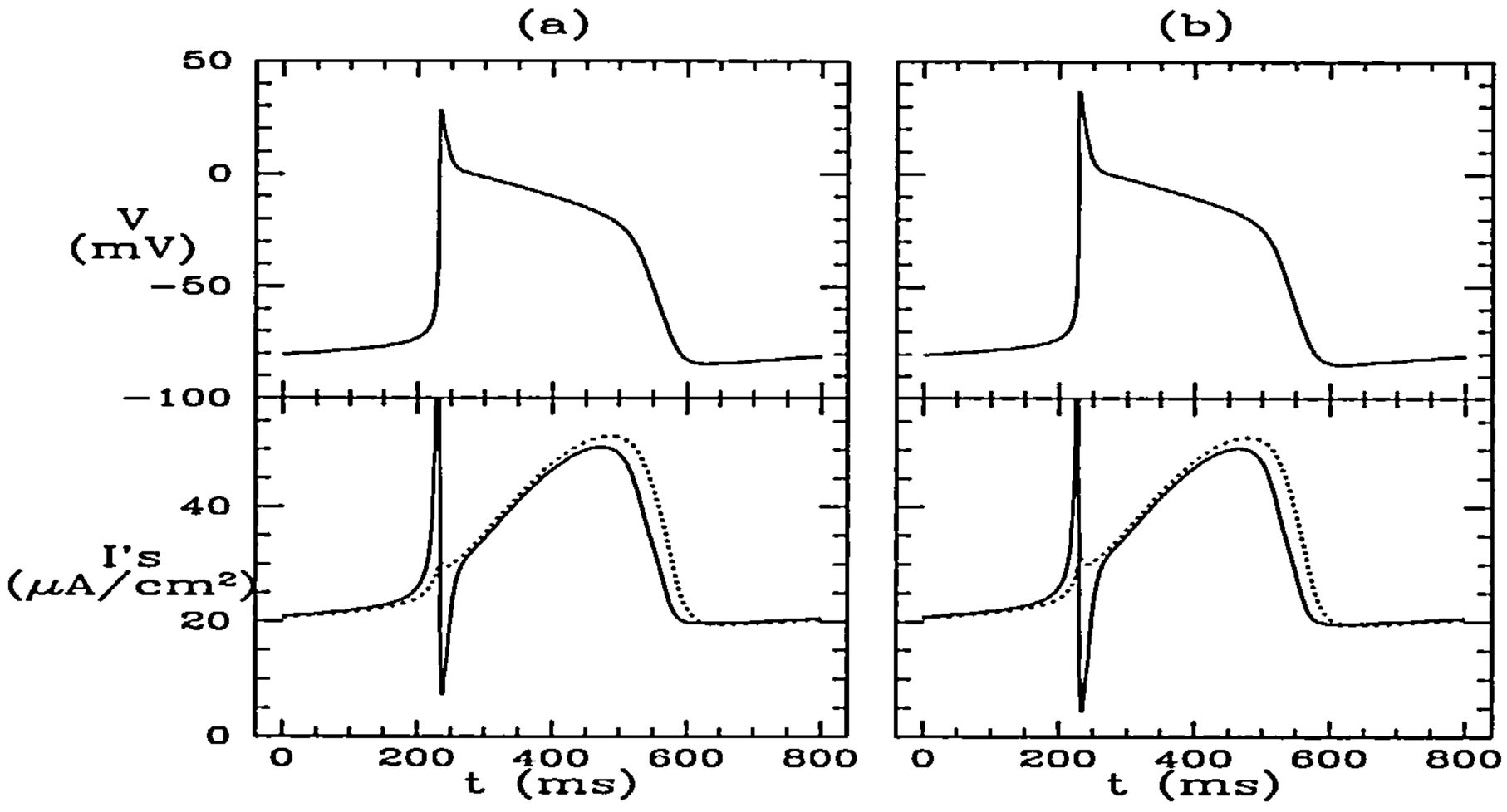

Figure 3.1: Results from simulations of the Noble model showing both voltage V and the currents $-I_{Na}$ (solid) and I_K (dotted) for (a) all four variables and (b) the three variable system obtained by setting m to its equilibrium value m_∞. Note that $-I_{Na}$ goes off the scale in both (a) and (b). $\tilde{g}_{Na} = 0.132$ is used in both plots giving excitable behaviour.

3.1.2 Change of Variables

We now change variables from V, n and h, to obtain the Noble model in terms of the voltage, sodium current and potassium current.

To simplify the notation we shall write I_1 as $-I_{Na}/C_m$ and I_2 as I_K/C_m. Hence I_1 and I_2 will represent the (scaled) inward and outward currents respectively. We shall also use the notation $\dot{x}$ to represent the time derivative of x. The Noble model, with m replaced by its equilibrium value $m_\infty(V)$, is

$$\begin{aligned}
\dot{V} &= I_1 - I_2 \\
I_1(V,h) &= -\frac{1}{C_m}(400m_\infty^3(V)h + \tilde{g}_{Na})(V - 40) \\
I_2(V,n) &= \frac{1}{C_m}(g_{K_1}(V) + 1.2n^4)(V + 100) \\
\dot{x} &= \alpha_x(V)(1-x) - \beta_x(V)x, \text{ where } x = h, n
\end{aligned}$$

h and n are gating variables so $0 < h, n < 1$. $m_\infty(V) > 0$ and is a sigmoidal function of voltage. Note also that, due to the structure of the equations, the voltage V is restricted to the range $-100 < V < 40$.

We shall now change from (V, h, n) variables to (V, I_1, I_2) variables. Note that with $-100 < V < 40$ and $0 < h, n < 1$ the map $(V, h, n) \longmapsto (V, I_1(V, h), I_2(V, n))$ is one-to-one and smooth with the Jacobian having non-zero determinant. Therefore by the Inverse Function Theorem it is a diffeomorphism. By the chain rule

$$\begin{aligned} \dot{I}_1 &= \frac{\partial I_1}{\partial V}\dot{V} + \frac{\partial I_1}{\partial h}\dot{h} \\ \dot{I}_2 &= \frac{\partial I_2}{\partial V}\dot{V} + \frac{\partial I_2}{\partial n}\dot{n} \end{aligned}$$

where

$$\begin{aligned} h &= \frac{-1}{400 m_\infty^3(V)}\left(\frac{C_m I_1}{V - 40} + \tilde{g}_{Na}\right) \\ n &= \left[\frac{1}{1.2}\left(\frac{C_m I_2}{V + 100} - g_{K_1}(V)\right)\right]^{\frac{1}{4}} \end{aligned}$$

Following some algebra we obtain

$$\begin{aligned} \frac{\partial I_1}{\partial V} &= \left(\frac{3m'_\infty(V)}{m_\infty(V)} + \frac{1}{V - 40}\right) I_1 + \frac{3m'_\infty(V)\tilde{g}_{Na}(V - 40)}{C_m m_\infty(V)} \\ \frac{\partial I_1}{\partial h}\dot{h} &= -\frac{(400 m_\infty^3(V) h_\infty + \tilde{g}_{Na})(V - 40) + C_m I_1}{C_m \tau_h} \\ \frac{\partial I_2}{\partial V} &= \frac{g'_{K_1}(V)(V + 100)}{C_m} + \frac{I_2}{V + 100} \\ \frac{\partial I_2}{\partial n}\dot{n} &= \frac{4(V + 100)}{C_m \tau_n} \times \\ &\qquad \left(1.2 n_\infty \left(\frac{1}{1.2}\left(\frac{C_m I_2}{V + 100} - g_{K_1}(V)\right)\right)^{\frac{3}{4}} - \frac{C_m I_2}{V + 100} + g_{K_1}(V)\right) \end{aligned}$$

where $m'_\infty(V)$ is the first derivative of $m_\infty(V)$ with respect to V and $g'_{K_1}(V)$ is the first derivative of $g_{K_1}(V)$ with respect to V. Re-writing this gives us the following system of differential equations.

$$\begin{aligned} \dot{V} &= I_1 - I_2 \\ \dot{I}_1 &= f_1(V, I_1)\dot{V} + f_0(V, I_1) \\ &= f_1(V, I_1)(I_1 - I_2) + f_0(V, I_1) \end{aligned} \tag{3.1}$$

$$\begin{aligned} \dot{I}_2 &= g_1(V, I_2)\dot{V} + g_0(V, I_2) \\ &= g_1(V, I_2)(I_1 - I_2) + g_0(V, I_2) \end{aligned}$$

where $f_1(V, I_1) = \frac{\partial I_1}{\partial V}$, $f_0(V, I_1) = \frac{\partial I_1}{\partial h}\dot{h}$, $g_1(V, I_2) = \frac{\partial I_2}{\partial V}$, and $g_0(V, I_2) = \frac{\partial I_2}{\partial n}\dot{n}$ as given above.

3.1.3 Simulations

The results from a simulation of the the above equations are shown in figure 3.2. It can be seen that, as it should, the model gives rise to the same action potentials

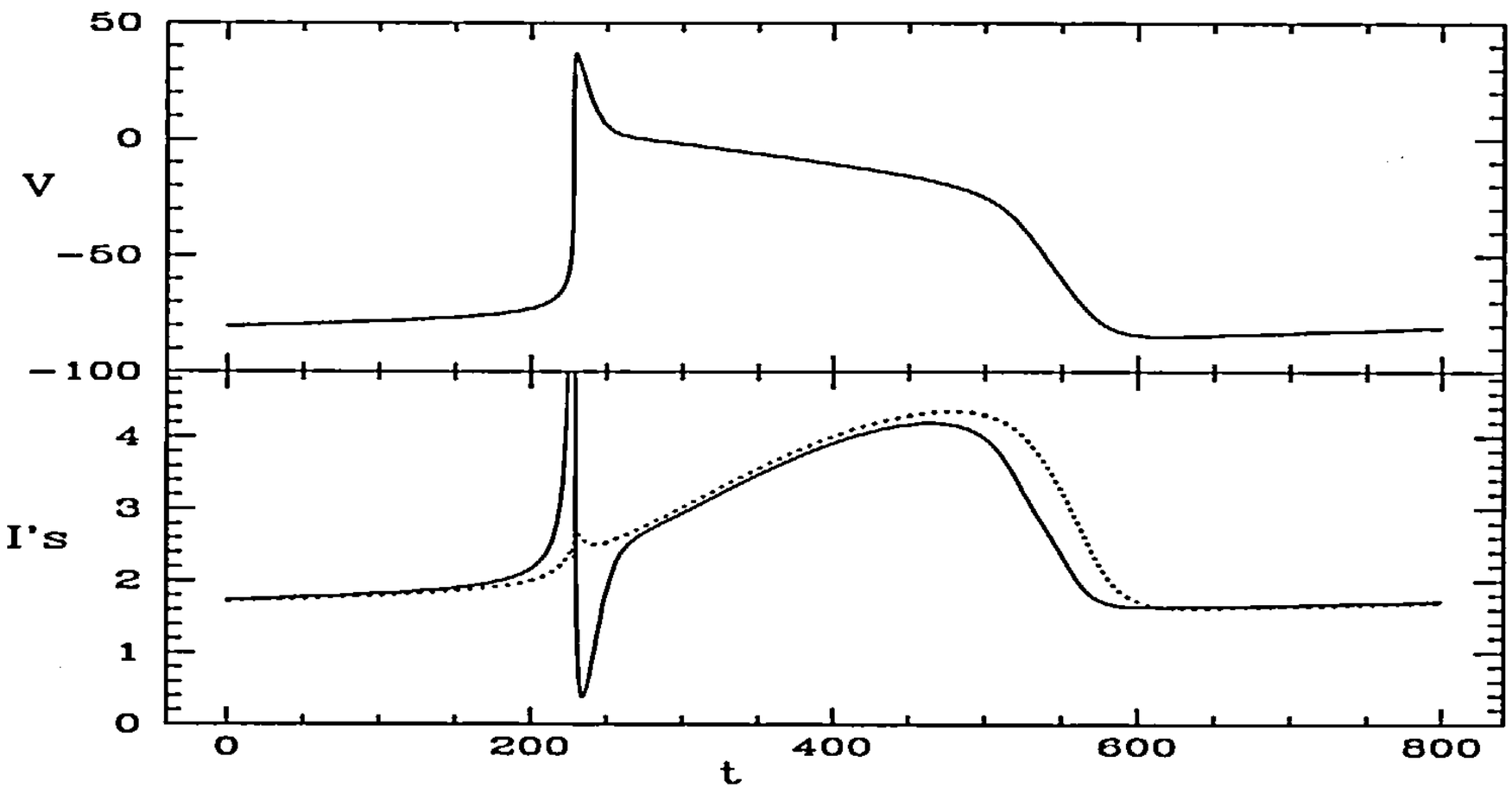

Figure 3.2: Results from a simulation of the Noble model in terms of current variables. Plotted is voltage, V, and the currents, I_1 (solid), and I_2 (dotted), against time. I_1 is truncated and reaches a value of around 140. Note that due to the scaling of the currents (by a factor of $1/C_m$) the I-axis of the current plot is also scaled. $\tilde{g}_{Na} = 0.132$ is used giving excitable behaviour.

and currents obtained from the traditional three-variable Noble model and that they therefore resemble those observed experimentally. Note that we shall omit the units (mV, $\mu A/cm^2$ etc.) in what follows as we will only be concerned with the qualitative aspects of the action potentials.

3.1.4 Phase Portrait Analysis

We can now gain insight into the dynamics from an analysis of the equation structure and the phase plane.

A first observation to make from the Noble current equations (3.1) is that the rate of change of voltage, $\dot{V}$, depends on the difference between the inward and outward currents, $I_1 - I_2$. Hence when these two currents cross, the rate of change of voltage changes sign. This simple, physically meaningful observation will be useful when considering the phase plane structure later in the chapter.

The results of a simulation, shown from a phase plane perspective (without null-clines), are plotted in figure 3.3. The change in currents is described below for the

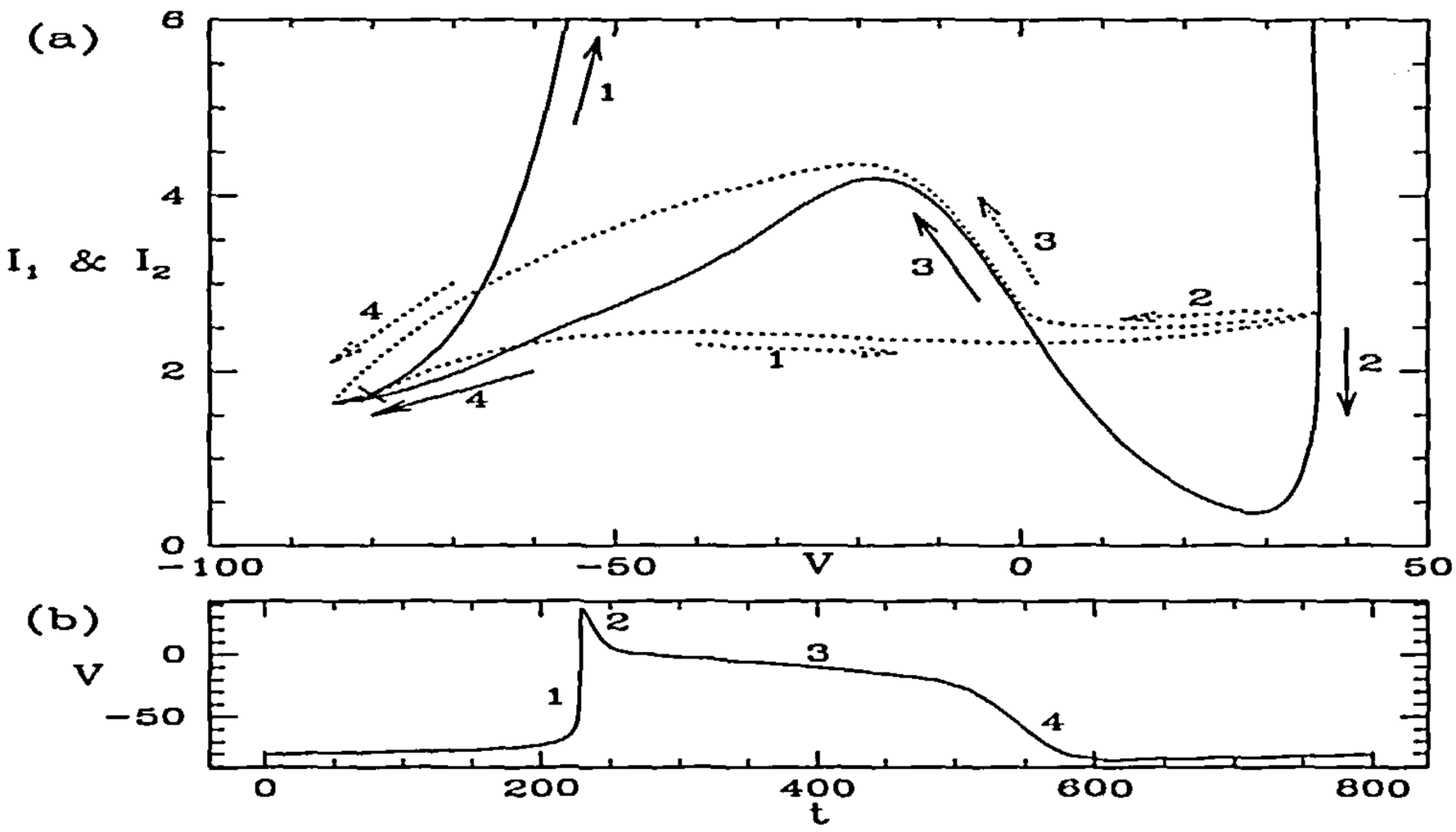

Figure 3.3: Simulation of the Noble currents model showing (a) the V–I phase plane and (b) the voltage action potential. In (a) the time directions of I_1 (solid) and I_2 (dotted) are indicated by arrows. The stable steady state is shown with a cross. Note also that I_1 reaches a maximum value of around 140.

four main phases of the action potential; upstroke, spike, plateau and repolarisation.

1. Upon the initiation of an action potential, the I_1 current becomes extremely

large causing the rate of change of voltage $\dot{V}$ $(= I_1 - I_2)$ to become large. This causes the voltage to sharply increase, during which I_2, the slower current, remains relatively constant. This is the fast upstroke of the action potential.

2. At high values of V, I_1, and hence $\dot{V}$, decrease. At a value of around 2.5, I_1 and I_2 cross, causing $\dot{V}$ to change sign. Therefore the voltage starts to decrease. The difference $I_1 - I_2$ (now negative) causes the voltage to decrease fairly rapidly to a value of around 0 when I_1 and I_2 become close in value. This corresponds to the spike of the action potential.

3. I_1 and I_2 are now very close so the value of $\dot{V}$ is small (and negative). This causes V to decrease relatively slowly generating the plateau of the action potential.

4. When I_1 and I_2 reach a value of around 4 the difference between them increases, and hence the rate of change of V increases (remaining negative) causing the voltage to decrease to low values. The two currents cross each other for the second time when V is around -85, so $\dot{V}$ changes sign once more and V slowly begins to increase back towards the steady state. The system thus returns to equilibrium.

After these four phases the action potential is complete. Note that if the original value of $\tilde{g}_{Na} = 0.14$ is used the equations are oscillatory and another action potential will be initiated. However, as mentioned previously, with $\tilde{g}_{Na}$ set to 0.132 the behaviour is excitable and the system will remain at equilibrium unless V is excited past threshold. In what follows we shall concentrate on the excitable case for which the (stable) fixed point is located at $V \approx -79.70$ and $I_1 = I_2 \approx 1.68$.

The above action potential scheme can also be described in terms of the I_1 and I_2 nullclines and this gives us a greater insight into the underlying mechanisms. The phase space is three-dimensional but we consider two-dimensional cuts. The V–I_1 nullcline therefore depends on the value of I_2, and the V–I_2 nullcline depends on the value of I_1. As I_2 changes during an action potential the structure of the V–I_1 nullclines varies corresponding and similarly as I_1 changes the V–I_2 nullclines

change. Various nullclines that occur throughout an action potential are shown in figures 3.4 and 3.5.

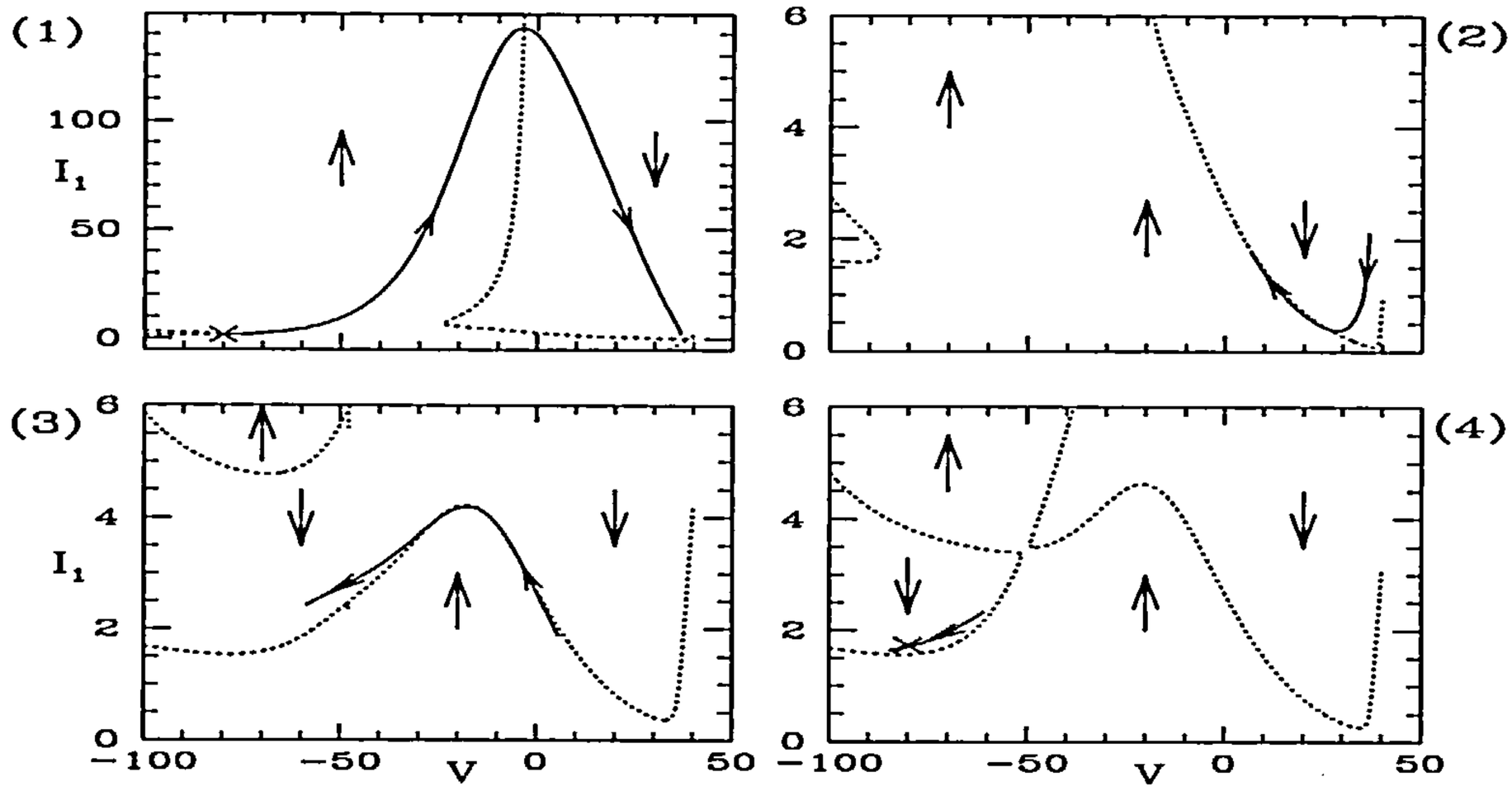

Figure 3.4: Four plots of the I_1 nullcline (dotted) for the Noble model with I_2 set to (1) 1.7, (2) 1.0, (3) 4.2 and (4) 3.14. Relevant parts of an actual simulation are also plotted (solid). The direction of the flow in different sections of the phase plane is illustrated by the larger arrows. Note that the scale of I_1 in (1) is different to allow the full upstroke to be shown. The stable fixed point is shown in (1) and (4) with a cross.

First let us concentrate on the I_1 nullclines (figure 3.4) and describe the four main phases of the action potential (upstroke, overshoot, plateau and repolarisation) using the nullcline structure.

1. From plot (1) it can be seen that as V is perturbed (to the right) from its steady state value, I_1 increases rapidly. This is because in this region of phase space $I_1 > 0$ and $\dot{I}_1 > 0$ and there is effectively a runaway dynamics in I_1. However, $\dot{V} > 0$ and the trajectory also moves to the right and crosses the I_1 nullcline (at a high value of I_1 with $V \approx -3$) and thereafter I_1 decreases. I_1 returns to low values with the voltage reaching a maximum of about 37.

Recall that V changes direction when the currents I_1 and I_2 cross.

2. I_1 continues to decrease until it crosses its nullcline at a value of around 0.3 and starts to increase again.

3. I_1 remains close to its nullcline for a while, slowly increasing (the rate of change of voltage here is small as I_1 and I_2 are close), until it again crosses its nullcline at a value of around 4.2. I_1 therefore begins to decrease signifying the end of the action potential plateau.

4. As I_1 continues to decrease, the nullcline structure changes (due to I_2 also decreasing), and I_1, (after touching I_2 when V changes direction once more) returns to equilibrium.

A similar analysis of the I_2 nullclines (figure 3.5) is outlined below.

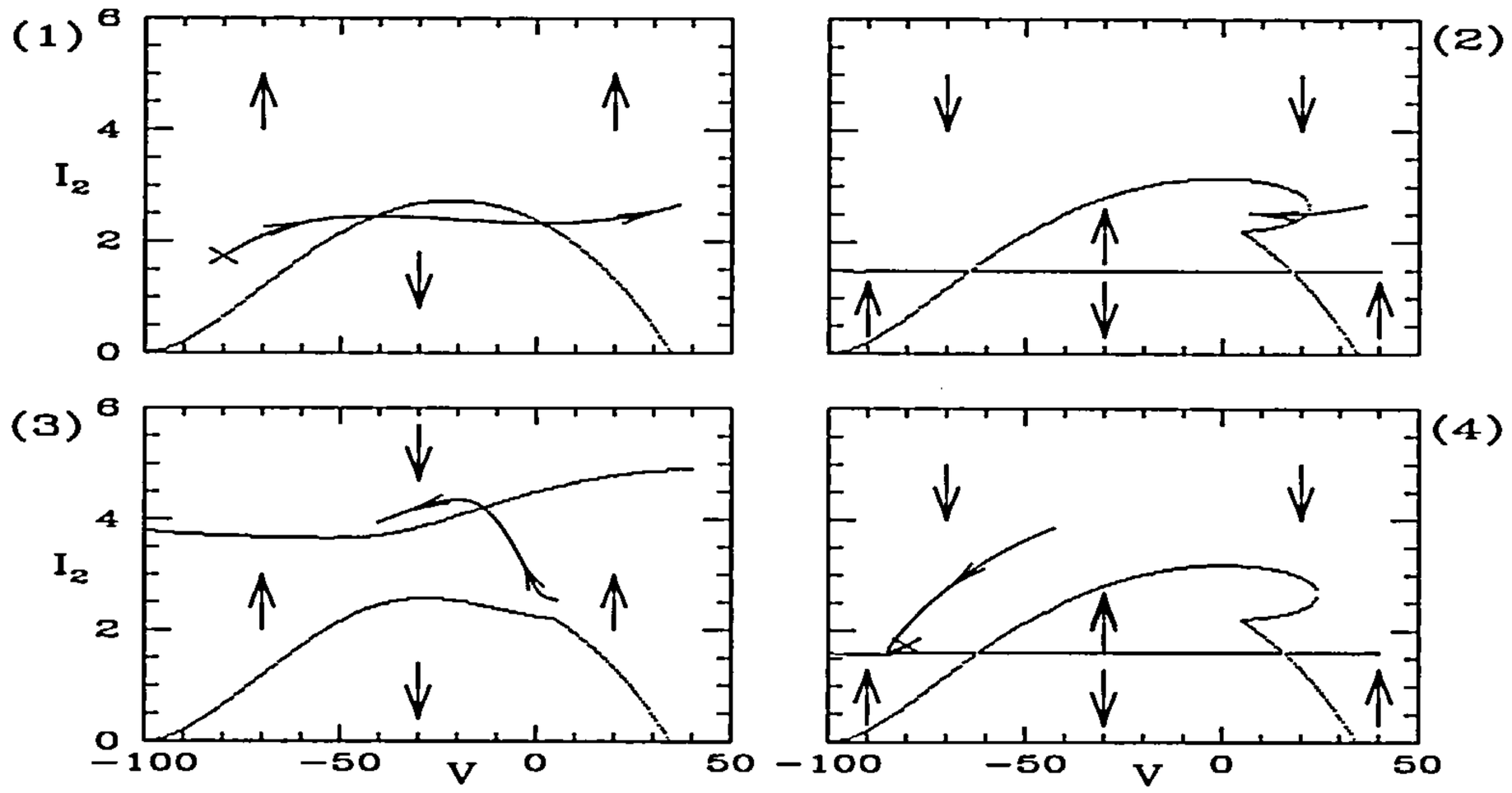

Figure 3.5: Four plots of the I_2 nullcline for the Noble model with I_1 set to (1) 100, (2) 1.5, (3) 3.8 and (4) 1.6. Again the relevant parts of an actual simulation are plotted together with the direction of the flow and the stable fixed point is shown in (1) and (4) with a cross.

1. As V increases rapidly (due to I_1 becoming large) I_2 changes only slightly in size whilst crossing its nullcline twice.

2. As I_1 and I_2 touch (at the highest value of V) the direction of V changes, as does the direction of I_2. Shortly afterwards I_2 crosses its nullcline and begins to increase.

3. I_2 slowly increases (recall that $\dot{V}$ is small here) following its nullcline (which is also increasing) until it catches up and crosses it at a value of around 4.4.

4. I_2 then decreases, once more following its nullcline, until the currents cross, V changes direction, and I_2 slowly increases to its equilibrium value.

There are a few main points to mention here arising from the analysis of the I_1 and I_2 nullcline figures. Looking at figure 3.4 we can see that the I_1 nullcline consists of essentially two components. These cross and, as the coupling varies (with changes in I_2), they split in different ways. In plots (1) and (2) (when $V < 3.14$) they are split so as to allow I_1 to increase rapidly giving the fast upstroke of the action potential. The same nullcline structure allows the I_1 current to cross the nullcline at a high value and return quickly to low values at high voltage. Note also that when I_1 reaches a sufficiently low value it crosses its nullcline again and begins to increase leading to the spike of the action potential. In plot (3) (when $V > 3.14$) the two components of the nullcline are split in the opposite direction. This enables the I_1 trajectory to follow closely that of I_2 giving rise to the plateau. In plot (4) (when $V = 3.14$) the two components cross and their shape can be clearly be seen.

From figure 3.5 we can see that the structure of the I_2 nullclines is different although it also consists of essentially two components. There is a quadratic-like component which gets distorted at low I_1 (as in plots (2) and (4)) and a component of the form $I_2 = I_1$. This second component gets distorted for higher values of I_1 (as in plot (3)) but is usually at roughly the same level as I_1.

The above analysis of how the currents and their nullclines change throughout an action potential gives us an insight into how the action potential occurs from a dynamical systems viewpoint. This study of the nullcline structure of the currents

in the Noble model will enable us to construct polynomial equations that have a similar form and that reproduce accurate voltages and currents.

3.2 Polynomial Model for Currents

We now present a polynomial model that reproduces the Noble dynamics to a very close approximation. The ideas come from the study of the Noble phase plane carried out in the previous section. We shall first present the equations that are used to reproduce the action potentials before explaining in detail how they are constructed.

3.2.1 Model Equations

We consider equations of the same general form as in the Noble model namely,

$$\begin{aligned} \dot{V} &= I_1 - I_2 \\ \dot{I}_1/\epsilon_1 &= f_1(V, I_1)\dot{V} + f_0(V, I_1) \\ \dot{I}_2/\epsilon_2 &= g_1(V, I_2)\dot{V} + g_0(V, I_2) \end{aligned} \tag{3.2}$$

ϵ_1 and ϵ_2 are constants. For our modelling the functions f_i and g_i $(i = 1, 2)$ are polynomials of the following form,

$$\begin{aligned} f_1(V, I_1) &= \alpha \\ f_0(V, I_1) &= -(VI_1 + \delta)(I_1 - h_f(V)) + \alpha(\beta - I_1) \\ g_1(V, I_2) &= I_2 - h_g(V) \\ g_0(V, I_2) &= \gamma(V + \bar{V}) \end{aligned} \tag{3.3}$$

where α, β, γ, δ, $\bar{V}$, are constants, $h_f(V)$ is a quartic polynomial, and $h_g(V)$ is a negative quadratic. I_1 and I_2 here are related to I_1 and I_2 in the previous section. That is, I_1 and I_2 represent the inward and outward currents respectively. Recall that the inward and outward currents in the real system contain not only Na^+ and K^+, as in the Noble model, but also Ca^{2+}, Cl^- etc. The above equations are

constructed from a detailed analysis of the Noble nullclines and shall be discussed further below. From here onwards we shall refer to this model as Model A.

3.2.2 Simulations

By choosing appropriate functions $h_f(V)$ and $h_g(V)$ and parameter values, as shown in table 3.1, we can get a very good match between Model A and the Noble model. A

$\epsilon_1 = 0.00375$	$\alpha = 20$	$\beta = 3.14$	$\delta = 170$	$\epsilon_2 = 0.02$	$\gamma = 0.005$	$\bar{V} = 80$

Table 3.1: Parameter values used for Model A.

comparison between the time series of two models is shown in figure 3.6. (The actual

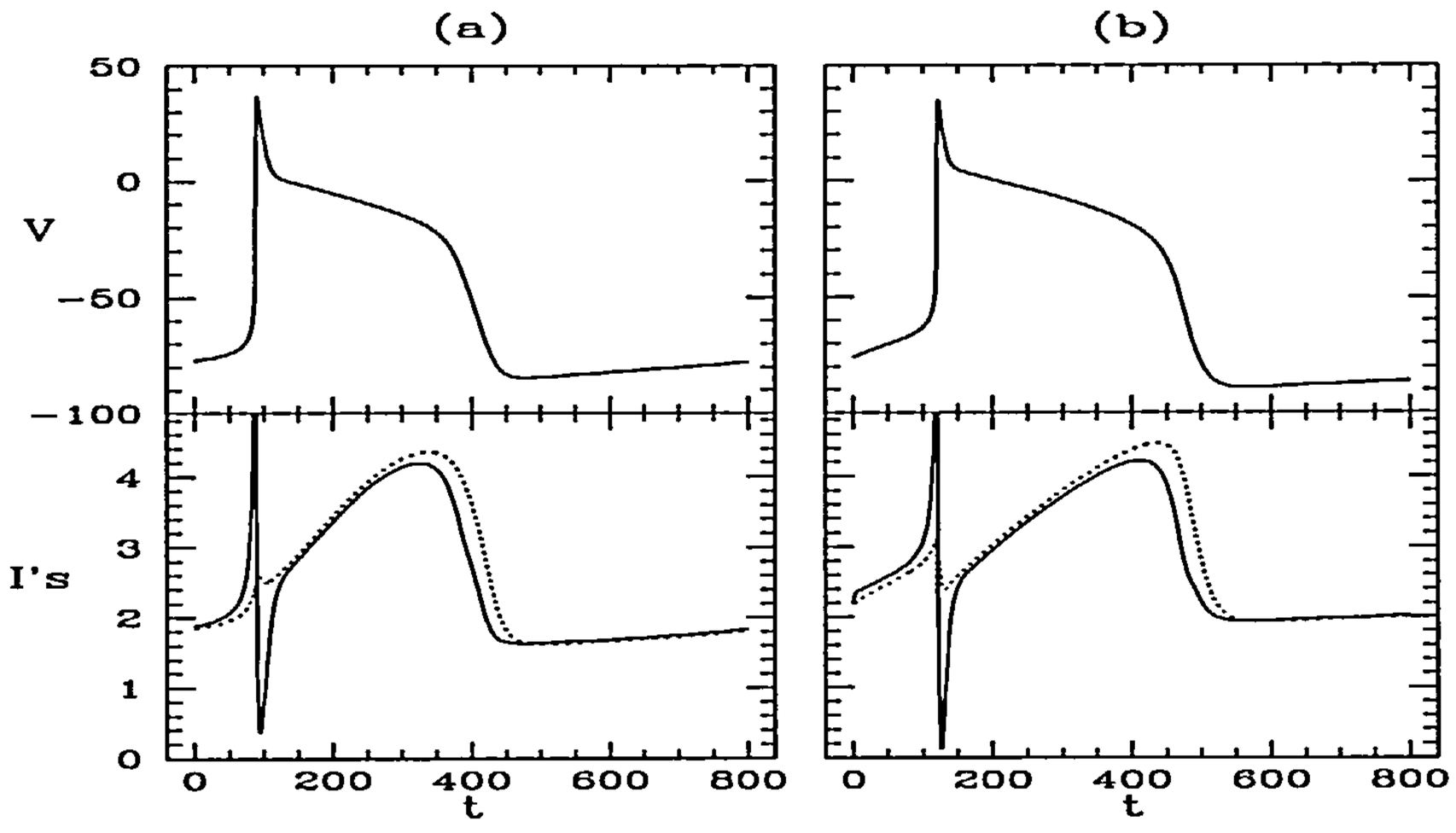

Figure 3.6: Comparison between (a) the Noble model and (b) Model A. The time series of voltage, V, and the inward and outward currents, I_1 (solid) and I_2 (dotted) are plotted. Note that the I_1 currents are truncated and reach a value of about 140 in both plots.

form of the the quartic and quadratic polynomials used is $h_f(V) = 6.8 \times 10^{-7}V^4 + 4.9 \times 10^{-5}V^3 - 1.5 \times 10^{-3}V^2 - 0.12V + 3.0$ and $h_g(V) = -0.0013(V + 20)^2 + 3.8)$.

The close behaviour of both the membrane voltage and the inward and outward currents is clearly illustrated. Model A has a stable steady state at $V = -80$ and $I_1 = I_2 \approx 2.19$, and the excitability threshold is at $V \approx -76.5$. (Recall that in the Noble model the stable steady state is at $V \approx -79.70$ and $I_1 = I_2 \approx 1.68$). There is also an unstable steady state at $V = -80$ and $I_1 = I_2 \approx 5.95$. Upon exciting the system past the threshold an action potential occurs. The action potential has the fast upstroke and the overshoot seen in the Noble model. Here we note that the speed and extent of the upstroke in I_1 may be altered by varying ϵ_1. Parameters have been used here so that the plateau of the action potential is of similar duration to that in the Noble model. Finally, the return to equilibrium is also on a similar time scale to that of the Noble model (and not as fast as the upstroke).

As mentioned above, parameter values are chosen so that the length of the plateau is similar to that in the Noble model. In fact the length of the plateau may be altered by changing the value of the parameter γ. Smaller values of γ lead to action potentials of longer duration whereas larger values of γ lead to action potentials of shorter duration. Two different plateau lengths are shown in figure 3.7.

We now recall that by lowering the value of the parameter $\tilde{g}_{Na}$ from a value of 0.14 to 0.132, the behaviour of the Noble model can be altered from oscillatory to excitable. The parameters used in table 3.1 lead to excitable behaviour Model A. However, if the parameter $\bar{V}$ is decreased then the behaviour can be made oscillatory. The actual equations will undergo a Hopf bifurcation and using the AUTO bifurcation package [50, 51, 52] we can calculate that the value of $\bar{V}$ at the bifurcation is approximately 72.24. Examples of oscillatory waves are shown in figure 3.8.

3.2.3 Phase Portrait Analysis

To explain why the behaviour of Model A is so close to that of Noble it will be useful to compare the phase portraits. The simulated trajectories of the two models are shown in the phase plane in figure 3.9. From these phase portraits the similarity in the behaviour of the inward and outward currents is once again evident.

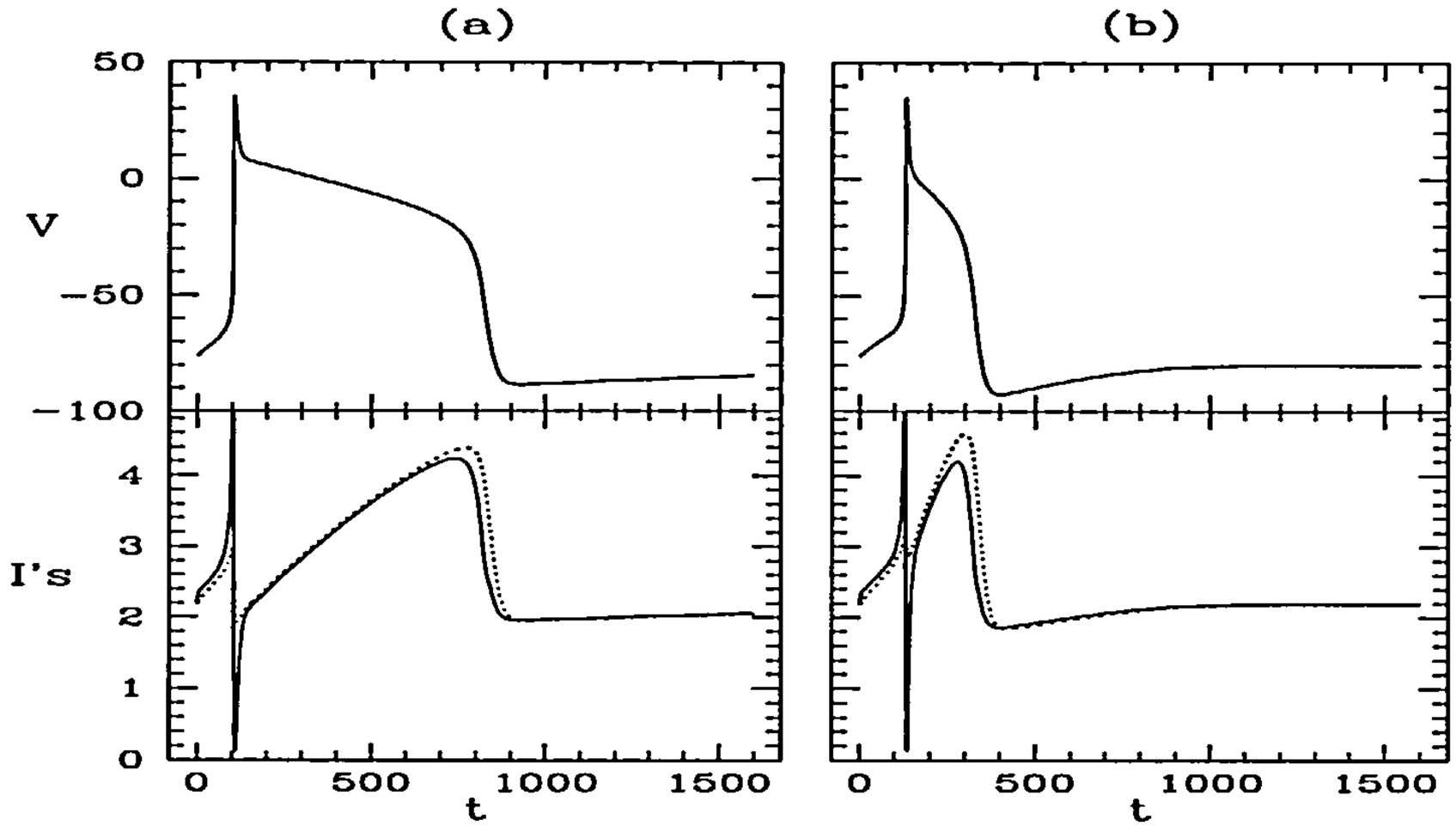

Figure 3.7: Different action potential durations for Model A. The time series of voltage, V, and the inward and outward currents, I_1 (solid) and I_2 (dotted) are plotted in both cases. Note that the time of simulation is double that used previously. (a) $\gamma = 0.0025$ (half its previous value) and the action potential duration is approximately double that in figure 3.6(b). (b) $\gamma = 0.01$ (double its previous value) and the action potential duration is approximately half that in figure 3.6(b). On increasing γ, the equations are not as excitable and ϵ_2 needs to be reduced to 0.018 to ensure excitation.

In a similar way to our analysis of the Noble model in the phase plane we can look at various nullclines that occur for Model A throughout an action potential. For this it will be more convenient to write equations (3.2) and (3.3) in the form (3.4) below.

$$\begin{aligned} \dot{V} &= I_1 - I_2 \\ \dot{I}_1/\epsilon_1 &= -(VI_1 + \delta)(I_1 - h_f(V)) + \alpha(\beta - I_2) \\ \dot{I}_2/\epsilon_2 &= (I_1 - I_2)(I_2 - h_g(V)) + \gamma(V + \bar{V}) \end{aligned} \tag{3.4}$$

Let us look at the equation structure in (3.4) and discuss why it is of the given form.

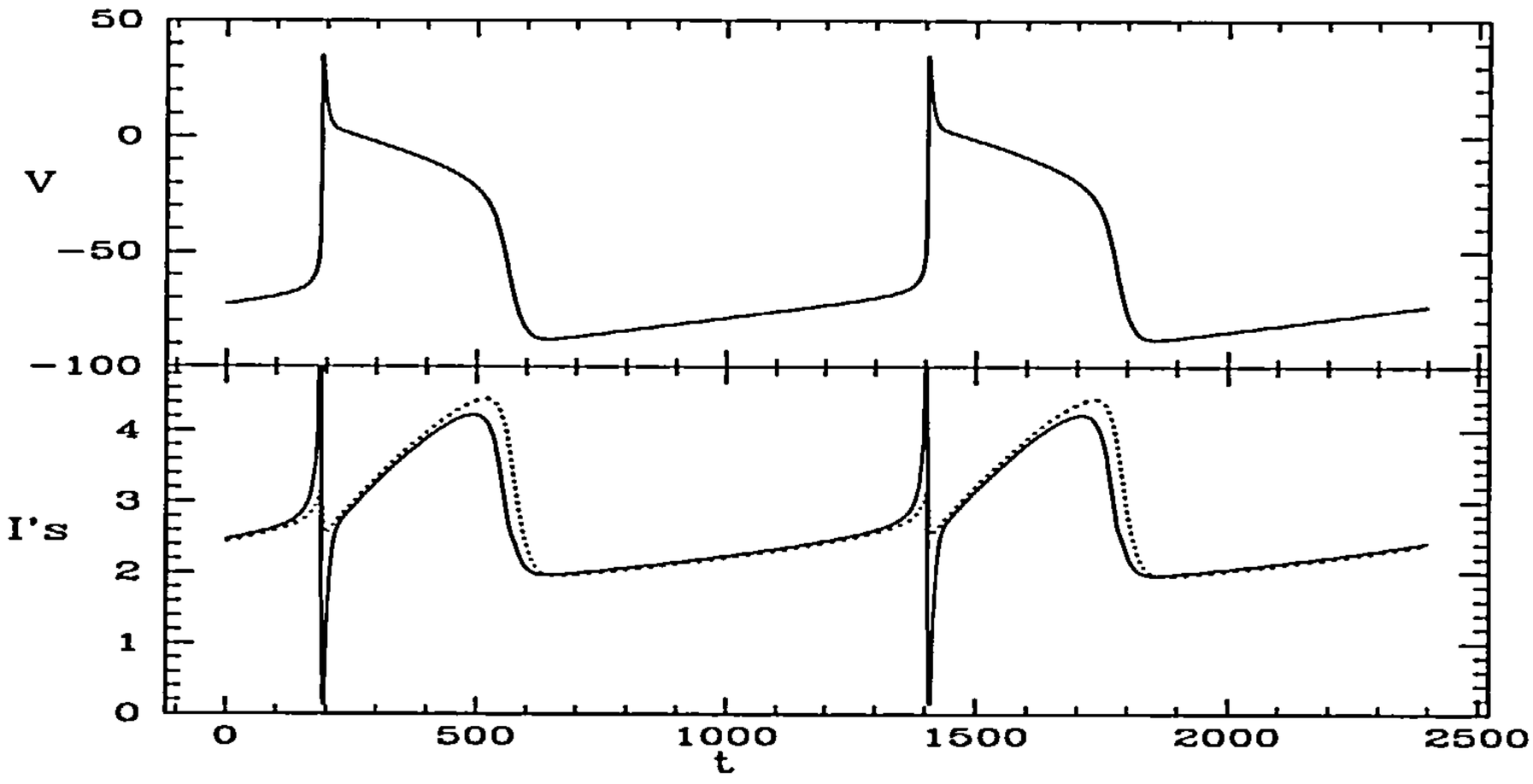

Figure 3.8: Oscillatory simulations for Model A. The time series of voltage, V, and the inward and outward currents, I_1 (solid) and I_2 (dotted) are plotted. These oscillatory waves are obtained by lowering the value of the parameter $\bar{V}$ from its original value of 80 to 72. This moves the stable steady state to $V = -72$ and $I_1 = I_2 \approx 2.49$ where it becomes unstable.

First observe that the $\dot{V}$ equation is kept the same as in the Noble equations. The simple relationship between the rate of change of voltage and the inward and outward currents is something we want to keep.

The $\dot{I}_1$ equation is constructed so that it is a product of two components. One component corresponds to a nullcline of the form $I_1 = -\delta/V$ and the other to a quartic nullcline, $I_1 = h_f(V)$. Added to these is a coupling term which depends on I_2 (as in the Noble model). The parameter β will determine the value of I_2 that causes the two components of the I_1 nullcline to split and will be given the value 3.14 to match the value observed in the Noble model. The parameter α will determine how, and to what extent, the two components of the I_1 nullcline will split.

The $\dot{I}_2$ equation is constructed so that it is a product of terms corresponding to nullclines $I_2 = I_1$ and the quadratic, $I_2 = h_g(V)$. Both these resemble the compo-

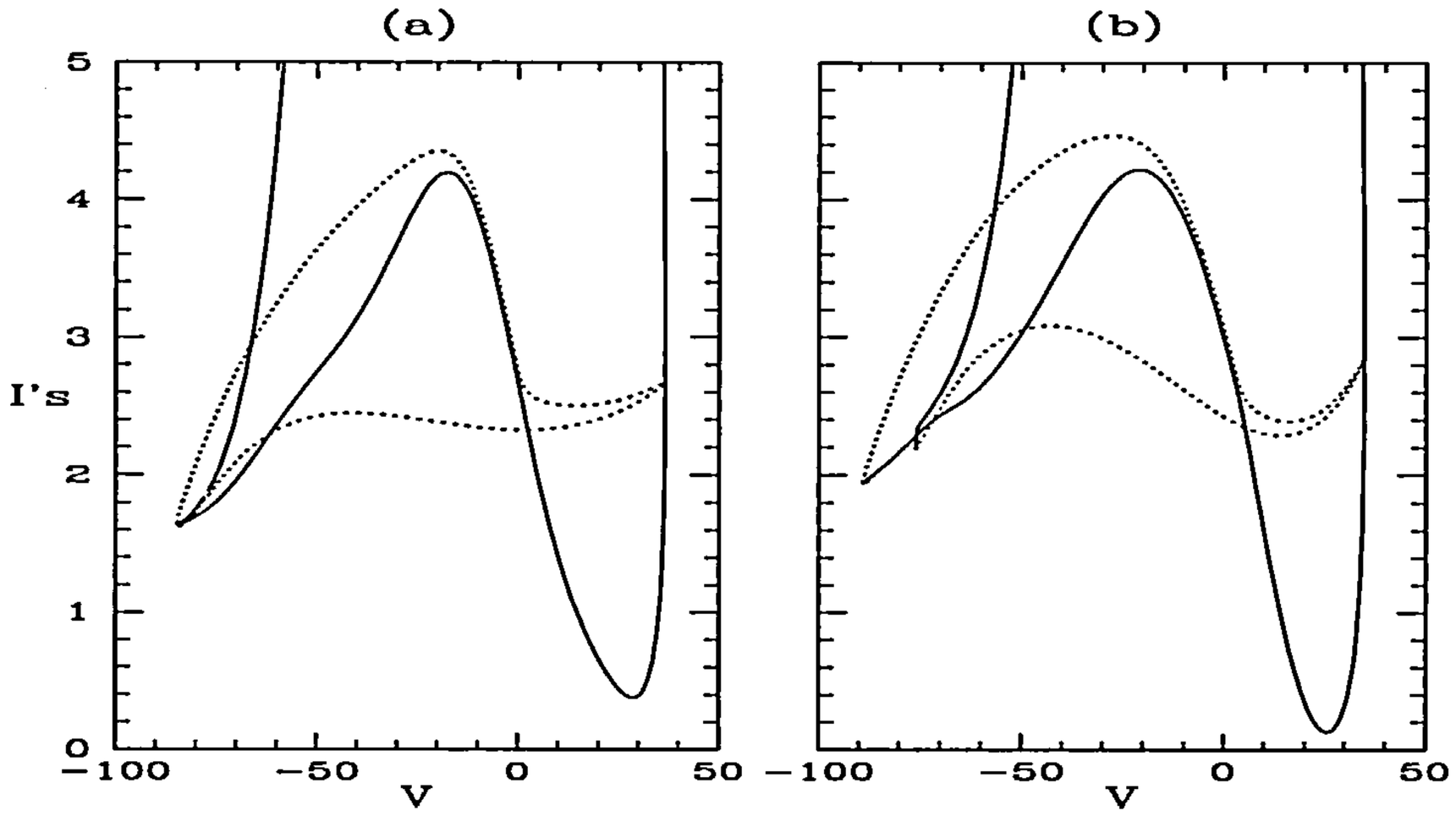

Figure 3.9: Phase portraits for (a) the Noble model and (b) Model A. I_1 (solid) and I_2 (dotted) are both plotted against V.

nents observed in the Noble I_2 nullclines. The coupling term is constructed so that the fixed point can be set at $V = -\bar{V}$. The stable fixed point in the Noble model is at $V \approx -79.70$ and we set $\bar{V} = 80$. The constant γ determines the strength of this coupling.

To help illustrate the behaviour of the nullclines resulting from the above equations some nullclines are plotted in figure 3.10.

It can be seen from plot (2) that when $I_2 = 3.14$ the two components of the I_1 nullclines cross. Recall that this was observed in the Noble model nullclines in the previous section (figure 3.4, plot (4)). From equations (3.4) it can be seen that this occurs as the parameter β is set to 3.14. The sign of α is chosen so that when $I_2 < \beta$ we will get a phase plane structure as in (1) allowing for the fast upstroke and spike, and if $I_2 > \beta$ we will get a phase plane structure similar to that in (3) allowing the plateau to be formed. The size of α ensures that the fixed point is stable at $V = -\bar{V} = -80$. From plots (4), (5) and (6) we can see the simple form of the I_2 nullclines. Both the quadratic component, the horizontal line at the level I_1, and

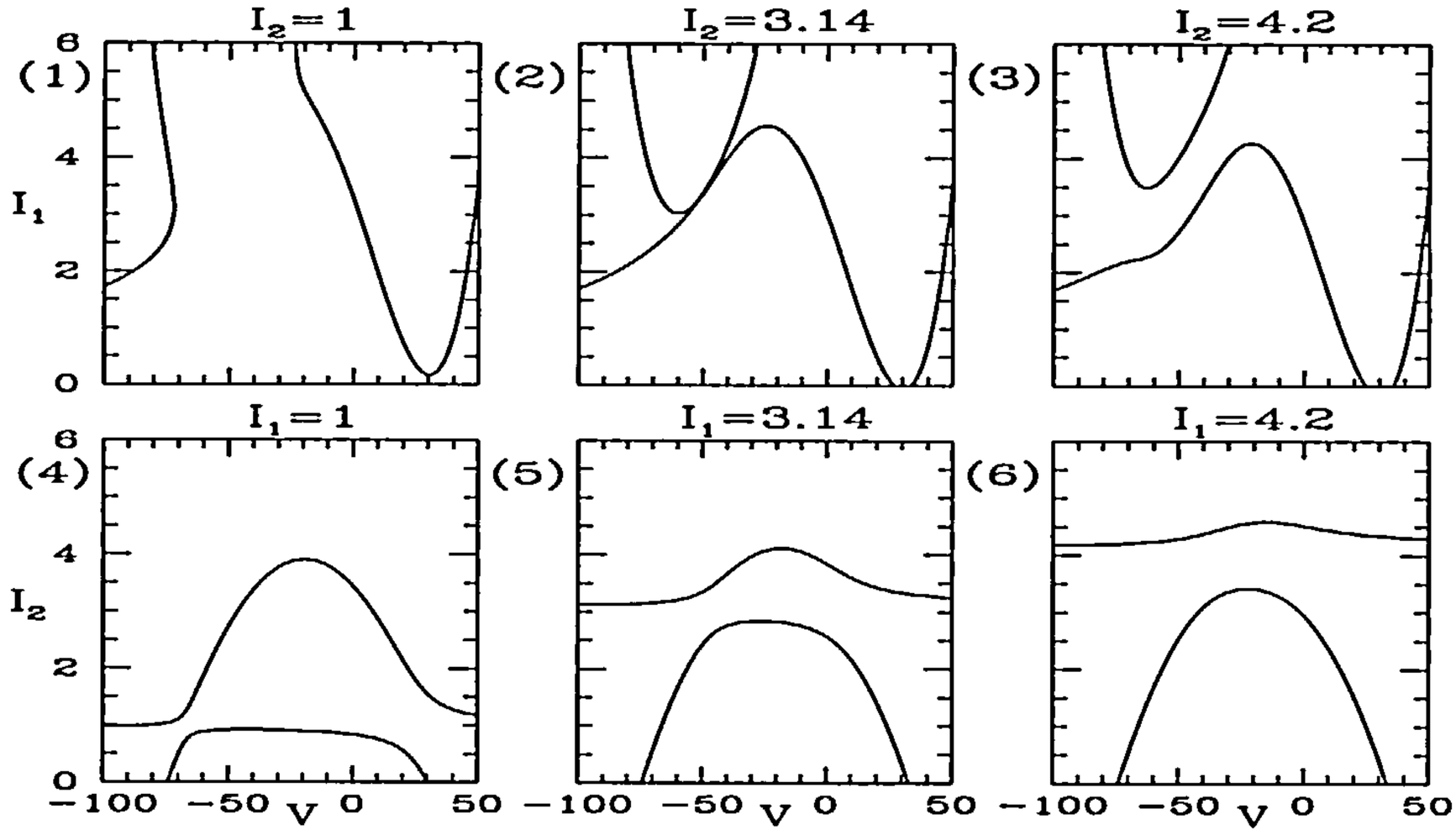

Figure 3.10: Example nullclines for Model A. Three I_1 nullclines are plotted for different values of I_2 ((1), (2) and (3)), and also three I_2 nullclines for different values of I_1 ((4), (5) and (6)).

the distortion due to the coupling term can clearly be seen.

We shall now plot relevant nullcline structures together with the appropriate simulation data for Model A and discuss how they change throughout an action potential. This is done for the I_1 nullclines in figure 3.11 and for the I_2 nullclines in figure 3.12.

It can be seen from figure 3.11 that the nullcline structures and dynamics of I_1 are extremely similar to those of Noble (figure 3.4). As V is increased slightly from its equilibrium value, the nullcline structure causes I_1 to increase rapidly (plot (1)). I_2 remains relatively constant throughout the upstroke so the I_1 nullcline structure does not change substantially. I_1 crosses its nullcline at a high value of I_1 and begins to fall again at higher values of V. I_1 and I_2 touch at the highest value of V and $\dot{V}$ changes sign causing V to start decreasing. I_1 continues to fall until, at a value close to 0, it crosses its nullcline again and begins to increase (plot (2)). As I_1 increases, following its nullcline, I_2 is also increasing. This causes the nullcline structure to

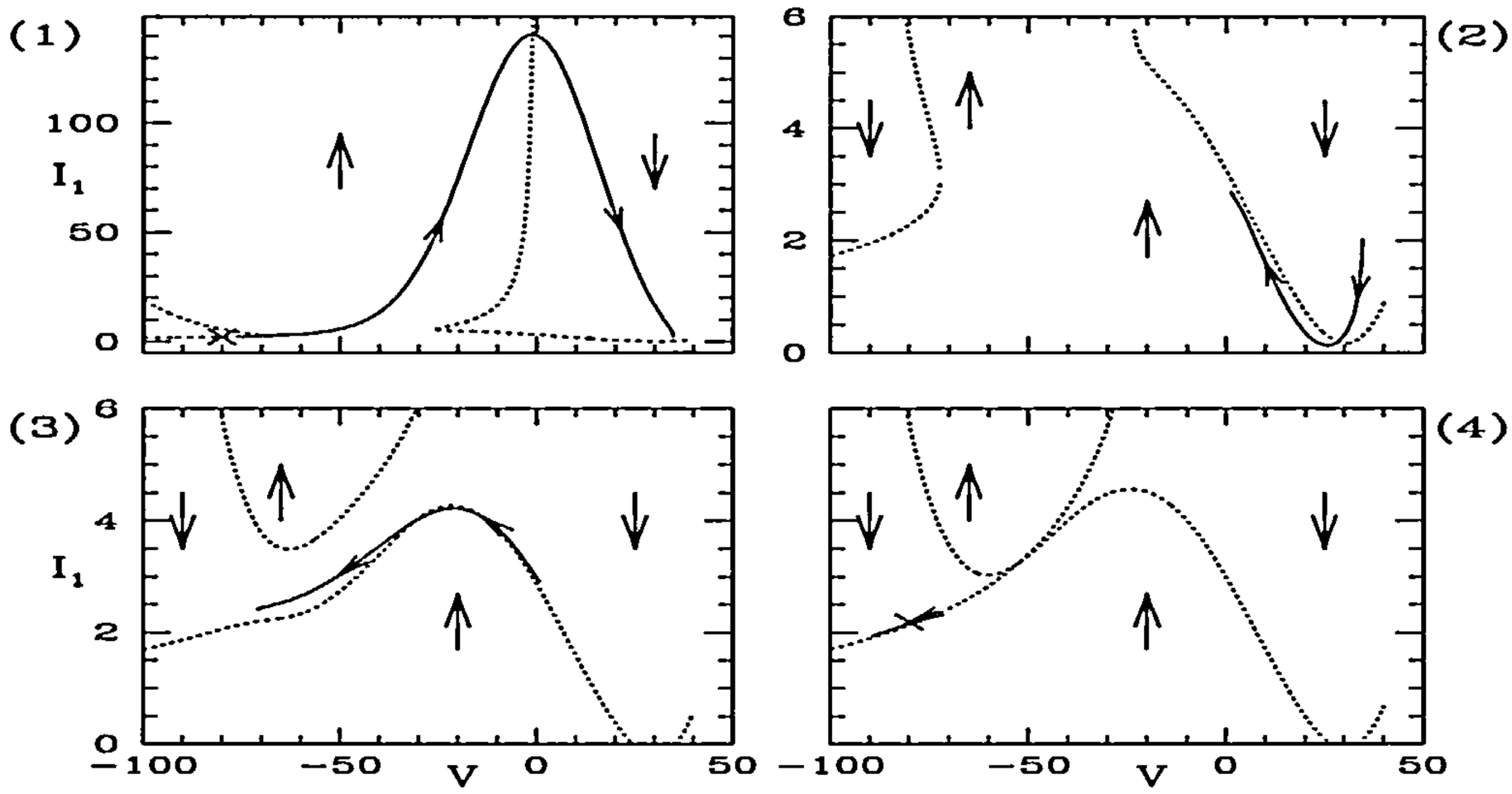

Figure 3.11: Four plots of the I_1 nullcline (dotted) for Model A with I_2 set to (1) 1.7, (2) 1.0, (3) 4.2 and (4) 3.14. Relevant parts of an actual simulation are also plotted (solid). The direction of the flow in different sections of the phase plane are illustrated by the larger arrows. Note that the scale of I_1 in (1) is different to allow the full upstroke to be shown. The stable fixed point is shown in (1) and (4) with a cross.

change (gradually and via the structure in (4)) to that shown in plot (3). As I_1 reaches a value close to 4, it crosses its nullcline and begins to decrease. I_2 is also decreasing here causing the nullcline structure to change first to that in (4) and eventually back to (1). In the meanwhile I_1 continues to decrease, touches I_2 where V changes direction, and increases slowly to its equilibrium value.

The I_2 nullcline structures (figure 3.12) can also be seen to be extremely close to those of the Noble model (figure 3.5). During the upstroke, when V increases rapidly, I_1 is large giving the nullcline structure shown in plot (1). I_2 remains relatively constant during the upstroke changing just slightly as it crosses the two branches of the the parabola component of the nullcline. After I_1 and I_2 touch at high V, and I_1 becomes small we get a nullcline structure as shown in (2). I_2 decreases, crosses its

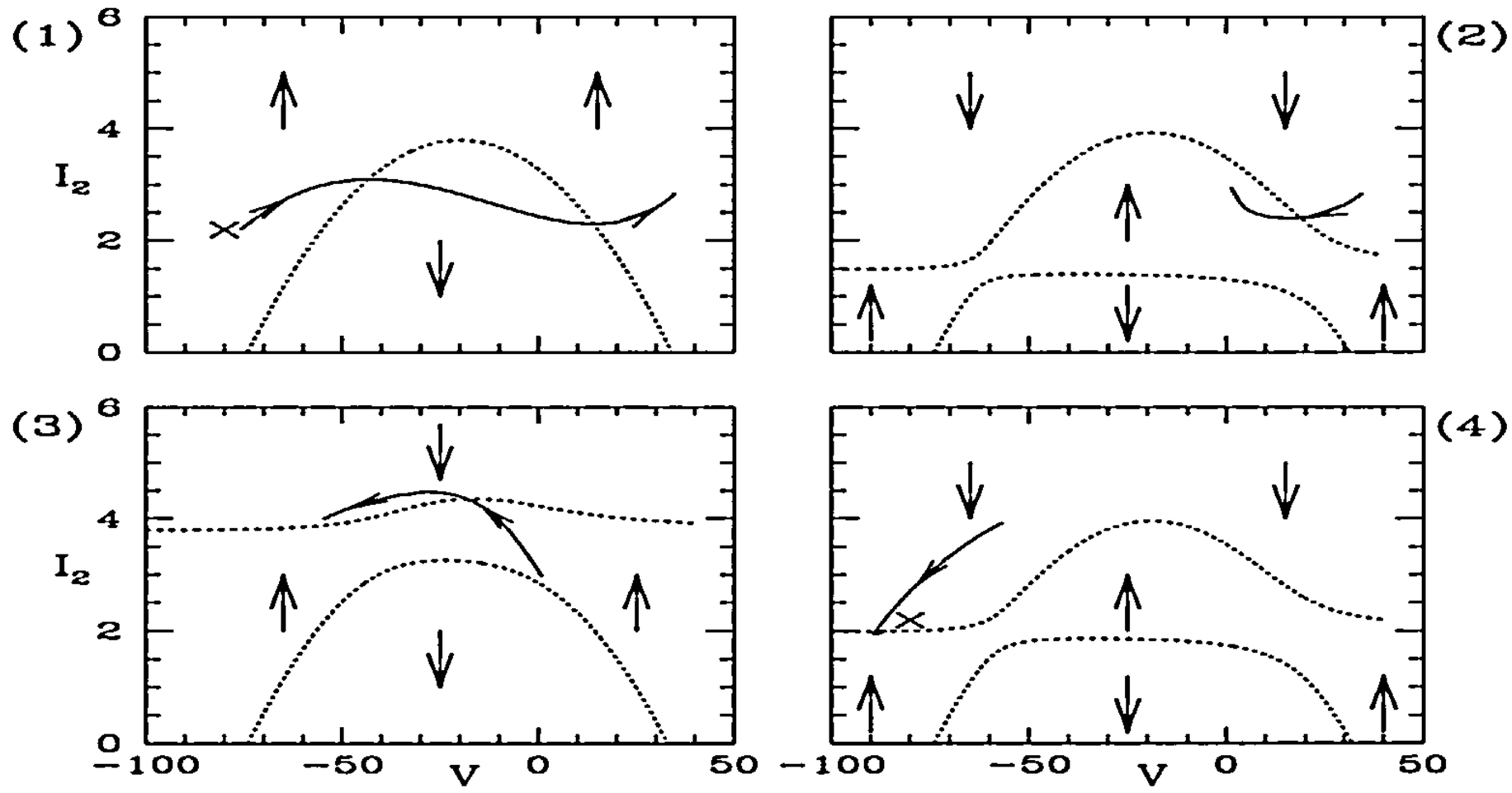

Figure 3.12: Four plots of the I_2 nullcline (dotted) for Model A with I_1 set to (1) 100, (2) 1.5, (3) 3.8 and (4) 1.6. Again the relevant parts of an actual simulation are plotted together with the direction of the flow and the stable fixed point is shown in (1) and (4) with a cross.

nullcline and begins to increase. I_1 is also increasing here so the nullcline structure changes to that in (3). I_2 continues to increase until it crosses the upper branch of the nullcline. I_1 is now decreasing resulting in a nullcline structure similar to that in (4). I_2 therefore decreases, changes direction as I_1 and I_2 touch at low V, and increases slowly to its equilibrium value.

3.3 Final Comments

In this chapter, following an analysis of the Noble model in the phase plane, we have constructed a polynomial model with three variables that gives action potentials matching very closely those of the Noble model.

Rather than analysing Model A in greater detail we can consider the same approach

using more simple equations. We do this in the following chapter.

Chapter 4

Simple Models

In the previous chapter we saw that a polynomial model can be constructed (Model A) that exhibits dynamics very similar to those of the Noble model. The general form of the equations is the same, the phase plane structure is similar, and the action potentials and currents generated resemble closely those obtained from simulations of the Noble model.

The behaviour of Model A can be captured more simply if we do not insist on quantitative results. We can use polynomial equations of a simpler form, but based on similar ideas, to obtain models that will give rise to action potentials and currents with the same underlying dynamics.

Recall that the model has the following important properties. The three variables correspond directly to physiologically relevant variables; membrane potential, inward current and outward current. Different ionic species are not distinguished and we are only concerned with the overall inward and outward currents. Also, the differential equations are expressed in terms of polynomial functions and on varying these we can change the behaviour of the two currents. This will enable us to obtain different types of action potentials.

In this chapter we shall carry out a study of simple polynomial models based on ideas introduced in the previous chapter. Later in the chapter we shall investigate models with the same form as Model A. However we shall first introduce two very

basic models which incorporate the fundamental ideas of our approach.

4.1 Simple Oscillator

The behaviour of Model A can be illustrated more clearly by considering the following simple oscillator.

$$\begin{aligned} \dot{V} &= I_1 - I_2 \\ \dot{I}_1 &= -I_1(1 + VI_1) - I_2 \\ \dot{I}_2/\epsilon &= (I_1 - I_2) + V + 2 \end{aligned} \tag{4.1}$$

Due to the simplicity of the equations, the important mechanisms behind the dynamics are more evident than in complicated models. Before presenting the results of a simulation let us highlight the key aspects of these equations.

- We keep the simple yet physiologically meaningful form of the $\dot{V}$ equation. When the currents cross, $\dot{V}$ changes sign, and when the difference of currents is large, so is $\dot{V}$.

- The $\dot{I}_1$ equation is the product of two terms plus a coupling term $-I_2$. Without coupling the I_1 nullclines are the constant $I_1 = 0$ and the hyperbola $I_1 = -1/V$. The leading term $-VI_1^2$ gives rise to the fast runaway of I_1 causing the sharp upstroke. The I_2 coupling means that the I_1 nullclines change qualitatively when I_2 changes sign.

- The $\dot{I}_2$ equation is as simple as possible whilst ensuring oscillations in the model. Almost any negative feedback form ($I_2 \approx -I_2$) is sufficient together with some dependence on I_1 and V. We keep the term $I_1 - I_2$ of the models in Chapter 3 and include linear coupling in V. The constant 2 is chosen to give oscillatory behaviour with not too sharp an upstroke.

Figure 4.1 shows a simulation of the above simple oscillator with ϵ set to the value of 0.25. From figure 4.1(a) we can see that we get oscillatory action potentials with

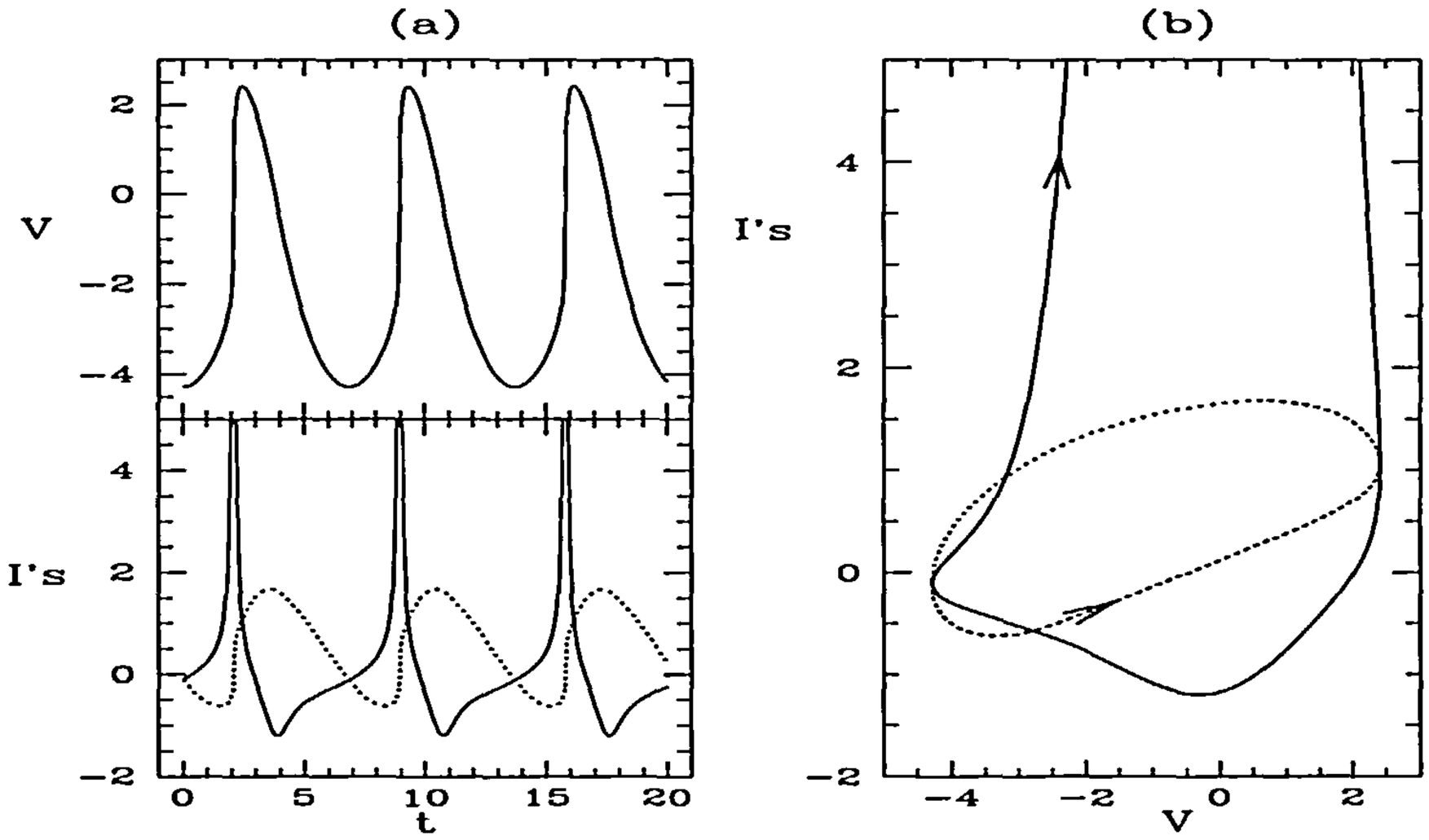

Figure 4.1: Simulation of the simple oscillator with $\epsilon = 0.25$. (a) The time series of V, I_1 (solid) and I_2 (dotted). (b) The phase plane. I_1 is truncated and reaches a value of around 57.

a relatively fast upstroke. The fast upstroke in V results from the fast increase in I_1 as can be seen from 4.1(b). Following this fast increase, I_1 begins to decrease at a high value (approximately 57) and falls to low levels. In the meanwhile, I_2 initially decreases, before increasing throughout the remainder of the upstroke. At a voltage of approximately 2.4 the currents cross resulting in the change of direction of voltage. I_1 continues to decrease until $V \approx -0.5$, when it increases again. I_2 on the other hand increases for the initial part of repolarisation before decreasing as the voltage becomes more negative. Note that I_1 and I_2 are closer in value during repolarisation than during the upstroke and thus repolarisation is slower in comparison. At a value of $V \approx -4.3$ the currents cross for a second time and the voltage begins to increase. An action potential is then complete and the next one begins.

The dynamics of the currents can be explained in more detail by looking at the nullcline structure of the equations. Let us first consider the I_1 nullcline. Example nullclines, for various values of I_2, are shown in figure 4.2. When $I_2 = 0$ (as in (a)) we

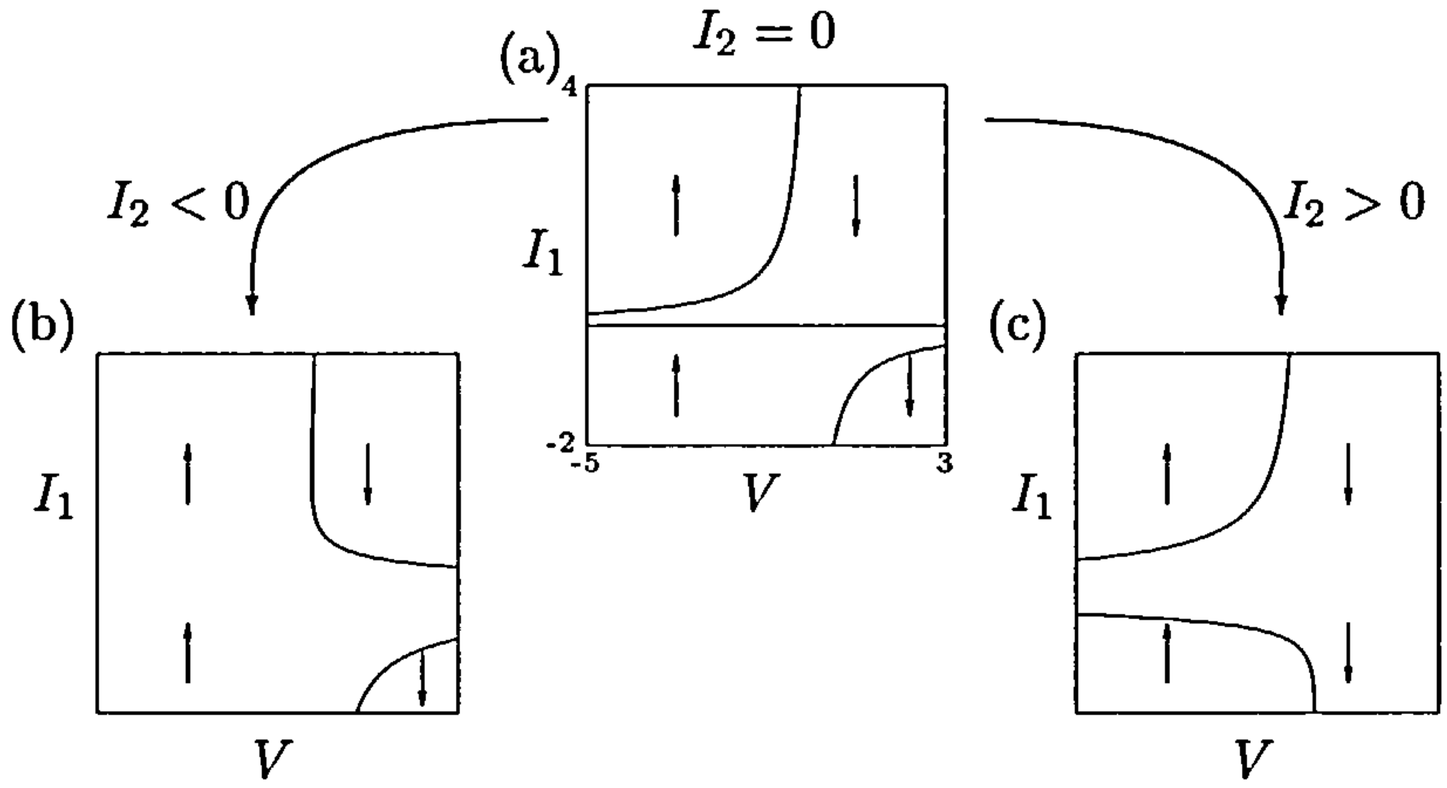

Figure 4.2: I_1 nullclines for the simple oscillator. The arrows indicate the direction of the flow.

are able to see the two main components of the I_1 nullclines; the component $I_1 = 0$ and the component $I_1 = -1/V$. When $I_2 < 0$, as in (b), the nullcline structure allows for the fast increase in I_1. Both I_1 and $\dot{I}_1$ (with leading term $-VI_1^2$) are greater than zero and we have the runaway behaviour in I_1 that in turn causes $I_1 - I_2$ and hence $\dot{V}$ to become large and cause the fast upstroke. Since $\dot{V}$ is also positive, V is increasing and I_1 will cross the central branch of its (hyperbola) nullcline at high values. I_1 then falls quickly throughout the second half of the upstroke. This is the essence of the voltage upstroke and fast inward current in all electrophysiological models.

To understand the remainder of the cycle, corresponding roughly to recovery in electrophysiological models, note that around midway through the upstroke (at $V \approx -0.5$), I_2 becomes positive and hence the nullcline structure of I_1 changes to that shown in (c). This nullcline structure remains throughout the remainder of the cycle. I_1 therefore continues to decrease throughout the initial part of repolarisation. Since $\dot{V}$ is now negative, I_1 will cross its nullcline at low values and begin to increase around midway through repolarisation. I_2 is decreasing at this point and when $V \approx -4.3$ the two currents touch for the second time. The direction of the rate of change of V then changes again and the voltage begins to increase. Shortly afterwards I_2 becomes negative again and the I_1 nullcline changes back to that shown in plot (b).

A new action potential begins.

The behaviour of the I_2 nullcline for the simple oscillator is straightforward. From equations (4.1) above we know that the I_2 nullcline is linear and is given by

$$I_2 = V + I_1 + 2$$

An example I_2 nullcline (for $I_1 = 0$) is shown in figure 4.3. As I_1 changes throughout

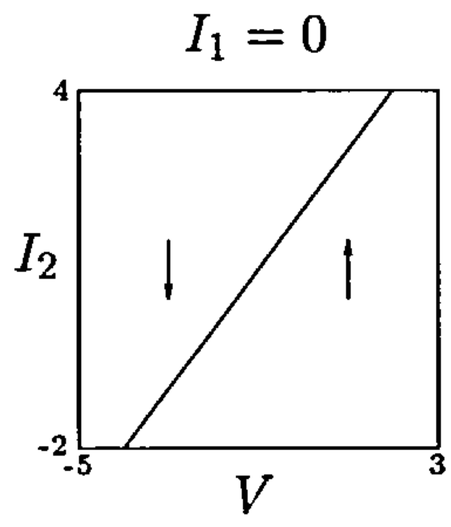

Figure 4.3: I_2 nullcline for the simple oscillator. Arrows indicating the direction of the flow are again drawn. Note that as I_1 varies the linear line will move up (positive I_1) and down (negative I_1).

an action potential, I_2 is above the nullcline and decreasing. During the upstroke V and I_1 increase quickly so I_2 crosses its nullcline and begins to increase. Note that I_1 is large during this period so the linear nullcline shown in figure 4.3 will be raised. Following the upstroke I_1 falls to low values and after the change in direction of V, when I_1 becomes negative, the I_2 nullcline becomes lower. I_2 continues to increase (with $\dot{V}$ negative) until it crosses its nullcline (at $V \approx 0.6$) and decreases throughout the remainder of repolarisation. The two currents cross for the second time at $V \approx -4.3$ where $\dot{V}$ becomes positive again and the action potential is completed.

This simple oscillator illustrates well two of the fundamental properties of our model. First, the dependence of $\dot{V}$ on $I_1 - I_2$. This causes V to increase rapidly throughout the upstroke (due to the large values of I_1) and ensures that the voltage changes direction when the inward and outward currents cross. Recall that this happens once at both high and low voltage for each action potential. The second important property is that there is a leading term of $-VI_1^2$ in the $\dot{I}_1$ equation, resulting from

the hyperbola component $I_1 = -1/V$. Therefore we get the runaway dynamics in I_1 causing the fast upstroke ($I_1 > 0$, $\dot{I}_1 > 0$).

Note that many of the aspects of Model A in the previous chapter (such as the excitability characteristic of voltage and the plateau) are not seen in this simple oscillator. Furthermore, the location and stability of the fixed points are different.

In the following section we shall modify the above oscillator to incorporate some further ideas from our analysis in Chapter 3.

4.2 Modified Simple Oscillator

We shall now alter the form of the $\dot{I}_2$ equation for the simple oscillator to include a second component in the nullclines. Recall that in Model A the $\dot{I}_2$ equation was of the form

$$\dot{I}_2/\epsilon_2 = (I_1 - I_2)(I_2 - h_g(V)) + \gamma(V + \bar{V})$$

where $h_g(V)$ is a polynomial function of V. Note that there is a term of the form $(I_2 - h_g(V))$ multiplying the component $(I_1 - I_2)$. We shall include a similar term in our simple oscillator giving the equations

$$\begin{aligned} \dot{V} &= I_1 - I_2 \\ \dot{I}_1 &= -I_1(1 + VI_1) - I_2 \\ \dot{I}_2/\epsilon &= (I_1 - I_2)(I_2 - V) + V + 3 \end{aligned} \tag{4.2}$$

The $\dot{V}$ and $\dot{I}_1$ equations are unaltered from the previous section. In this simple oscillator model $h_g(V) = V$ is used. The form of the coupling in the I_2 equation has been kept the same as in the previous section with a slight alteration in the constant term ($\gamma = 1$ and $\bar{V} = 3$ rather than $\bar{V} = 2$).

A simulation of the above oscillator is shown in figure 4.4 with ϵ set to the value of 0.09. The observed action potentials are again oscillatory and have a similar shape to those in the previous section. The slight differences are that the wavelength

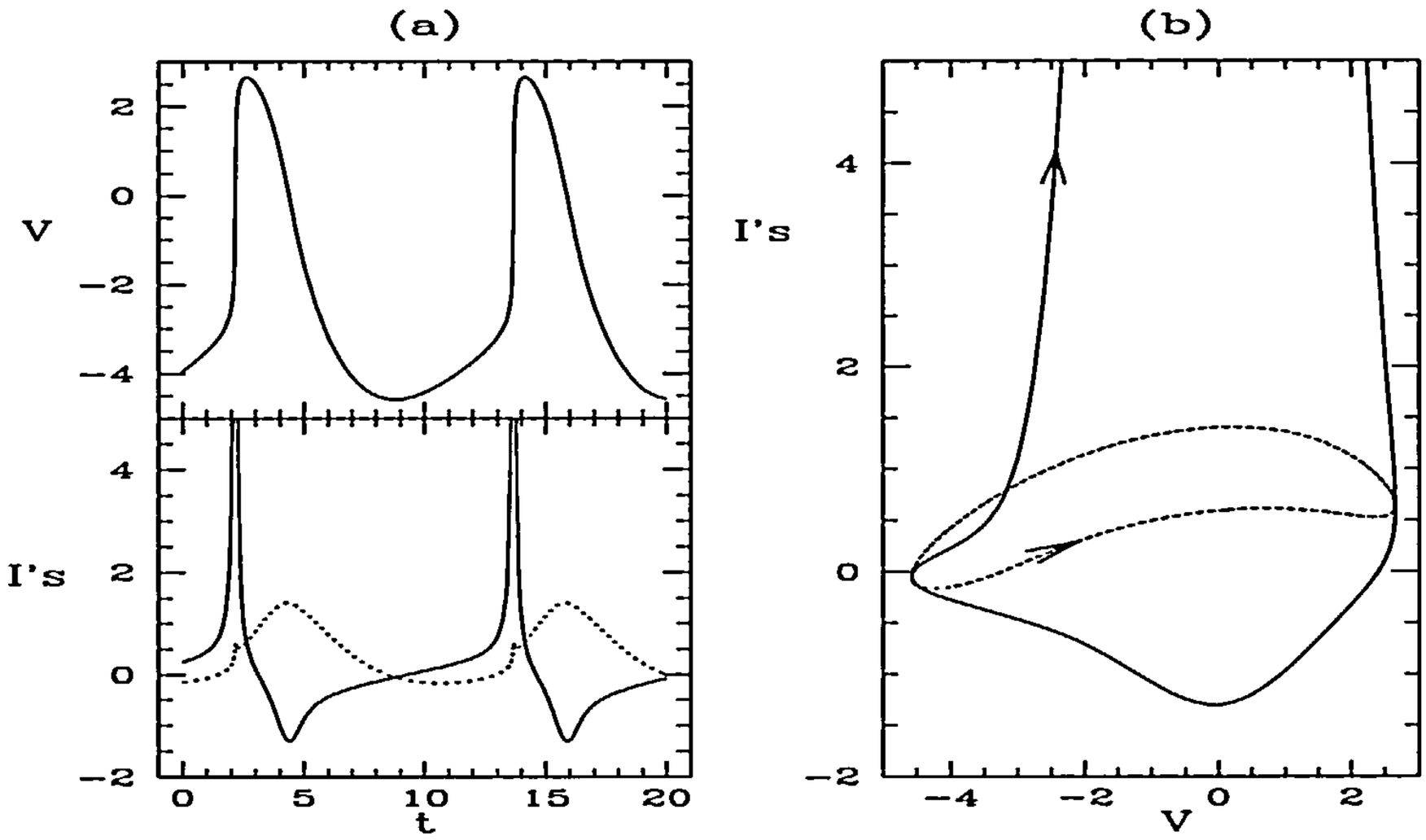

Figure 4.4: Simulation of the modified simple oscillator with $\epsilon = 0.09$. (a) The time series of V, I_1 (solid) and I_2 (dotted). (b) The phase plane. I_1 is again truncated and reaches a value of around 75.

of the action potentials is slightly longer and the upstroke is sharper. (I_1 reaches higher values). From figure 4.4(b) we can see that the phase plane behaviour of the current I_1 is essentially the same due to the $\dot{I}_1$ equation remaining unaltered. There is however a change in the behaviour of I_2. During the upstroke $\dot{I}_2$ becomes positive almost immediately and towards the end of the upstroke it begins to decrease. A difference to the previous oscillator is that as the currents touch at high V, and the voltage changes direction, I_2 also changes direction and begins to increase again. Midway through repolarisation I_2 starts to decrease and continues decreasing until the voltage reaches its minimum value. Here the currents again touch, the voltage changes direction and the I_2 current begins to increase again.

This slight difference in the dynamical behaviour of the I_2 can be explained from the nullclines. Example nullclines for I_2 are shown in figure 4.5. Note that the dependence of the nullclines on I_1 is relatively simple. In general, as I_1 increases, the I_2 nullclines are raised, and as I_1 decreases, the nullclines are lowered.

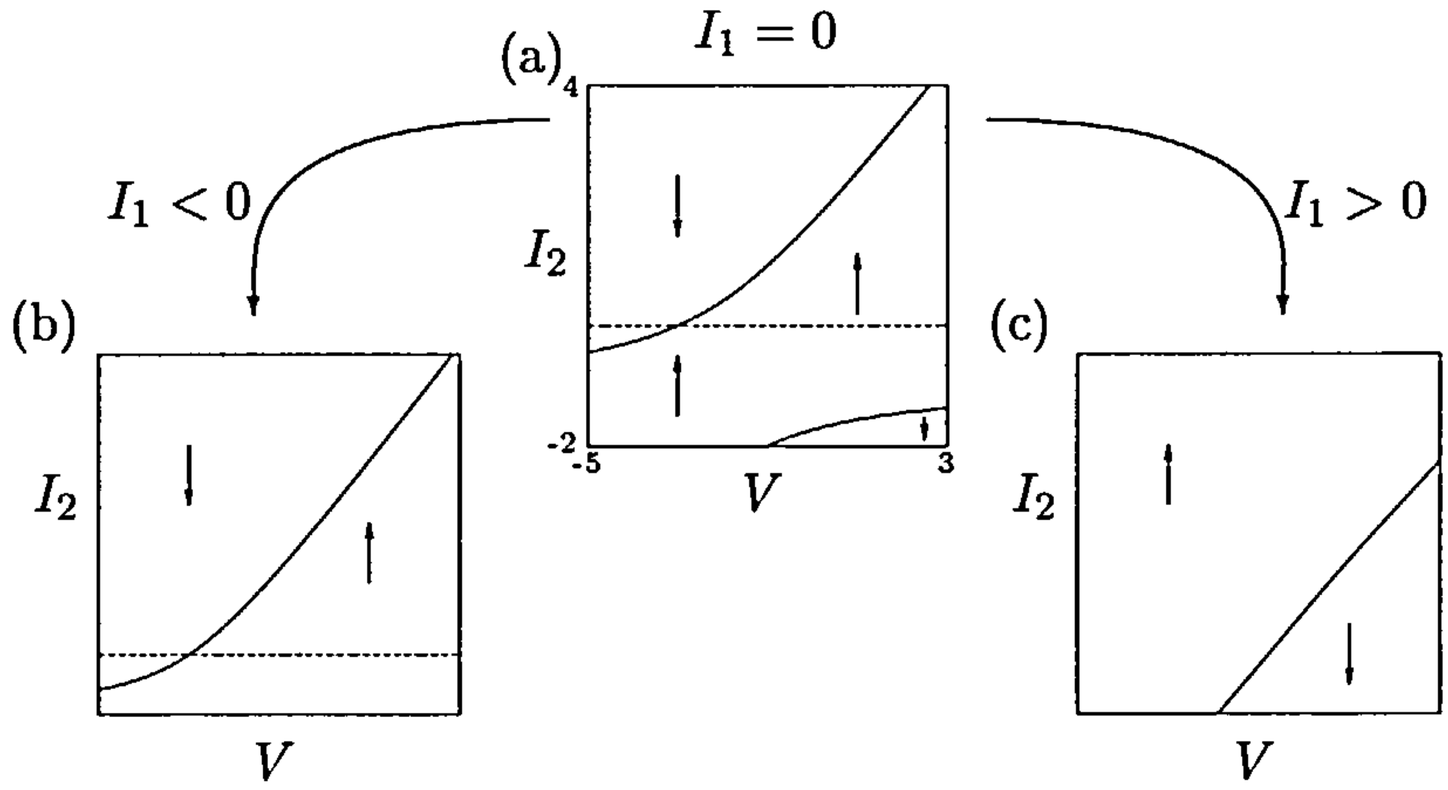

Figure 4.5: I_2 nullcline for the modified simple oscillator. Arrows indicating the direction of the flow are again drawn. The dashed line in (a) and (b) is the level $I_2 = I_1$ (0 and -1 respectively). $I_1 = 10$ in (c) so no dashed line is visible.

During the upstroke, when I_1 is large, the I_2 nullcline structure will be as in (c). Therefore I_2 will increase until it crosses its nullcline towards the end of the upstroke and begins to decrease. I_1 falls at the end of the upstroke and the I_2 nullcline will fall correspondingly. When I_1 reaches a value of $I_1 \approx 0.6$, the currents touch and V changes direction. The I_2 nullcline is then similar to that in (a) but with the level of the dashed line $I_2 = I_1$ at around 0.6. I_2 therefore begins to increase again. I_1 is at low values throughout repolarisation so the I_2 nullcline structure will be as in (b). I_2 increases until V reaches a value of around 0.2 at which I_2 crosses its nullcline and begins to decrease. This continues throughout repolarisation until the currents touch again at a value of approximately -0.05. The I_2 nullcline structure is again similar to (a) and as the voltage begins to increase, I_2 decreases for a short time before crossing its nullcline. I_2 then begins to increase again as another action potential is initiated.

Due to the additional component in the $\dot{I}_2$ equation, I_2 changes direction more than twice during the course of each action potential. When the currents cross and $(I_1 - I_2)$ changes sign the effect is seen not only in the $\dot{V}$ equation (with V changing direction) but also in the $\dot{I}_2$ equation. For example, as I_1 falls towards the end of an action potential, the I_2 nullclines are also falling (from a nullcline similar to that

in figure 4.5(c) to one similar to (b)). Therefore as the voltage changes direction, I_2 crosses its (falling) nullcline and also changes direction. A similar situation occurs as the I_2 nullclines are raised (as I_1 increases) when the currents cross at the minimum value of V.

4.3 General Modelling Approach

Having investigated the principal ideas of our approach using the above simple oscillators we shall now consider a general modelling approach based on the ideas laid out thus far in this and the previous chapter.

4.3.1 Equation Structure

The form of the equations that we shall consider is

$$\begin{aligned} \dot{V} &= I_1 - I_2 \\ \dot{I}_1/\epsilon_1 &= f_1(V, I_1)\dot{V} + f_0(V, I_1) \\ \dot{I}_2/\epsilon_2 &= g_1(V, I_2)\dot{V} + g_0(V, I_2) \end{aligned}$$

V is the voltage, I_1 represents the inward current and I_2 the outward current. As in the previous chapter, it will be more convenient from the viewpoint of mathematical analysis to rewrite the above equations in the form

$$\begin{aligned} \dot{V} &= I_1 - I_2 \\ \dot{I}_1/\epsilon_1 &= -(VI_1 + \delta)(I_1 - h_f(V)) + \alpha(\beta - I_2) \\ \dot{I}_2/\epsilon_2 &= (I_1 - I_2)(I_2 - h_g(V)) + \gamma(V + \bar{V}) \end{aligned} \tag{4.3}$$

We may calculate the location of the fixed points for equations (4.3). These are given by

$$\begin{aligned} V &= -\bar{V} \\ I_1 = I_2 &= \frac{1}{2\bar{V}}\left(K \pm \sqrt{K^2 - 4\bar{V}(\alpha\beta + \delta h_f(-\bar{V}))}\right) \end{aligned} \tag{4.4}$$

where $K = \bar{V}h_f(-\bar{V}) + \delta + \alpha$ and $\bar{V} \neq 0$. There are two fixed points, both at $V = -\bar{V}$, but with different values of I_1 and I_2. Also note that, depending on the values of the parameters, we may get complex values for I_1 and I_2.

4.3.2 Essential Ideas

The essential ideas behind the above choice of polynomial model have already briefly been mentioned. However before proceeding with our study of the models we shall re-iterate the main points.

1. The $\dot{V}$ equation has the simple and physically meaningful form of the difference between the two currents I_1 and I_2. Thus if one of the currents is substantially larger than the other then the voltage V changes at a corresponding high rate. Similarly, if the size of the two currents is comparable then the rate of change of voltage is slow. An important consequence of the form of $\dot{V}$ is that the rate of change of voltage V changes sign when the two currents I_1 and I_2 cross.

2. The $\dot{I}_1$ equation consists basically of two nullcline components together with a coupling term.

   - The first of these two components is of the form $I_1 = -\delta/V$. Together with appropriate coupling this enables us to model the fast upstroke of an action potential as outlined previously.
   - The second component of the nullcline structure is of the form $I_1 = h_f(V)$, where $h_f(V)$ is a polynomial equation in V. By altering its form we can change the structure of the I_1 nullclines. This enables us to specify the path for the trajectory of I_1, especially in the plateau and repolarisation phases, and hence alter the resulting action potentials.
   - The coupling term is a simple linear function of I_2. It determines the value that I_2 takes when the structure of the I_1 nullclines changes between the breaking apart of the two components in the two different directions (one allowing for the upstroke and the other for the return to equilibrium).

3. As in the $\dot{I}_1$ equation, the $\dot{I}_2$ equation consists of two main nullcline components together with a coupling term.

   - The first component of the $\dot{I}_2$ equation is of the form $I_2 = I_1$. Thus as I_1 changes, I_2 attempts to move towards the same value. Also note that as $\dot{V}$ changes sign, and I_1 and I_2 cross, the sign of this component of the I_2 equation changes. If the coupling is small then the direction of the current I_2 also changes sign close to the change of direction in V.
   - The second component of the nullcline structure is of the form $I_2 = h_g(V)$, where $h_g(V)$ is a polynomial equation in V. As with $h_f(V)$, altering the form of $h_g(V)$ enables us to alter the trajectory of I_2 and thus change the property of the resulting action potentials.
   - The coupling term in the $\dot{I}_2$ equation is of the form $\gamma(V + \bar{V})$. When the system is at equilibrium $I_1 = I_2$ and this term fixes the location of the fixed point at $V = -\bar{V}$. γ controls the strength of the coupling.

In the following analysis of these equations we will principally be concerned with studying the effects of changing the parameters α, β, γ, $\bar{V}$ and ϵ_2, and the two polynomial functions which describe the nullclines, $h_f(V)$ and $h_g(V)$. We note here that a common behaviour of ionic models as parameters are changed is that a steady state will lose or gain its stability as the result of a Hopf bifurcation. The model will therefore either be excitable, with a stable steady state, or oscillatory (autorhythmic) with a stable limit cycle.

4.3.3 Alternative Form of Equations

The coupling term chosen in the $\dot{I}_2$ equation above is of the form $\gamma(V + \bar{V})$. This fixes the value of V at the fixed point to be $-\bar{V}$. From the $\dot{I}_1$ equation the value of I_1 and I_2 at the fixed point is then given by equation (4.4).

Rather than fixing the value of V at the fixed point by appropriate coupling in the $\dot{I}_2$ equation, we may instead fix the value of I_1 and I_2. This is easily done by changing the coupling from $\gamma(V + \bar{V})$ to $\gamma(I_2 - \bar{I})$. (The change of sign is to keep

the parameter $\bar{I}$ positive). The value of I_2 (and hence I_1) at the fixed point then has a value of $\bar{I}$ and our equations become

$$\begin{aligned} \dot{V} &= I_1 - I_2 \\ \dot{I}_1/\epsilon_1 &= -(VI_1 + \delta)(I_1 - h_f(V)) + \alpha(\beta - I_2) \\ \dot{I}_2/\epsilon_2 &= (I_1 - I_2)(I_2 - h_g(V)) + \gamma(I_2 - \bar{I}) \end{aligned}$$

The value of V at the fixed point is determined by the $\dot{I}_1$ equation and depends on the form of $h_f(V)$. For example if $h_f(V)$ is constant ($h_f(V) = k$ say) then we get one fixed point with $V = \frac{\alpha\beta+\delta k-(\alpha+\delta)\bar{I}}{\bar{I}(\bar{I}-k)}$ (providing $\bar{I} \neq 0, k$). If $h_f(V)$ has a more complicated form then we have more fixed points. Indeed if $h_f(V)$ is a polynomial of order n then we have $n+1$ solutions to the fixed point equation (of which some may be complex).

From this point onwards we shall concentrate on equations (4.3), that is with the coupling $\gamma(V + \bar{V})$ in the $\dot{I}_2$ equation. The analysis using $\gamma(I_2 - \bar{I})$ is similar.

4.4 Initial Choices

When we were matching the polynomial model to Noble in the previous chapter, the functions $h_f(V)$ and $h_g(V)$ were given particular forms. The principal reason for this was to match the nullclines with those of the Noble model (re-written in terms of the currents) ensuring that the trajectory of the currents I_1 and I_2 followed a similar path to I_1 and I_2 in the Noble model. Recall that $h_f(V)$ was set to be a quartic and $h_g(V)$ was set to be a (negative) quadratic. In this chapter we are not concerned with quantitative results (such as the voltage varying between values of around -100 and 40 as in the Noble model) and we are free to alter the forms of $h_f(V)$ and $h_g(V)$. Furthermore, for the remainder of this chapter we set $\delta = 1$ (resulting in the hyperbola component of the nullcline $I_1 = -1/V$) and $\epsilon_1 = 1$ (so that ϵ_2 gives us simple control over the respective time scales of the two current equations $\dot{I}_1$ and $\dot{I}_2$).

Our initial choice for $h_f(V)$ and $h_g(V)$ is as simple as possible whilst ensuring the excitability characteristic of the equations. Note that the two simple oscillators discussed at the beginning of the chapter ($h_f(V) = 0$, $\alpha = 1$, $\beta = 0$, $h_g(V) = V$, $\gamma = 1$) gave oscillatory but not excitable behaviour.

We take $h_f(V)$ to be a constant, in particular 1, and $h_g(V)$ to be a linear function of V through the origin, i.e. $h_g(V) = k_1 V$. Using the AUTO bifurcation package developed by Doedel and his collaborators [50, 51, 52] we can perform a bifurcation analysis of these equations. With k_1 as the bifurcation parameter (and the parameter values shown in table 4.1), we find that if $k_1 \gtrsim 5.23$ then the fixed point (at $V = -\bar{V}$) is stable and we get excitable behaviour. We initially choose a value of 6. Our initial choices for $h_f(V)$ and $h_g(V)$ are therefore

$$\begin{aligned} h_f(V) &= 1 \\ h_g(V) &= 6V \end{aligned}$$

4.4.1 Simulation

Results from a simulation of equations (4.3) using these simple choices of $h_f(V)$ and $h_g(V)$ are shown in figure 4.6. The parameter values used are shown in table 4.1 and give the stable fixed point at $V = -3$ and $I_1 = I_2 = \frac{2}{3}$. (Note that there is also an unstable fixed point at $V = -3$ and $I_1 = I_2 = 1$). The equations (with these

$\alpha = 1$	$\beta = 1$	$\gamma = 0.5$	$\bar{V} = 3$	$\epsilon_2 = 0.015$

Table 4.1: Parameter values used for the simple model.

parameter values) are excitable (the threshold is at $V \approx -2.95$) and perturbing the voltage to a value of $V = -2.9$ results in an action potential as shown.

The action potential has a fast upstroke, resulting from the fast increase in I_1. There is no overshoot as I_1 continues to decrease after the upstroke. The plateau phase is short and we can see that this is due to the fact that I_1 and I_2 are not particularly close during the plateau phase. $\dot{V}$ is therefore larger at this point of the trajectory resulting in a faster change in V and a shorter plateau. The repolarisation phase

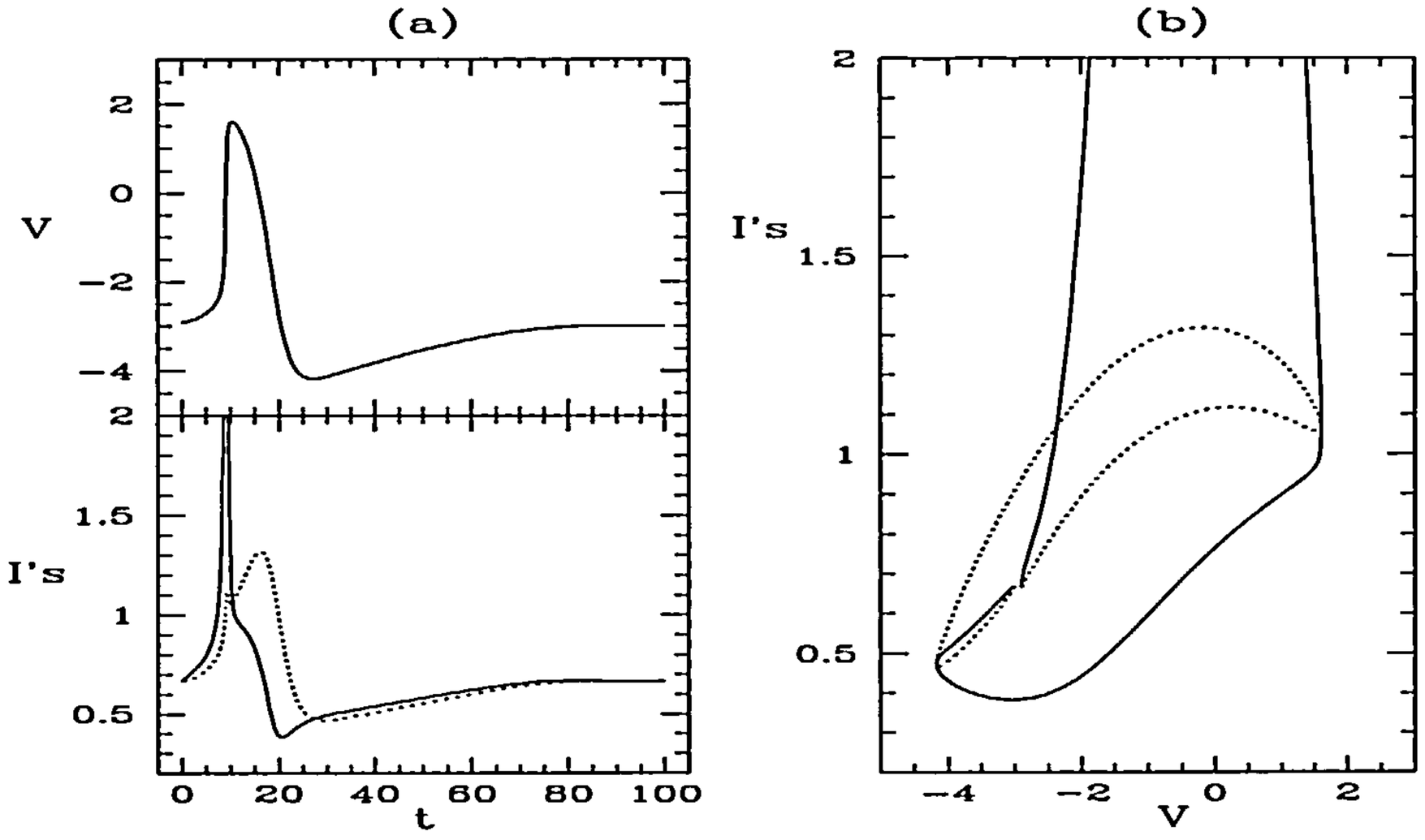

Figure 4.6: Simulation of equations (4.3) using the parameter values in table 4.1 and $h_f(V) = 1$ and $h_g(V) = 6V$. Both (a) the time series of the voltage and currents and (b) the phase plane are plotted. I_1 is shown as a solid line and I_2 as a dotted line. I_1 is truncated and reaches a value of around 8 on the upstroke.

of the action potential is also fast, although not as fast as the upstroke, and this is followed by a slow return to the equilibrium value.

4.4.2 Phase Portrait Analysis

The reason behind our choices for $h_f(V)$ and $h_g(V)$, and why the action potentials are as those observed, can be made clearer by looking at the nullcline structures.

The nullcline structure for I_1 is shown in figure 4.7 (using the parameter values in table 4.1). In figure 4.7(a), when $I_2 = 1$, the coupling term in the $\dot{I}_1$ equation is zero (as $\beta = 1$). We can clearly see the two components of the I_1 nullclines, $I_1 = -1/V$, and $I_1 = h_f(V) = 1$. $\alpha > 0$ and so when $I_2 < 1$, the two components of the nullclines split to give a nullcline structure as in plot (b). Any (positive) perturbation of V from the steady state value at -3 (shown with a cross) causes I_1 to increase quickly leading to the upstroke of the action potential. In (c), when

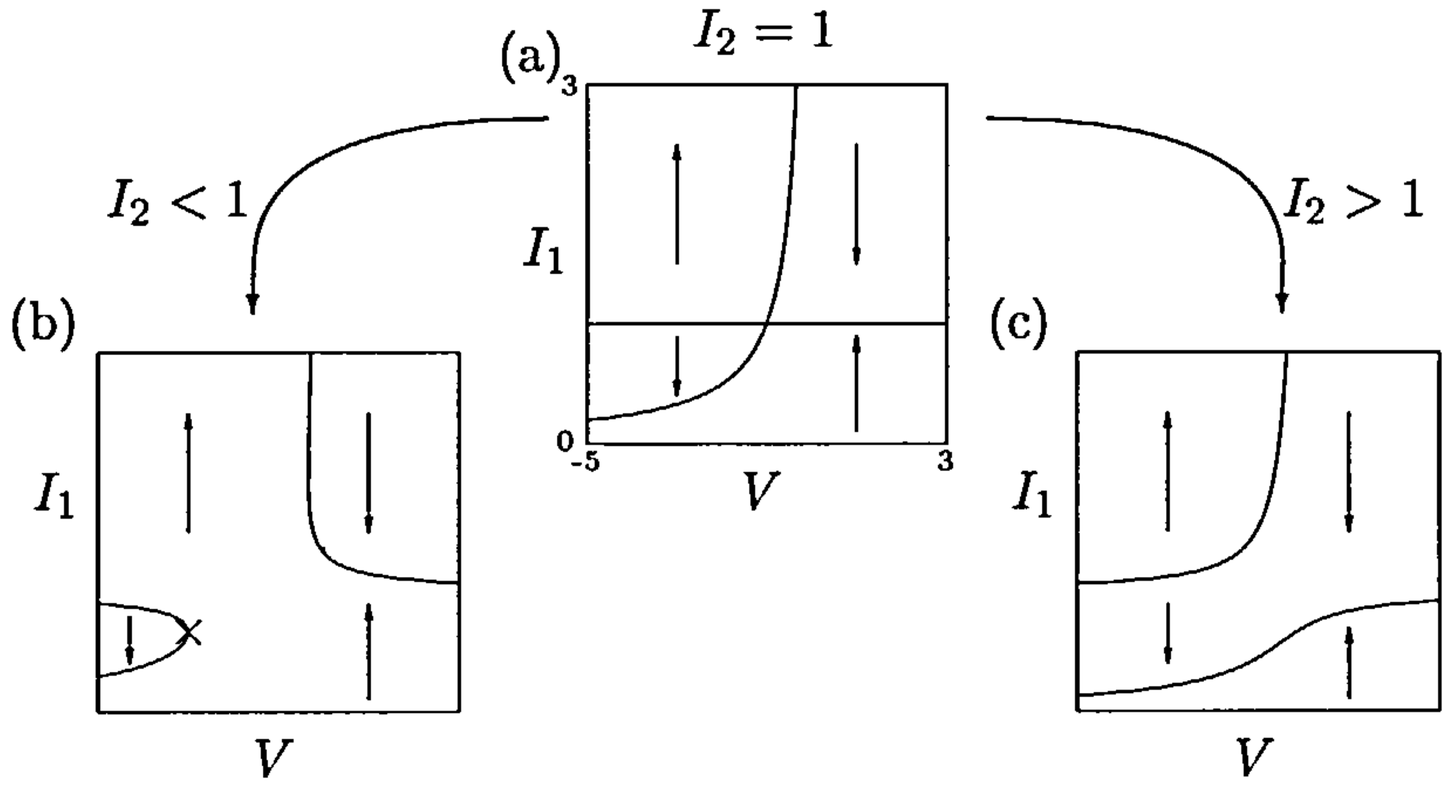

Figure 4.7: I_1 nullclines for the simple model. The arrows indicate the direction of the flow and the stable fixed point is shown in (b) with a cross. In (b) $I_2 = \frac{2}{3}$ has been used and in (c) $I_2 = 1.3$.

$I_2 > 1$, the nullclines split in the opposite direction and I_1 follows the lower branch of the resulting nullcline structure on its return to equilibrium.

Now let us look at the I_2 nullclines which are shown in figure 4.8. In 4.8(a), the I_2

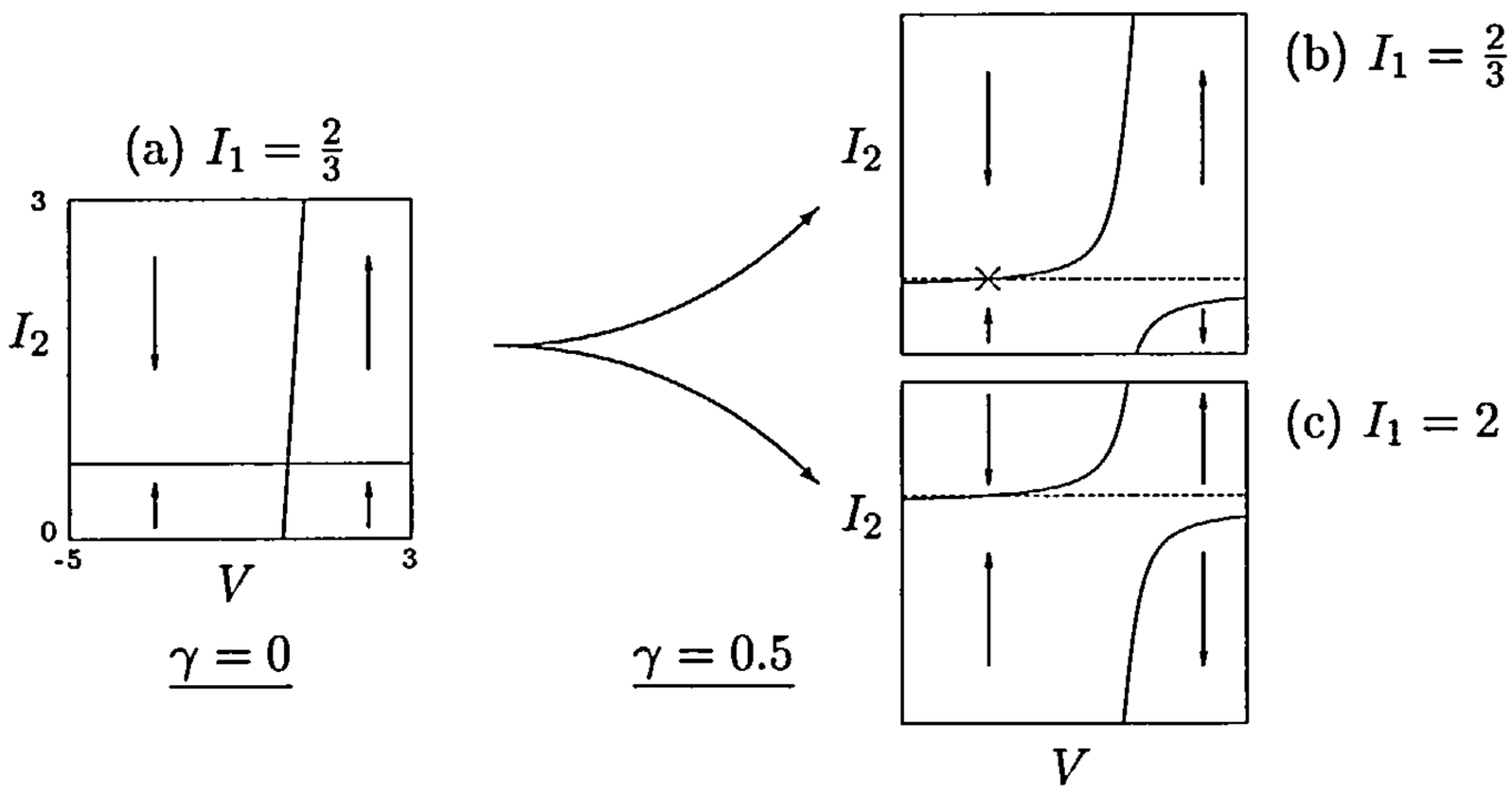

Figure 4.8: I_2 nullclines for the simple model. Arrows indicating the direction of the flow are again drawn and in (b) the stable fixed point is shown with a cross. The dashed line in plots (b) and (c) indicates the height $I_2 = I_1$.

nullclines are drawn with $\gamma = 0$. This puts the coupling term in the $\dot{I}_2$ equation equal

to zero so that the two components of the nullclines can be seen. The horizontal line is the term $I_2 = I_1$ and so is at the level I_1 ($\frac{2}{3}$ in this example). The sloped line is the curve $I_2 = h_g(V) = 6V$. The effect of adding coupling (with $\gamma \neq 0$) is shown in (b) with $I_1 = \frac{2}{3}$, and in (c) with $I_1 = 2$. We have used $\gamma = 0.5$. It can be seen that as I_1 varies the horizontal component of the I_2 nullclines moves up and down and the effect of the coupling is to break apart the two nullcline components as shown.

In this simple polynomial model the basic ideas behind the phase plane dynamics are the same as those in the Noble model and polynomial model discussed in the previous chapter. The main difference in the resulting action potential is that there is no overshoot on the upstroke and the plateau is of a shorter duration. (This is in fact similar to slow response waves as discussed in Chapter 2).

Later in this chapter we shall investigate the effect of altering the form of the functions $h_f(V)$ and $h_g(V)$. First of all however we shall look at the effect of changing the parameter values from those given in table 4.1.

4.5 Effect of the Parameters

4.5.1 The Parameter α

The equation for I_1 with $h_f(V) = 1$, and $\beta = 1$, is

$$\dot{I}_1 = -(VI_1 + 1)(I_1 - 1) + \alpha(1 - I_2) \tag{4.5}$$

From this equation we can see that the main effect of α is to change the strength of the coupling in the $\dot{I}_1$ equation. At the fixed point the nullclines are split so that the fixed point is on one part of the I_1 nullcline (as in figure 4.7 (b)) and a small increase in V causes the trajectory to move off the nullcline leading to a quick increase in I_1 and the upstroke. As α varies (for fixed I_2) the appropriate section of the nullcline changes slightly becoming smaller (as α increases) or larger (as α decreases) suggesting that α helps determine the excitability of the system.

However, from equation (4.5), we know that the location of the stable fixed point in I also depends on α and is given by $I_1 = I_2 = \frac{1+\alpha}{3}$. (The unstable fixed point is at $I_1 = I_2 = 1$). Therefore as α is decreased, the value of I_1 and I_2 at the stable fixed point decreases (linearly) and as α is increased the value increases. The effect of changes in α on the fixed point and the I_1 nullclines is shown in figure 4.9.

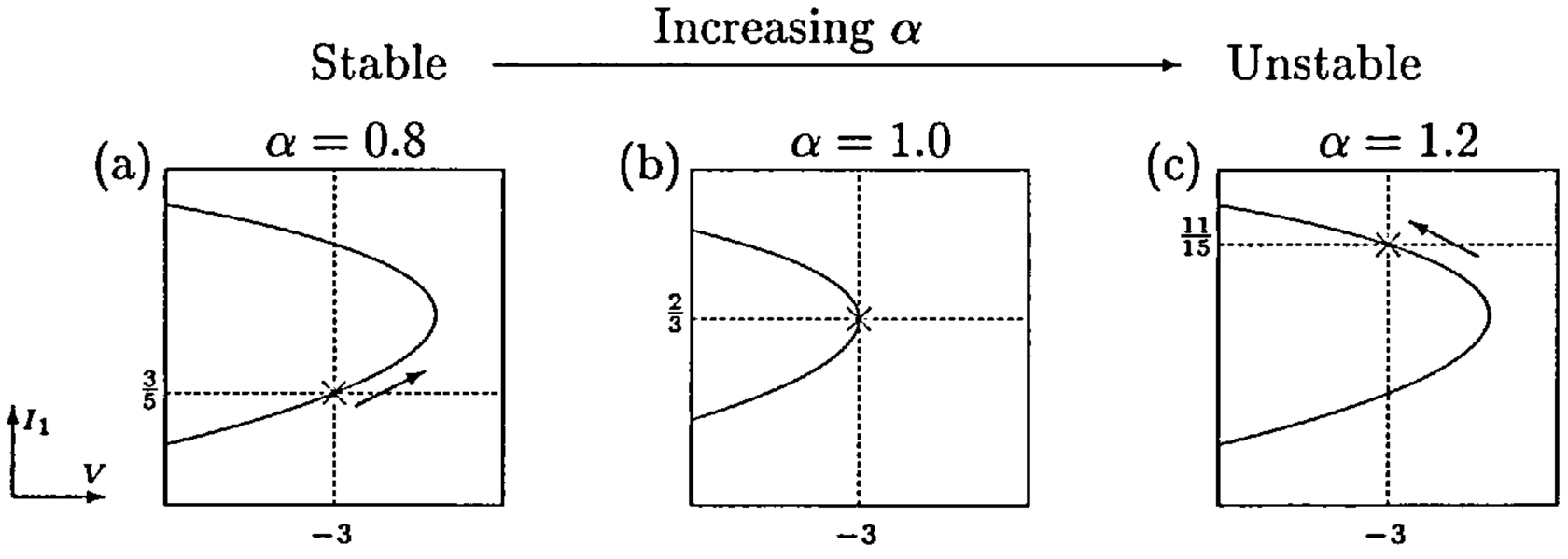

Figure 4.9: Dependence of the fixed point on α. As α increases, the value of I_1 at the fixed point increases (as shown by the arrows) whilst remaining on the (α-dependent) I_1 nullcline.

When $\alpha = 0.8$ the fixed point is stable and the I_1 nullclines are as in (a). The system is not particularly excitable in the sense that the threshold for excitation is large. As α increases, the value of I_1 at the fixed point also increases with the nullclines moving to the left (and hence the equations becoming more excitable) until, at $\alpha = 1$, we have the null cline structure in (b), with the rightmost part of the nullcline at $V = -3$. As α continues to increase the nullclines move to the right with the fixed point increasing and becoming unstable. We can check this behaviour using the AUTO bifurcation package with α as the bifurcation parameter. Indeed, as α is increased past a value of $\alpha \approx 1.075$, a supercritical Hopf bifurcation occurs and the fixed point becomes unstable leading to a stable limit cycle and oscillatory waves. Note that, whereas the value of I_1, and hence I_2, at the fixed point change with α, the value of V remains at -3 as it is fixed by the $\dot{I}_2$ equation.

4.5.2 The Parameter β

With $h_f(V) = 1$, and $\alpha = 1$, the $\dot{I}_1$ equation is

$$\dot{I}_1 = -(VI_1 + 1)(I_1 - 1) + \beta - I_2 \tag{4.6}$$

The parameter β determines when the I_1 nullclines change qualitatively from the simple two components $I_1 = h_f(V)$ and $I_1 = -1/V$. Decreasing β will mean that the "window" in the I_1 nullclines allowing the fast increase of I_1 (and hence the upstroke of the action potential) closes more quickly as I_2 increases on the upstroke. This results in reduced excitability. Increasing β extends the size of the "window" as I_2 has to get larger before it is closed. The result is increased excitability or oscillatory waves.

Changing β also affects the value of I_1 (and I_2) at the fixed point. From equation (4.6), and with $\bar{V} = 3$, the stable fixed point is at $I_1 = \frac{1}{6}(5 - \sqrt{13 - 12\beta})$. (The unstable fixed point is at $I_1 = \frac{1}{6}(5 + \sqrt{13 - 12\beta})$). Thus as β decreases, the value of I_1 at the stable fixed point decreases, and as β increases, the value increases. The behaviour of the nullclines and the stable fixed point as β varies is similar to that as α varies (shown in figure 4.9). The situation in 4.9(b) (when the rightmost part of the nullcline is at $V = -3$) occurs when $\beta = 1$. Note that when $\beta > \frac{13}{12}$ the two fixed points become complex.

The effect of β on the stability of the fixed point can be verified using the AUTO package and indeed there is a supercritical Hopf bifurcation at $\beta \approx 1.02$. Furthermore, there is a limit point at $\beta = \frac{13}{12}$.

4.5.3 The Parameter γ

Now let us recall the equation for I_2 with $h_g(V) = 6V$.

$$\dot{I}_2/\epsilon_2 = (I_1 - I_2)(I_2 - 6V) + \gamma(V + \bar{V})$$

It can be seen that the parameter γ determines the strength of the coupling in the I_2 equation and as γ increases the breaking apart of the two I_2 nullcline components

(as in figure 4.8(b) and (c)) becomes larger. However, γ does not affect the location of the fixed points and for reasonable values of γ ($0 < \gamma < 1$) the fixed point at $V = -3$ and $I_1 = I_2 = \frac{2}{3}$ remains stable.

When the two currents I_1 and I_2 are close, γ has a greater effect on the rate of change of I_2 as the coupling term dominates the I_2 dynamics. The main effect of changing γ is therefore seen on the plateau of an action potential and in the slow recovery back to equilibrium that occurs immediately after an action potential (when I_1 and I_2 are close). Larger γ's give shorter plateaus and recovery times and vice-versa.

4.5.4 The Parameter $\bar{V}$

$\bar{V}$ determines the location of the fixed point in V via the $\dot{I}_2$ equation. With the other parameters fixed at the values in table 4.1, the value of I_1 and I_2 at the stable fixed point is $\frac{2}{\bar{V}}$. (The unstable fixed point is at $I_1 = I_2 = 1$). Therefore as $\bar{V}$ increases, the value of V ($= -\bar{V}$), I_1, and I_2, at the fixed point decrease. Similarly, if V decreases they increase. The effect of changes in V on the fixed point and the I_1 nullclines is shown in figure 4.10. The fixed point is located on the rightmost part

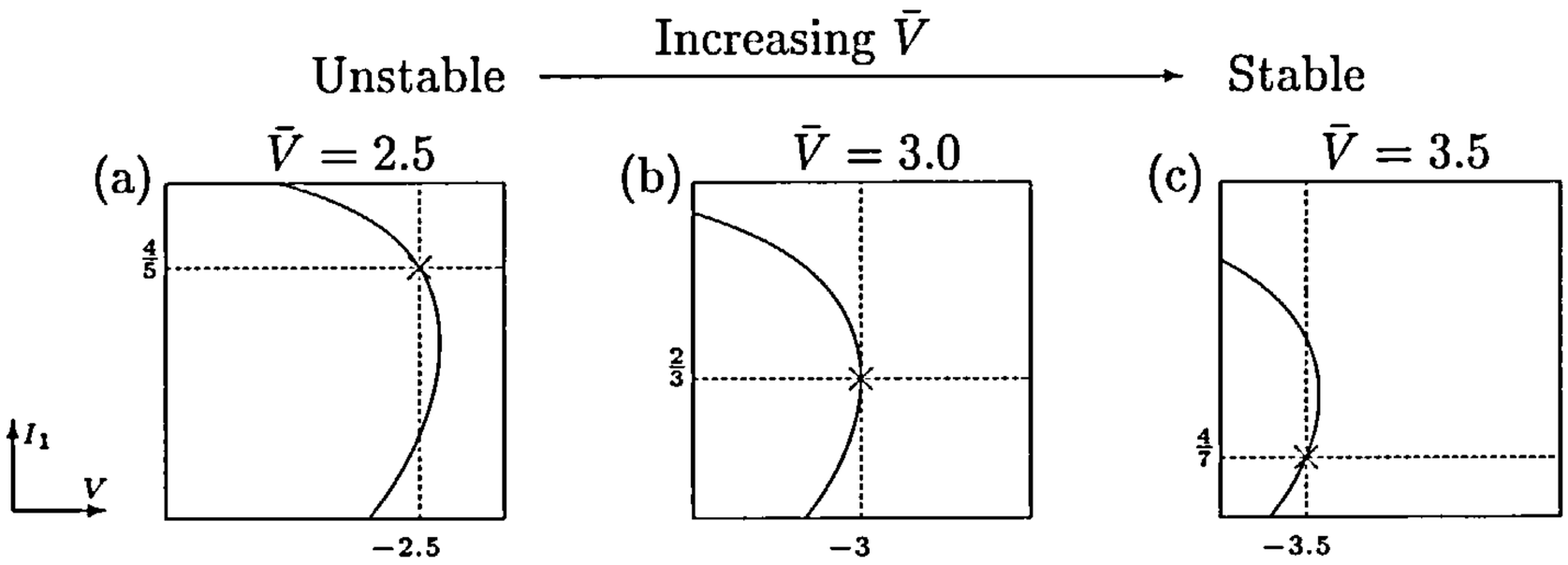

Figure 4.10: Dependence of the fixed point on $\bar{V}$. As $\bar{V}$ increases, the value of I_1 at the fixed point decreases whilst remaining on the ($\bar{V}$-dependent) I_1 nullcline.

of the nullcline, as shown in (b), when $\bar{V} = 3$.

Using AUTO we find that, on decreasing $\bar{V}$, a supercritical Hopf bifurcation occurs at $\bar{V} \approx 2.90$, and the fixed point becomes unstable. Oscillatory waves therefore occur. On increasing $\bar{V}$ from it's initial value of 3, the fixed point remains stable with the

value of V at the fixed point becoming more negative and I_1 and I_2 decreasing.

The parameter $\bar{V}$ is useful for changing the behaviour of the equations in two ways. It can be used both for altering the speed of the upstroke and for changing the character of the equations from excitable to oscillatory.

If we wish to increase the size of I_1 on the upstroke, leading to a sharper upstroke in the action potential, the fixed point of the equations may be moved to more negative values of V by increasing the value of $\bar{V}$ (whilst altering α to keep the excitability characteristic). For example, with $\bar{V} = 3.5$ and $\alpha = 1.25$ (so that the fixed point is on the rightmost part of the nullcline as before) and with the other parameters unaltered, the fixed point is at $V = -3.5$ and $I_1 = I_2 = \frac{1+\alpha}{\bar{V}} = \frac{9}{14}$. The equations are excitable and the value of I_1 gets about four times as big on the upstroke compared with its size when $\bar{V} = 3$ and $\alpha = 1$. A wave of this type is shown in figure 4.11. There is no great difference in the shape of the wave but the upstroke is now sharper

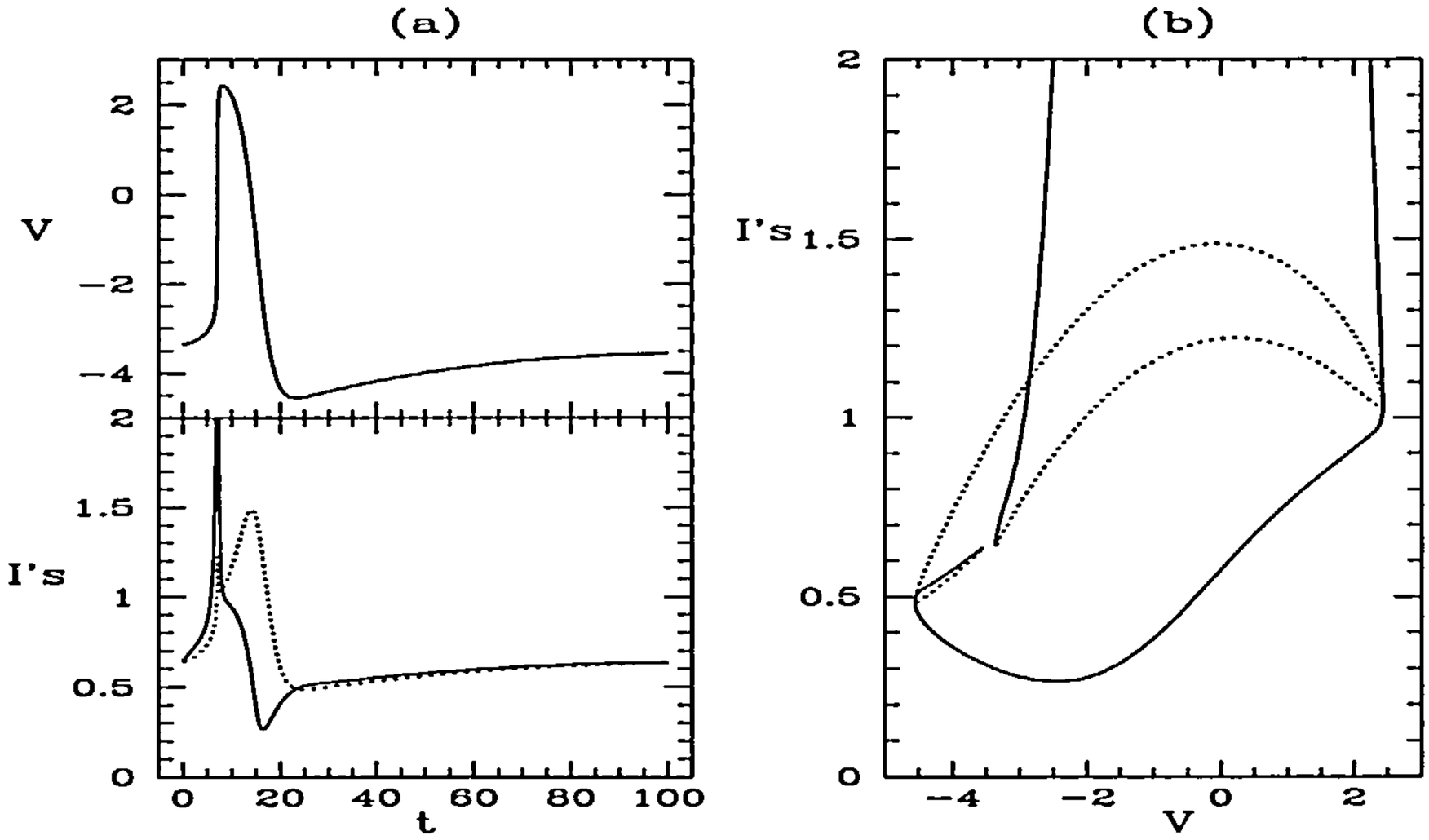

Figure 4.11: Simulation of equations (4.3) with $\bar{V} = 3.5$ and $\alpha = 1.25$. Both (a) the time series of the voltage and currents and (b) the phase plane are plotted. I_1 is shown as a solid line and I_2 as a dotted line. I_1 is truncated and reaches a maximum value of about 34.

and V gets slightly more positive.

$\bar{V}$ can also be used to make the equations oscillatory. If $\bar{V}$ is changed to a value of 2.8 whilst keeping the other parameters fixed as in table 4.1, oscillatory waves are observed. Recall that there is a Hopf bifurcation at $\bar{V} \approx 2.90$. The stable fixed point becomes unstable and during the slow recovery to equilibrium, V continues to increase past the fixed point causing the trajectory to cross the I_1 nullcline and move into the "upstroke window". An example of an oscillatory wave obtained by altering the value of $\bar{V}$ in this manner is shown in figure 4.12.

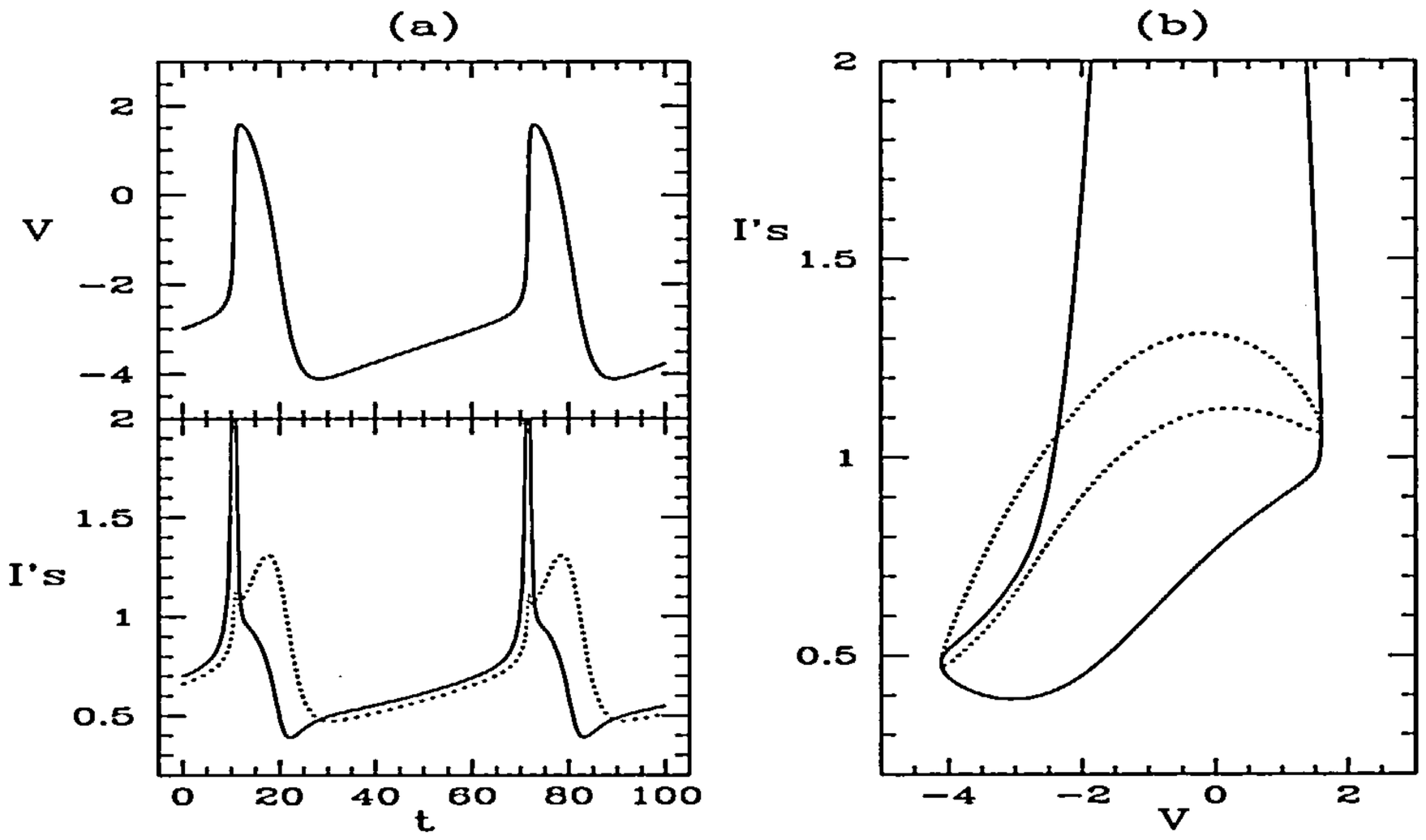

Figure 4.12: Simulation of the simple model showing oscillatory behaviour resulting from decreasing $\bar{V}$ to a value of $\bar{V} = 2.8$. Both (a) the time series of the voltage and currents and (b) the phase plane are plotted. I_1 is shown as a solid line and I_2 as a dotted line.

4.5.5 The Parameter ϵ_2

The parameter ϵ_2 controls the rate of change of I_2 relative to the rate of change of I_1 and does not affect the location of the fixed points or the nullcline structures. Reducing ϵ_2 results in I_2 changing more slowly with respect to the rate of change

of I_1. This leads to oscillatory behaviour (a Hopf bifurcation occurs at $\epsilon_2 \approx 0.0130$) and more negative values of V after an action potential as the speed of recovery of I_2 is reduced. Increasing ϵ_2 results in a faster relative rate of change in I_2. This gives rise to smaller plateaus, as I_2 is moving more quickly, and in less excitability, as the rate of change of I_2 at the start of an action potential is quicker causing the "window" of excitability to close more quickly.

4.6 Effect of the Functions $h_f(V)$ and $h_g(V)$

In this section we investigate the behaviour of the action potentials generated by our simple model (equations 4.3) as the functions $h_f(V)$ and $h_g(V)$ are altered.

4.6.1 The Function $h_f(V)$

The function $h_f(V)$ helps to fix the structure of the I_1 nullclines. Up to now we have been using $h_f(V) = 1$. Below we shall investigate the simple model for various different functions of $h_f(V)$; constant, linear, quadratic, cubic and quartic. We shall keep $h_g(V) = 6V$.

Constant: $h_f(V) = k$

We have already seen examples of the type of behaviour of equations (4.3) when $h_f(V)$ is a constant, in particular when $h_f(V) = 1$. The main effect of changing the value of the constant k, thus raising or lowering the horizontal component of the nullcline, is to alter the nullcline structure close to the fixed point. The value of I_1 at the stable fixed point depends on k and is given by $I_1 = \frac{1}{6}(2 + 3k - \sqrt{9k^2 - 8})$. If we increase k, the value of I_1 at the stable fixed point decreases, and the size of the nullclines close to the fixed point becomes larger. As k is decreased, the value of I_1 at the fixed point increases, and the size of the nullclines decreases. Note that as k decreases past $k = \sqrt{\frac{8}{9}}$ the fixed points become complex. The behaviour of

the nullclines and the stable fixed point as k varies is similar to that as $\bar{V}$ varies (shown in figure 4.10). When $k = 1$ we have the situation shown in 4.10(b) with the rightmost part of the nullcline at $V = -3$.

From a bifurcation analysis we find that as k is increased from 1, the fixed point in I_1 remains stable and decreases in value. The equations become less excitable. As k is decreased from 1 the fixed point becomes unstable, undergoing a Hopf bifurcation (at $a \approx 0.986$), and we get oscillatory behaviour. As k is decreased past $\sqrt{\frac{8}{9}} \approx 0.943$ and the fixed points become complex we get a limit point in the bifurcation diagram.

Linear: $h_f(V) = k_1 V + k_2$

First note that if $k_1 = 0$ and $k_2 = 1$ we have the previous case when $h_f(V) = 1$. We investigate the behaviour as k_1 becomes negative. We will not be concerned with k_1 becoming positive as this destroys the nullcline structure close to the fixed point which we need for the system to be excitable. Also, we shall "rotate" the linear curve around the point $(V, I_1) = (-3, 1)$ to keep the location of the fixed point at $(-3, \frac{2}{3})$. i.e $k_2 = 1 + 3k_1$. As the size of k_1 decreases, the excitability increases until the equations undergo a Hopf bifurcation (at $k_1 \approx -0.0385$) and the waves become oscillatory. As k_1 continues to decrease, the frequency of oscillation increases and the action potential duration decreases. An example of such waves is shown in figure 4.13. Other than the oscillatory behaviour, we can see that I_1 initially gets lower during repolarisation and then remains at a relatively constant value. Also, the upstroke is quicker and the action potential duration is shorter than in previous simulations.

These differences may be explained by looking at the change in the I_1 nullclines, shown in figure 4.14. As k_1 decreases, and the gradient of $h_f(V)$ (visible in (a) without coupling) becomes more negative, the nullcline structure becomes lower at high values of V. I_1 thus attains lower values following the upstroke resulting in a greater distance between I_1 and I_2, a larger $\dot{V}$, and hence a smaller action potential duration. During repolarisation the lower part of the nullcline is almost horizontal (as in (c)) so I_1 remains relatively constant throughout the return to equilibrium.

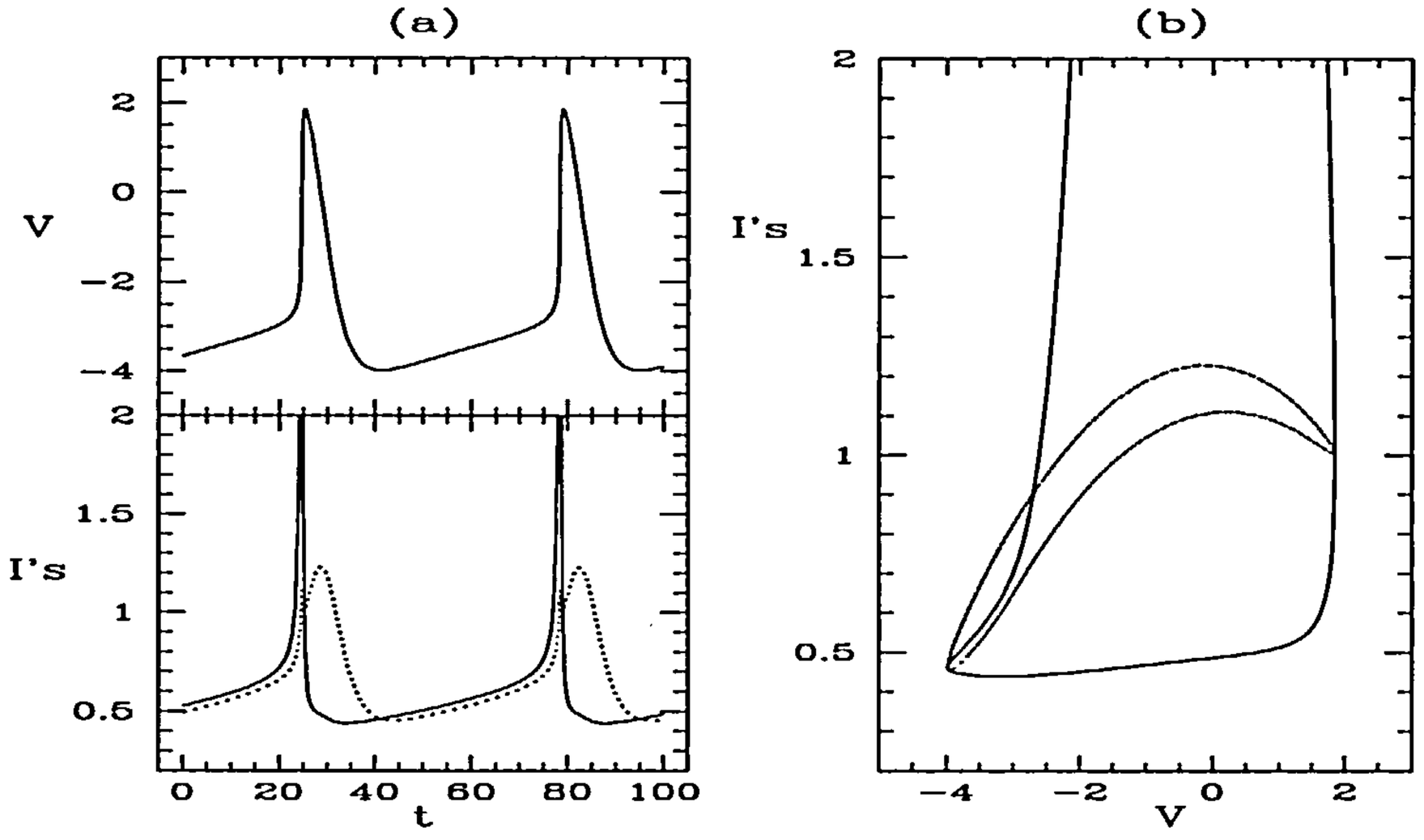

Figure 4.13: Simulation of equations (4.3) with a linear $h_f(V)$, in particular $h_f(V) = -0.1V + 0.7$ ($k_1 = -0.1$). The normal parameter values (table 4.1) are used. Both (a) the time series of the voltage and currents and (b) the phase plane are plotted. I_1 is shown as a solid line and I_2 as a dotted line.

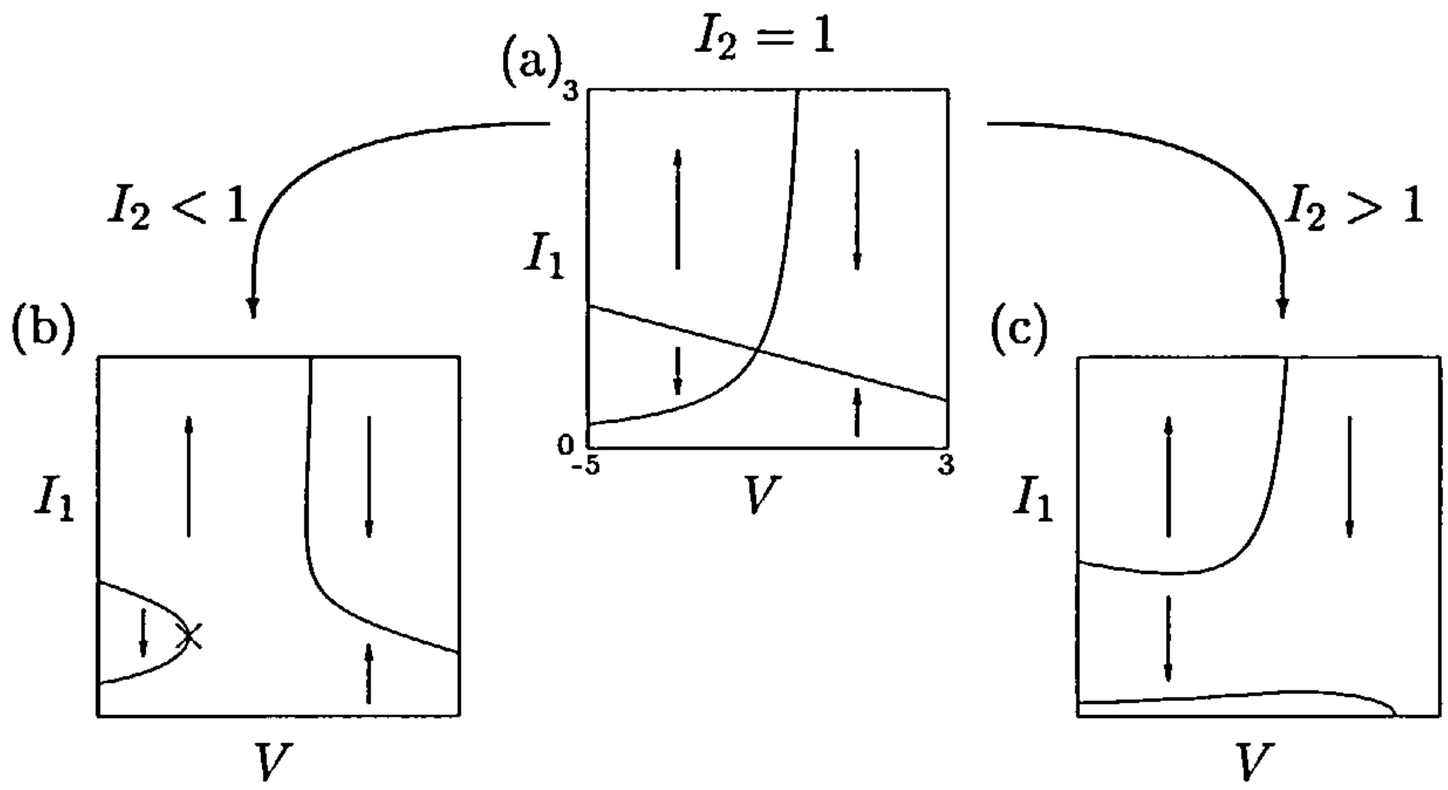

Figure 4.14: I_1 nullclines for the simple model with $h_f(V) = -0.1V + 0.7$. The arrows indicate the direction of the flow and the fixed point is shown in (b) with a cross.

Quadratic: $h_f(V) = k_1(V - k_2)^2 + k_3$

As in our study of linear forms of $h_f(V)$ we shall initially consider parabolas that pass through the point $(V, I_1) = (3, -1)$ to keep the location of the fixed point at $(-3, \frac{2}{3})$. We shall only consider positive parabolas ($k_1 > 0$). (Negative parabolas will destroy the fixed point nullcline structure when k_1 becomes sufficiently negative). Furthermore, we shall initially use $k_2 = 0$ and hence $k_3 = 1 - 9k_1$. Once again, if $k_1 = 0$, we have our original choice of $h_f(V) = 1$. If k_1 is increased from 0, a Hopf bifurcation occurs almost immediately ($k_1 \approx 0.0064$) and we get oscillatory waves. As k_1 continues to increase, the frequency of oscillation increases, the action potential duration decreases, and I_1 attains lower values during repolarisation. The results from a simulation are shown in figure 4.15. The action potential duration

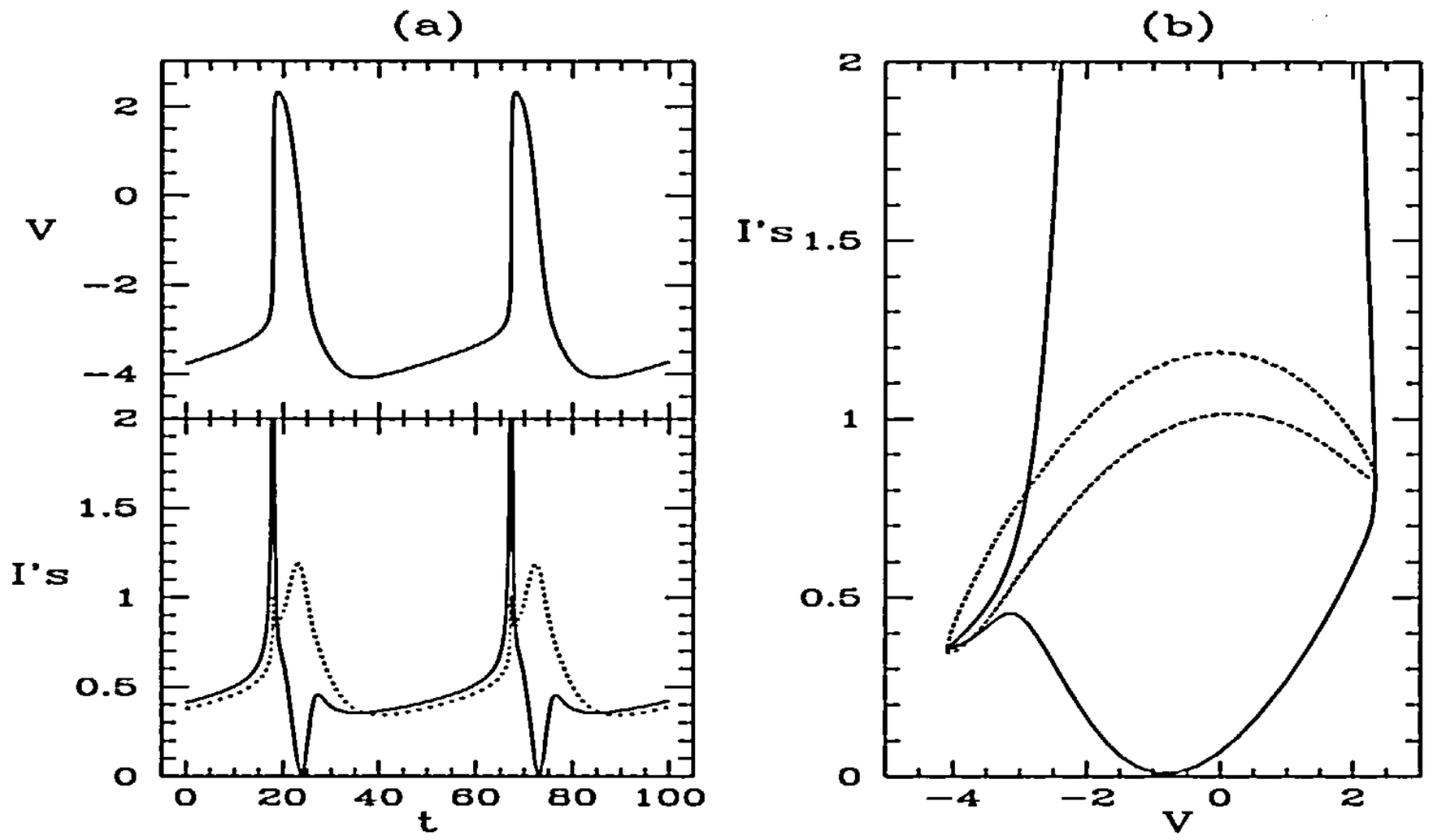

Figure 4.15: Simulation of equations (4.3) with a quadratic $h_f(V)$, in particular, $h_f(V) = 0.1V^2 + 0.1$ ($k_1 = 0.1$). The normal parameter values (table 4.1) are used. Both (a) the time series of the voltage and currents and (b) the phase plane are plotted. I_1 is shown as a solid line and I_2 as a dotted line.

is shorter than in the original equations and the upstroke is also a lot sharper with V attaining higher values. Another difference is that I_1 reaches lower values during

repolarisation (making it faster) before increasing back towards its equilibrium value.

We can help explain these differences by looking at the nullcline structure for a quadratic $h_f(V)$ as shown in figure 4.16. As k_1 increases, the parabola (shown in

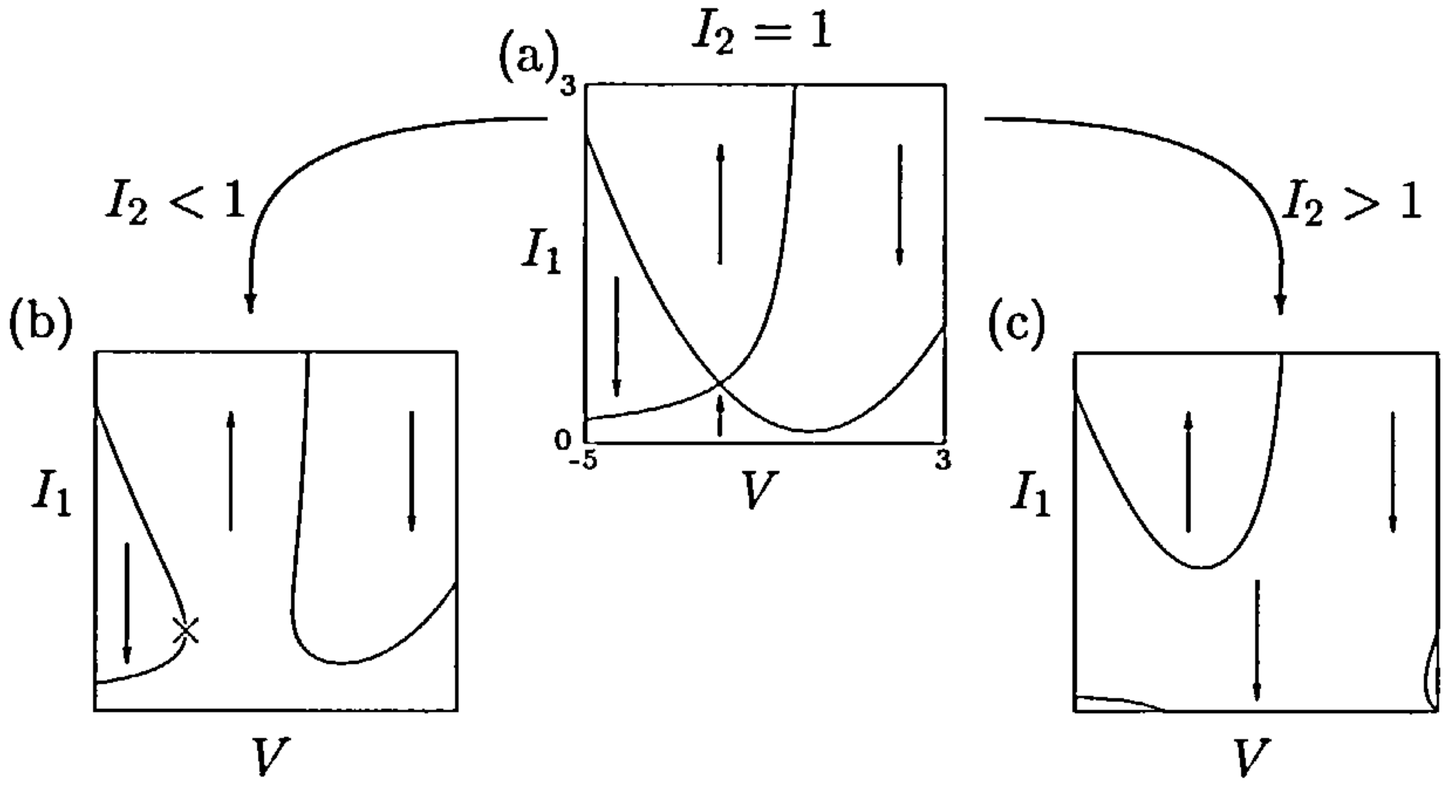

Figure 4.16: I_1 nullclines for the simple model with $h_f(V) = 0.1V^2 + 0.1$. The arrows indicate the direction of the flow and the fixed point is shown in (b) with a cross.

(a)) becomes lower at $V = 0$ giving nullclines as in (c) when $I_2 > 1$. This explains the low values of I_1 during repolarisation. The fact that I_1 reaches lower values during the repolarisation phase means that, for the same reason as in the previous section, the action potentials are short and repolarisation is fairly quick.

Now let us fix k_1 and k_3 (both at 0.1 as before) and consider varying k_2. (Note that the value of I_1 and I_2 at the fixed point changes). Changing k_2 moves the parabolic part of the nullcline to the left (negative k_2) or right (positive k_2). With (small) negative k_2 we get oscillatory waves of increasing frequency until k_2 passes $k_2 \approx -0.097$. The nullcline structure is then altered sufficiently to destroy the required structure of the nullclines and we get complex fixed points. On increasing k_2 the frequency of the oscillations decreases and a Hopf bifurcation occurs at $k_2 \approx 0.59$. We then get excitable behaviour with a stable fixed point. This can be explained from the nullcline structure. If the parabolic part of the nullcline is moved to the left then the nullcline structure close to the fixed point decreases in size

encouraging oscillatory behaviour. If the parabola is moved to the right then the nullcline structure enlarges, and excitable behaviour is preferred.

Cubic

In the previous cases, the behaviour of I_1 is simple. It initially increases (causing the upstroke) before decreasing throughout the plateau and repolarisation phases. It then increases briefly as it approaches its equilibrium value. A consequence of this behaviour is that the plateau of the action potential is short and we do not get an overshoot on the upstroke. Both of these behaviours may be obtained if I_1 begins to increase following the upstroke. This will give the overshoot and cause I_1 and I_2 to be close on the plateau, giving lower values of $\dot{V}$, and hence a longer action potential duration. This can be achieved by using a cubic or quartic function for $h_f(V)$. We shall initially investigate a cubic structure.

The result of a simulation with an appropriate choice of cubic $h_f(V)$ is shown in figure 4.17. Note that ϵ_2 is increased to 0.025. This speeds up the recovery of I_2 preventing V from getting too negative during repolarisation (resulting in oscillatory waves). α and β are altered to keep the excitability characteristic. Excitable behaviour occurs with the stable fixed point at $V = -3$ and $I_1 = I_2 \approx 0.44$. It can be seen that the action potential now has an overshoot and the plateau is longer.

Our simple model with a cubic $h_f(V)$ can be made oscillatory by decreasing the value of $\bar{V}$ in the usual way. With the same $h_f(V)$ and parameters as above, but with $\bar{V} = 2.8$, we get oscillatory waves as shown in figure 4.18.

Example nullcline structures for a cubic $h_f(V)$ are shown in figure 4.19. Note that the cubic function $h_f(V)$ can clearly be seen in (a). We can help explain the effects of using a cubic $h_f(V)$ from this figure. Throughout the upstroke the nullclines are as in plot (b). This allows I_1 to increase rapidly upon a small increase in V from the stable fixed point, cross its nullcline at high I_1, and decrease rapidly at high V. Shortly after V changes direction, I_1 crosses its nullcline at low values and begin to increase. This is a consequence of the cubic form of $h_f(V)$. $I_2 > 1$ here, and the

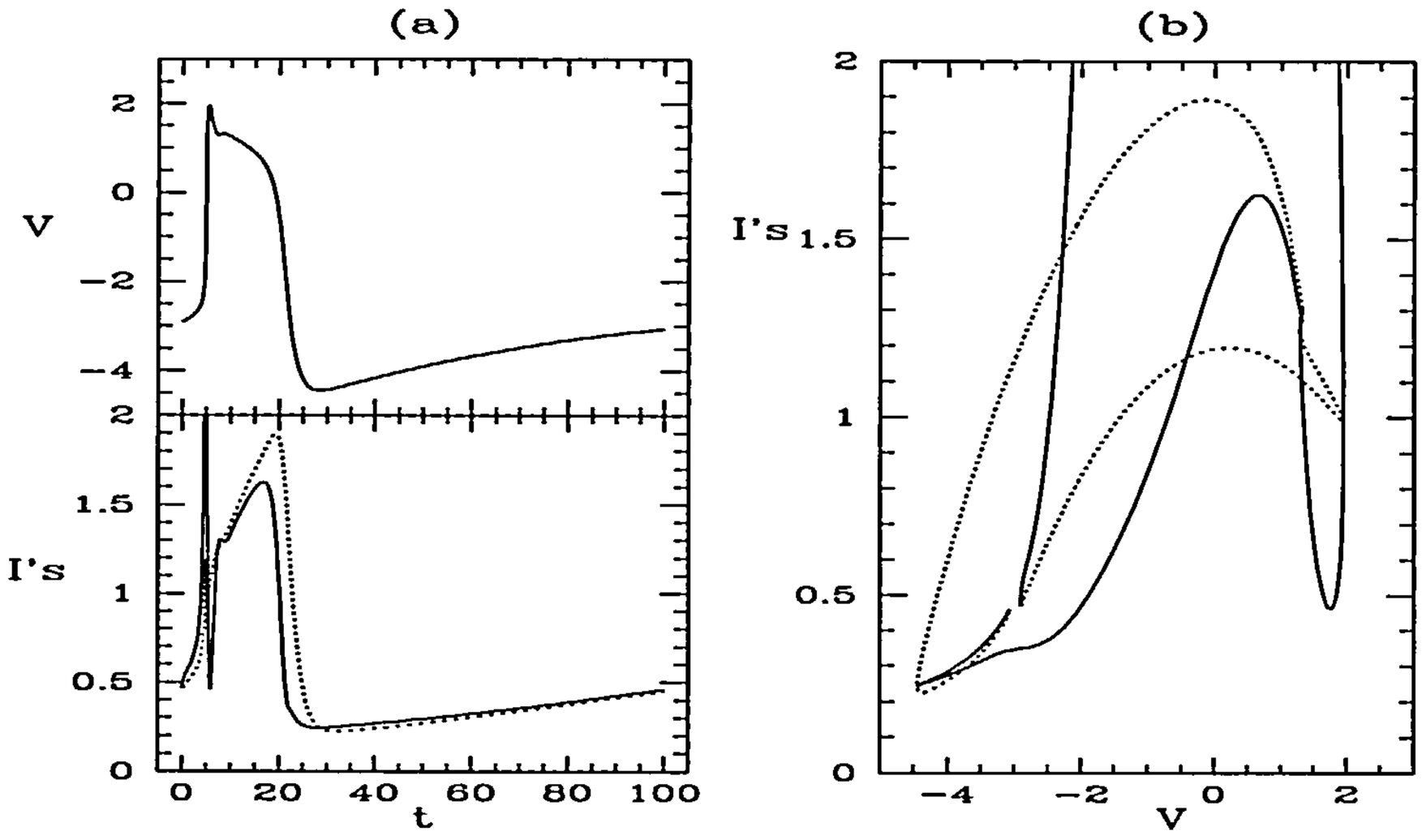

Figure 4.17: Simulation of equations (4.3) with a cubic $h_f(V)$, in particular $h_f(V) = -0.2(V + 2.6)(V + 0.9)(V - 1.5) + 1$, showing excitable behaviour. The normal parameter values (table 4.1) are used with the changes $\alpha = 0.8$, $\beta = 1.2$, and $\epsilon_2 = 0.025$. Both (a) the time series of the voltage and currents and (b) the phase plane are plotted. I_1 is shown as a solid line and I_2 as a dotted line.

relevant nullcline structure is that in plot (c). Up until I_1 attains similar values to I_2 (at a value of around 1.2) we have the overshoot. As I_1 reaches values close to I_2 we get a slower rate of change in V giving the plateau. Upon reaching values of around 1.5, I_1 crosses its nullcline again and begins to decrease following the lower branch of the nullcline structure in (c). Towards the end of repolarisation I_2 becomes less than 1 and the nullcline structure reverts back to that in (a) (via (b)). V changes direction as the two currents touch each other and I_1 increases slowly to its equilibrium value (shown with a cross).

Quartic

As mentioned in the previous section, a quartic form for $h_f(V)$ will give rise to waves with a fast upstroke, an overshoot and longer plateaus. Also recall that in

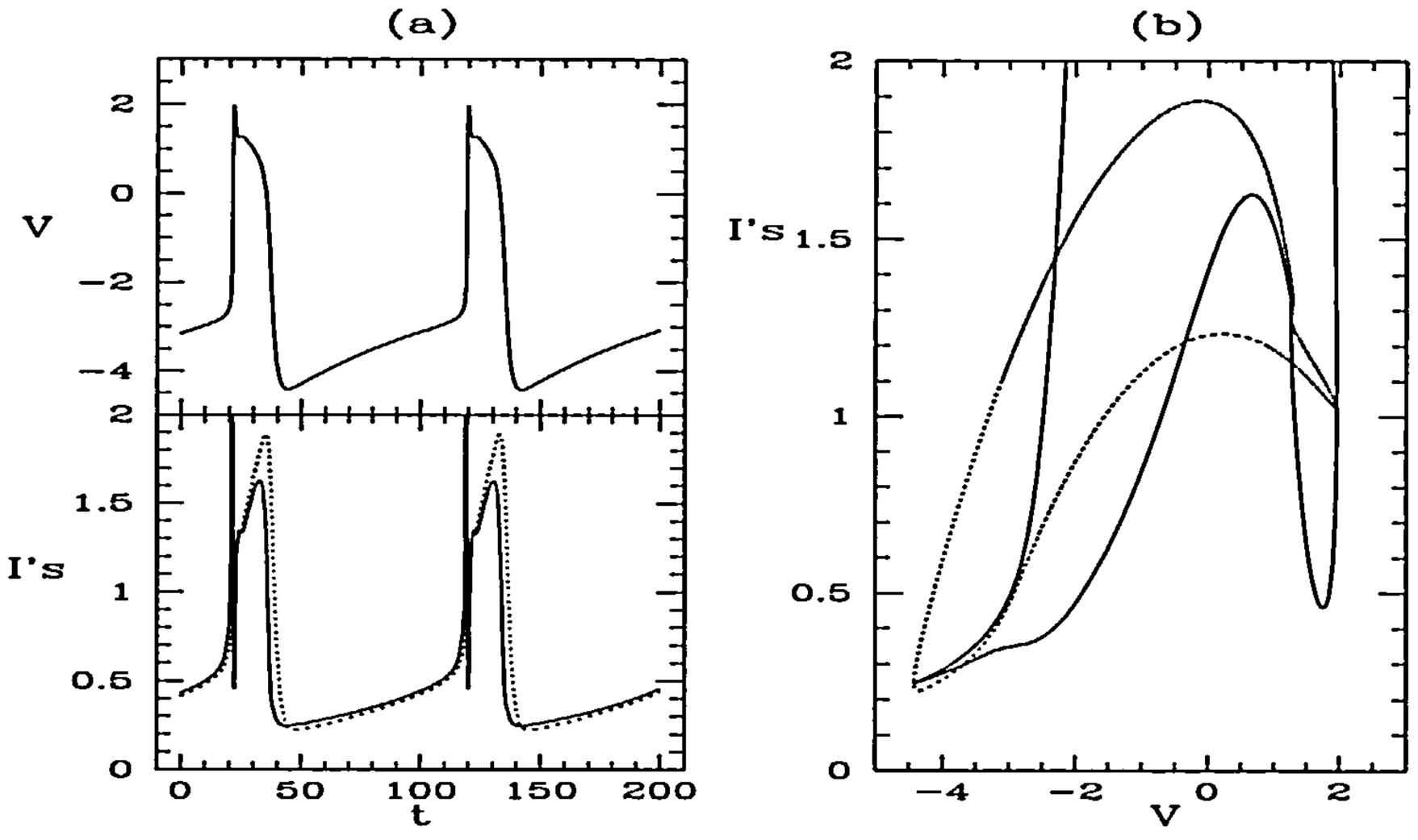

Figure 4.18: Simulation of equations (4.3) with a cubic $h_f(V)$ showing oscillatory behaviour. The same $h_f(V)$ and parameter values as in figure 4.17 are used with the change $\bar{V} = 2.8$.

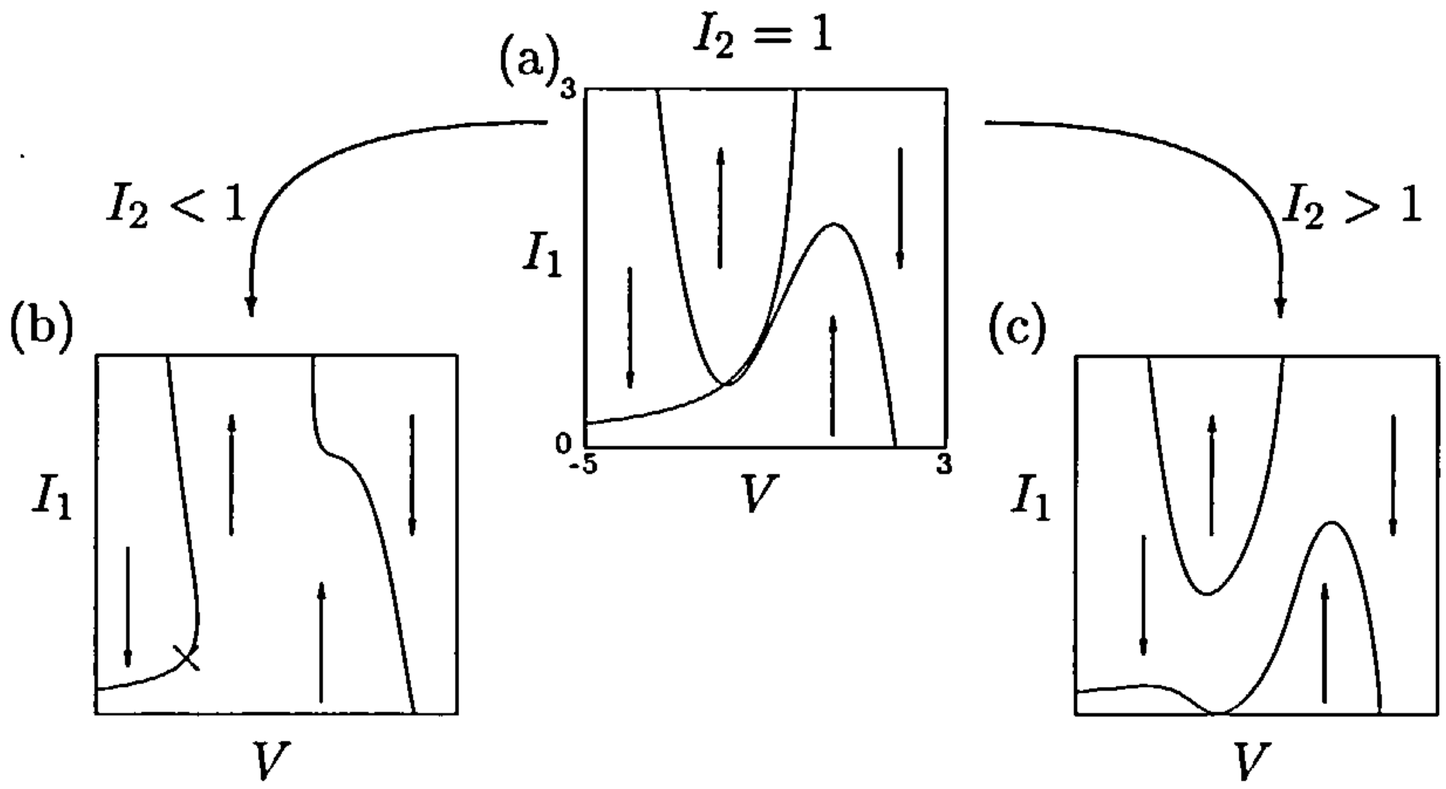

Figure 4.19: I_1 nullclines for the simple model with $h_f(V) = -0.2(V + 2.6)(V + 0.9)(V - 1.5) + 1$. The arrows indicate the direction of the flow and the fixed point is shown in (b) with a cross.

our approximation to the Noble model in the previous chapter we used a quartic polynomial for $h_f(V)$ to match the I_1 dynamics.

A simulation of our simple model with a quartic structure for $h_f(V)$ is shown in figure 4.20. We can see that the action potential is of the fast response type and is

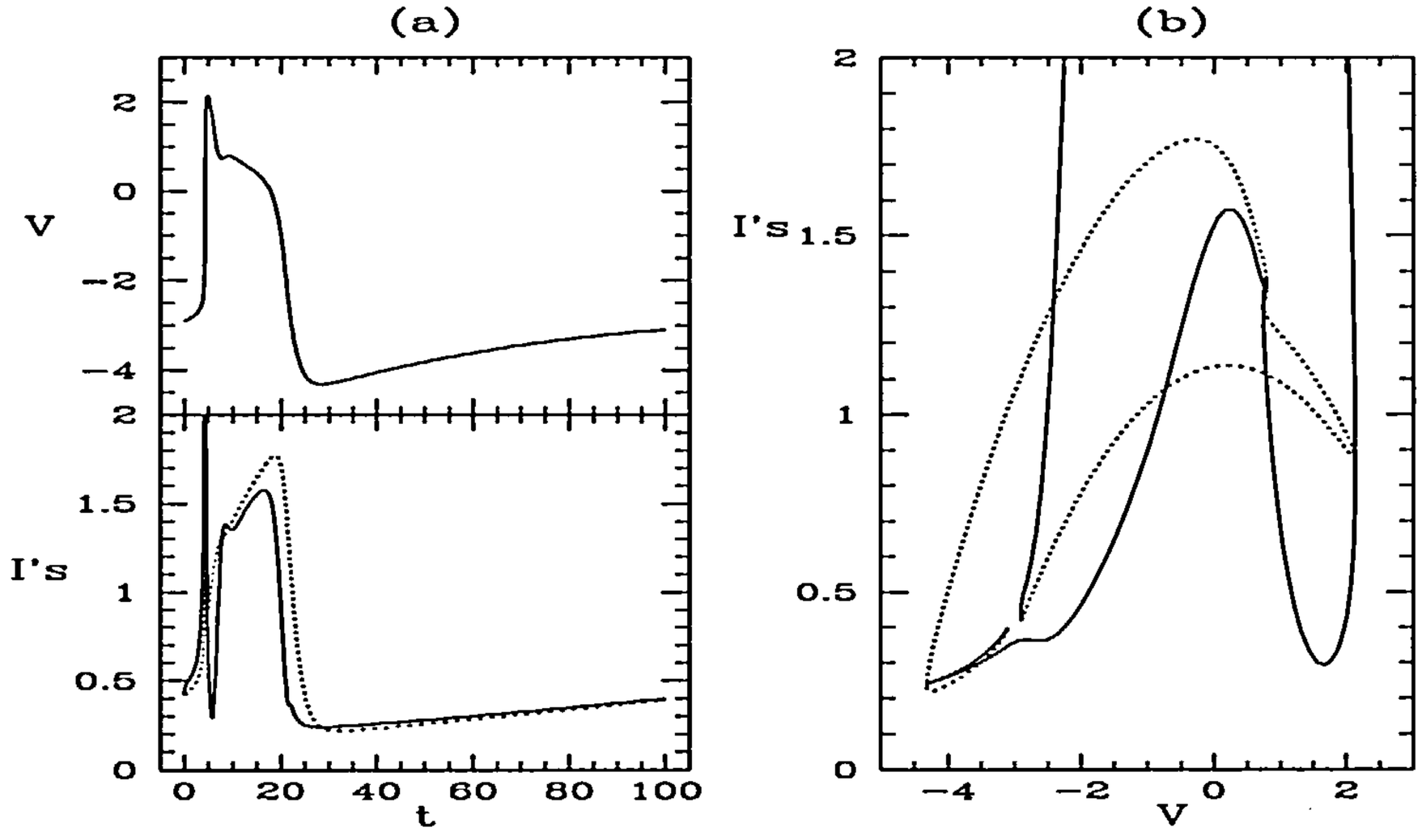

Figure 4.20: Simulation of equations (4.3) with a quartic $h_f(V)$, in particular $h_f(V) = 0.125(V^2-4)^2$. The normal parameter values (table 4.1) are used with the change $\epsilon_2 = 0.025$ and $\beta = 1.2$. Both (a) the time series of the voltage and currents and (b) the phase plane are plotted. I_1 is shown as a solid line and I_2 as a dotted line.

very similar to that with a cubic $h_f(V)$. In the quartic case the plateau is slightly longer and the overshoot is larger. The behaviour is excitable with the stable fixed point at $V = -3$ and $I_1 = I_2 \approx 0.43$ and, as before, the equations can be made oscillatory by lowering the value of $\bar{V}$.

Example nullcline structures for a quartic $h_f(V)$ are shown in figure 4.21. The quartic structure of $h_f(V)$ that we have chosen can be seen in plot (a). A similar behaviour to that of the cubic nullclines is seen. The quartic structure ensures that I_1 increases after the upstroke generating the overshoot and plateau in a similar manner to the previous section.

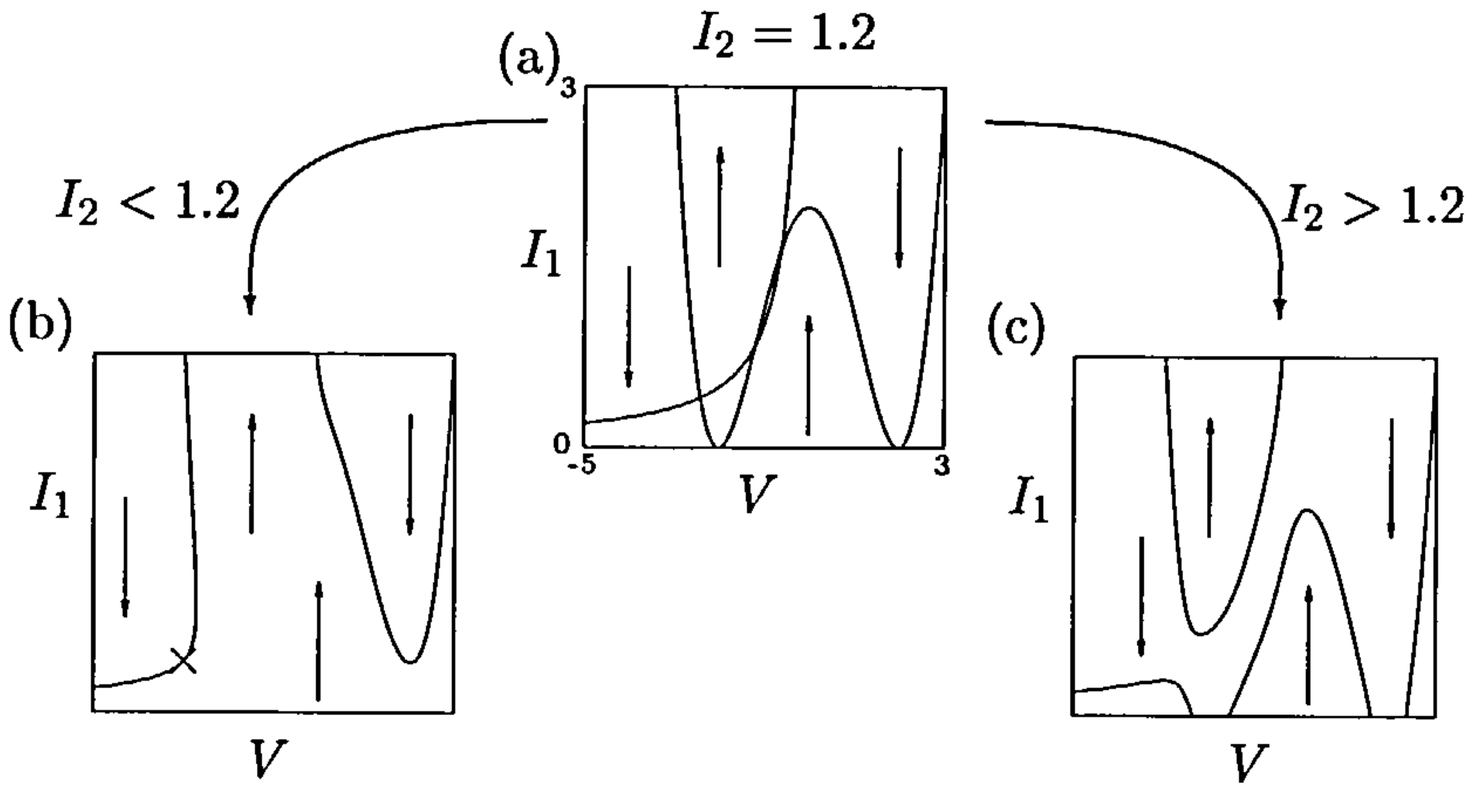

Figure 4.21: I_1 nullclines for the simple model with $h_f(V) = 0.125(V^2 - 4)^2$. The arrows indicate the direction of the flow and the fixed point is shown in (b) with a cross.

4.6.2 The Function $h_g(V)$

The function $h_g(V)$ helps to fix the structure of the I_2 nullclines. In this section we shall investigate our equations for different functions of $h_g(V)$; linear and quadratic, whilst keeping $h_f(V) = 1$. Note that changes in the function $h_g(V)$ do not alter the location of the fixed points.

Linear: $h_g(V) = k_1 V + k_2$

In choosing the initial form for $h_g(V)$ $(= 6V)$ we investigated varying k_1 whilst keeping $k_2 = 0$. We found that on decreasing k_1, thus decreasing the gradient of the curve $h_g(V)$, we get a Hopf bifurcation at $k_1 \approx 5.23$ giving oscillatory waves. Increasing k_1 increases the gradient of the curve $h_g(V)$. The stable fixed point remains but the plateau becomes shorter.

Small changes in the parameter k_2 have no major effect on the waves. On increasing k_2, $h_g(V)$ is raised. The result is that I_2 remains lower on the upstroke and the currents touch at a higher V. During repolarisation I_2 attains higher values. The result of a simulation is slightly higher amplitude excitable waves. On decreasing

k_2, we still get excitable waves but of a smaller duration. The reason for this is that I_2 gets higher on the upstroke leading to larger differences between the two currents during the plateau and repolarisation. Therefore there is a faster change in voltage throughout the plateau and repolarisation phases giving a shorter action potential duration.

Quadratic: $h_g(V) = k_1(V - k_2)^2 + k_3$

Recall that we used a (negative) quadratic in Model A, our polynomial approximation to the Noble model. The principal reason for this was to match the slight fluctuations in I_2 on the upstroke.

The results from a simulation using a quadratic $h_g(V)$ are shown in figure 4.22. The main effect on the I_2 trajectory is that it is flatter on the upstroke and does

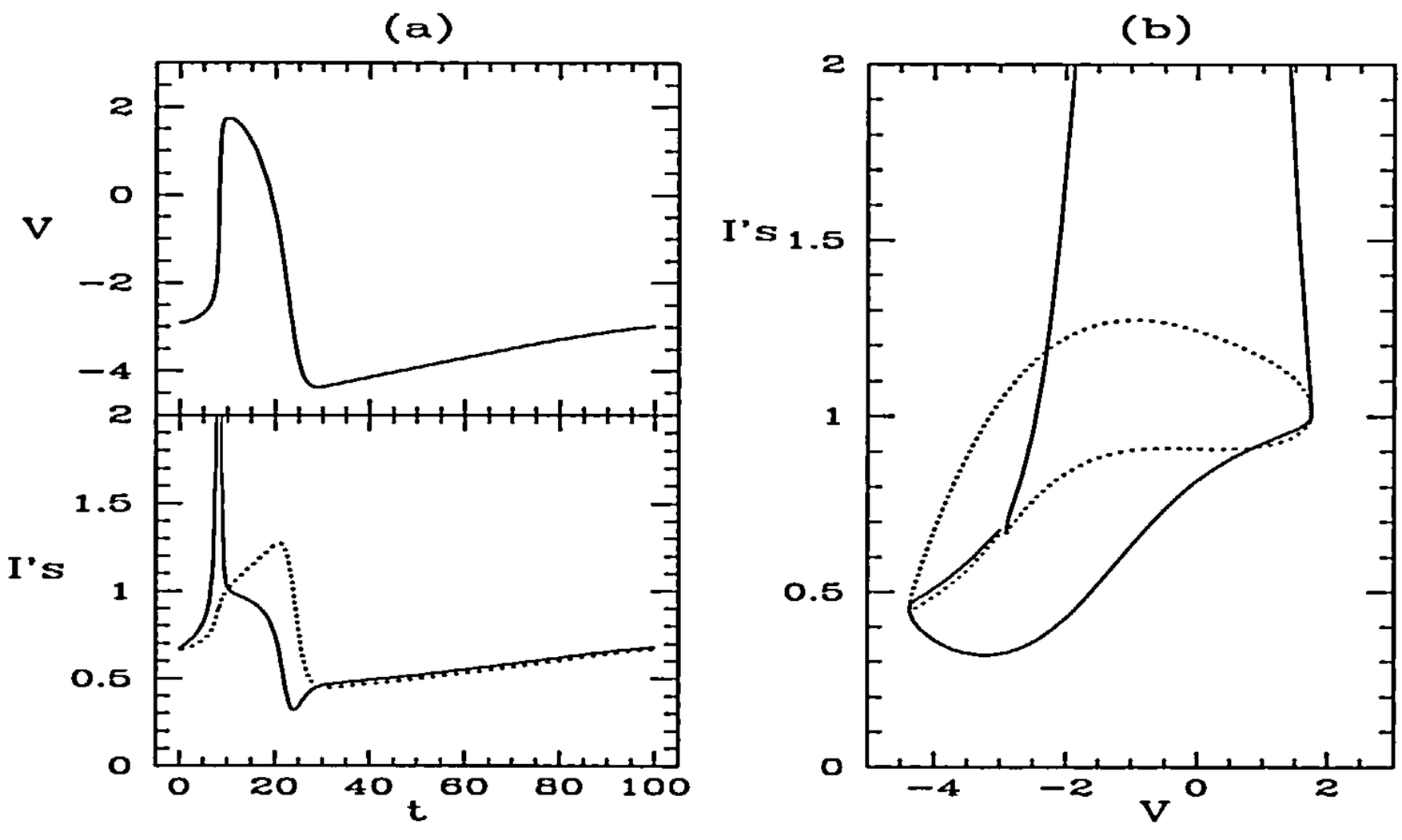

Figure 4.22: Simulation of equations (4.3) with a quadratic $h_g(V)$, namely $h_g(V) = -2V^2 + 1.5$ ($k_1 = -2$, $k_2 = 0$ and $k_3 = 1.5$). The parameter values in table 4.1 are used. Both (a) the time series of the voltage and currents and (b) the phase plane are plotted. I_1 is shown as a solid line and I_2 as a dotted line.

not reach as high values as previously. Therefore I_1 and I_2 are close throughout

the plateau phase and the resulting action potentials are of longer duration. The behaviour is excitable although can be changed to oscillatory in the usual manner by slightly decreasing $\bar{V}$.

We now look at the nullcline structure. Examples are shown in figure 4.23. In (a)

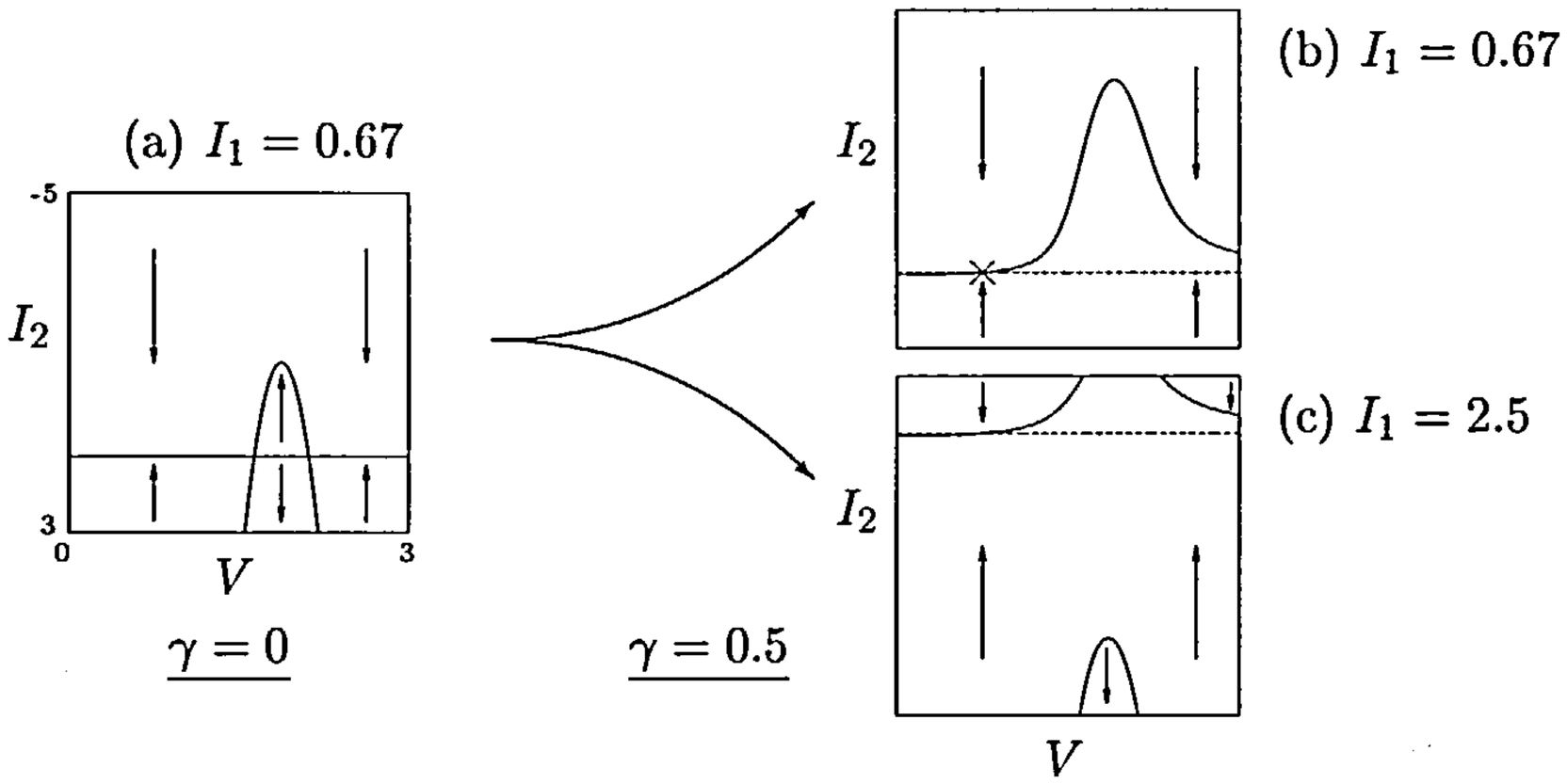

Figure 4.23: I_2 nullclines for the simple model with $h_g(V) = -0.2V^2 + 1.5$. The arrows indicate the direction of the flow and the fixed point is shown in (b) with a cross.

the I_2 nullclines are plotted with $\gamma = 0$ so that the structure of the parabola is clear. The effect of the coupling (with $\gamma > 0$) is shown in (b) and (c). During the upstroke, when I_1 is large, the I_2 nullclines are similar to those in (c). As a result of the middle (negative) parabola component of the nullclines, I_2 remains lower, and flatter, on the upstroke as noticed from the simulations. This results in the slightly longer plateau.

If γ is increased then the breaking apart of the two nullcline components of $\dot{I}_2$ is greater. As mentioned in section 4.5.3, the effect is to shorten the plateau and speed up the recovery to equilibrium. If γ is increased past $\gamma \approx 0.82$ then a Hopf bifurcation occurs and we get oscillatory waves.

If k_1 is made more negative the the parabola becomes steeper. The rate of change of I_2 away from its steady state value upon the initiation of an action potential is greater causing the system to be less excitable (as the I_1 nullclines close more

quickly). Increasing k_1 past a value of $k_1 \approx -1.91$, thus increasing the size of the parabola, causes a Hopf bifurcation to occur. I_2 stays lower on the upstroke and we get oscillatory waves.

If k_3 is reduced then the parabola is lowered. Excitable waves remain although the plateau length is reduced due to I_2 attaining higher values on the upstroke. Increasing k_3 raises the parabola and I_2 remains lower on the upstroke and the plateau length increases. If k_3 is increased past $k_3 \approx 2.31$ a Hopf bifurcation occurs and we get oscillatory waves.

We can also change the parameter k_2. If k_2 is increased, then the parabola moves to the right. I_2 then moves faster on the upstroke causing the system to be less excitable and shorter plateaus to occur. On decreasing k_2 the parabola moves to the left. I_2 stays lower on the upstroke and oscillatory waves result. (A Hopf bifurcation occurs at $k_2 \approx 0.069$).

One last point to note is that the behaviour of I_2 here is slightly different to the behaviour of Model A. This is due to I_1 continuing to decrease during repolarisation. Due to the coupling of the equations, I_1 affects the I_2 nullclines and hence the I_2 dynamics. As I_1 is low on the return to equilibrium the I_2 nullcline is similar to that in figure 4.23(b) throughout repolarisation. The trajectory of I_2 during repolarisation is fairly flat and does not get close to I_1 giving rise to the long plateau (and higher values of I_2). In the next section we will use a quadratic form of $h_g(V)$ together with a quartic form of $h_f(V)$.

4.6.3 The Functions $h_f(V)$ and $h_g(V)$

Just as in Model A of the previous chapter that closely approximates the Noble equations, we can investigate a simulation of the equations in this chapter with $h_f(V)$ as a quartic and $h_g(V)$ as a quadratic.

The results of a simulation are shown in figure 4.24. We have used forms of $h_f(V)$ and $h_g(V)$ discussed earlier in this chapter. Note that $\beta = 1.3$ is used (as I_2 now attains higher values) and $\epsilon_2 = 0.035$ (to prevent V getting too negative or oscillatory waves

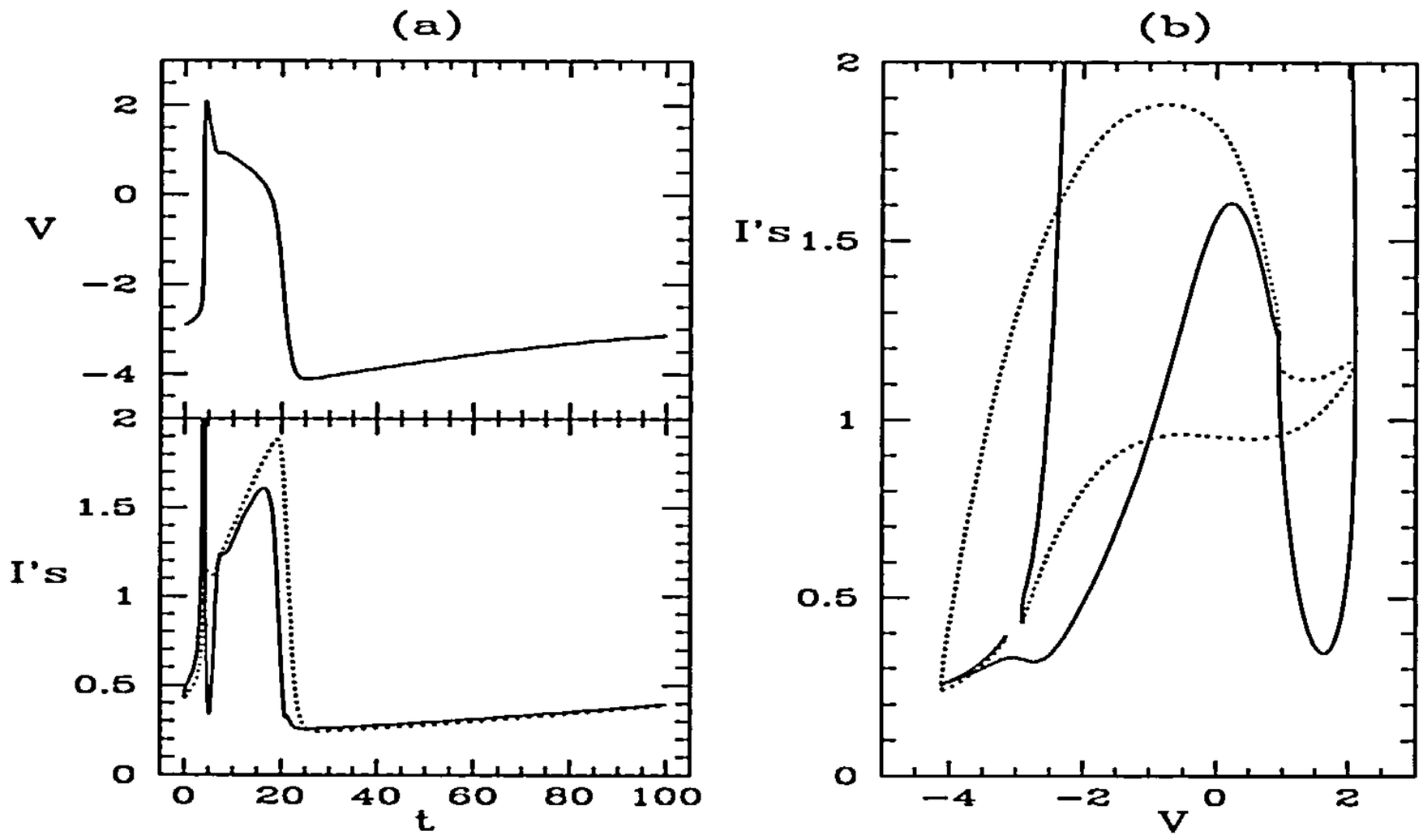

Figure 4.24: Simulation of equations (4.3) with a quartic $h_f(V)$ and a quadratic $h_g(V)$. $h_f(V) = 0.125(V^2 - 4)^2$ and $h_g(V) = -2V^2 + 1.5$. The normal parameter values (table 4.1) are used with the changes $\beta = 1.3$ and $\epsilon_2 = 0.035$. Both (a) the time series of the voltage and currents and (b) the phase plane are plotted. I_1 is shown as a solid line and I_2 as a dotted line.

occurring). We can see that these equations are excitable and have a fixed point at $V = -3$ and $I_1 = I_2 \approx 0.44$. The main features of a fast response action potential are seen. The upstroke is sharp and there is an overshoot giving a brief period of recovery. There is then a relatively long plateau phase before repolarisation of the action potential occurs. Repolarisation is fairly fast although not as quick as the upstroke and there is then a relatively long recovery to the equilibrium value. These equations can be made oscillatory in the usual way by increasing the value of $\bar{V}$.

4.7 Final Comments

We have investigated the behaviour of our simple model (equations (4.3)) for different parameter values and for different functions of $h_f(V)$ and $h_g(V)$. Changing these values alters the structure of the nullclines and hence the behaviour of the equations.

Not only can the behaviour of the equations be changed from oscillatory to excitable but by choosing appropriate functions $h_f(V)$ and $h_g(V)$ we can obtain action potentials of both the fast and slow response type.

Furthermore, by changing both the structure of $h_f(V)$ and $h_g(V)$ and the values of the parameters, we can change many properties of the action potentials. Examples include the location and stability of the fixed points (giving both excitable and oscillatory behaviour), the amplitude of the the action potentials, the size and speed of the upstroke, the extent of the overshoot, and the length of the plateau.

Chapter 5

Spatial Investigations

Thus far we have concentrated on single cell models of action potentials. However, during the heartbeat the action potential impulse spreads across the heart, from cell to cell (at velocities ranging from $0.03ms^{-1}$ in the sinoatrial node to $0.6ms^{-1}$ in the atria and ventricles). Recall that the normal pattern of propagation is as follows. The impulse is initiated at the sinoatrial node (the normal pacemaker of the heart) and spreads across the atrium before passing through the atrioventricular node. The impulse then travels through the bundle of His and the Purkinje fibres, and spreads out into the ventricular muscle. This allows synchronous electrical activation and, therefore, synchronous contraction of the thick ventricle walls. To model this propagation of voltage across the heart one needs to combine single cell excitation models, as in the previous chapter, with a model describing propagation between cells.

Since cardiac tissue is cellular it should ideally be studied as a discrete system of coupled cells. Unfortunately in many cases this is not possible due to the computational requirements of simulating vast systems of coupled differential equations. To overcome this computational difficulty cellular automata models can be used [2, 59]. These models are rather abstract and, although computationally efficient, they are unrealistic from the viewpoint of electrophysiology and the resulting wave patterns often reflect the geometry of the lattice used. Therefore continuum models based on partial differential equations are frequently employed in the study of action potential propagation. In reality the heart is a highly inhomogeneous anisotropic

medium and in using a partial differential equation to model it we are assuming that the tissue behaves as a continuum, neglecting the fine-scale properties of electrical propagation within and between cells. The partial differential equations for heart tissue are parabolic, nonlinear and of the reaction-diffusion type. Such partial differential equation models, together with an excitability property, provide the most common computational approach to wave phenomena in cardiac tissue and this is the approach we use here. In recent years work has been carried out on models of the heart with a more realistic spatial structure [39, 37, 41, 59]. However this approach is extremely computationally demanding, especially if electrophysiological models of excitation are used.

In this chapter we are concerned with spatial simulations using the ionic current models discussed in the previous chapters. We shall concentrate principally on one-dimensional studies but towards the end of the chapter will include some two-dimensional simulations.

Before proceeding we shall briefly discuss the theory of propagation in cardiac tissue.

5.1 Theory of Propagation

The propagation of an electrical impulse depends upon the flow of electric current along muscle fibres from excited to resting regions. In some regions of the heart, such as the Purkinje fibres, the flow is along a cylindrical fibre and so propagation can be treated as one-dimensional. However in most regions of the heart, such as the atria and ventricles, the geometry is more complicated and the impulse spreads across a higher dimensional space. The theory of multidimensional propagation in excitable tissue is complex and we shall only discuss the one-dimensional case here. Higher dimensional analysis can be found in [47].

Cardiac cells are roughly cylindrical and one-dimensional propagation (across many cells) may be modelled by considering the cardiac tissue as a simple cylindrical cable as shown in figure 5.1. Here the axial flow of current is denoted by I_a, and the

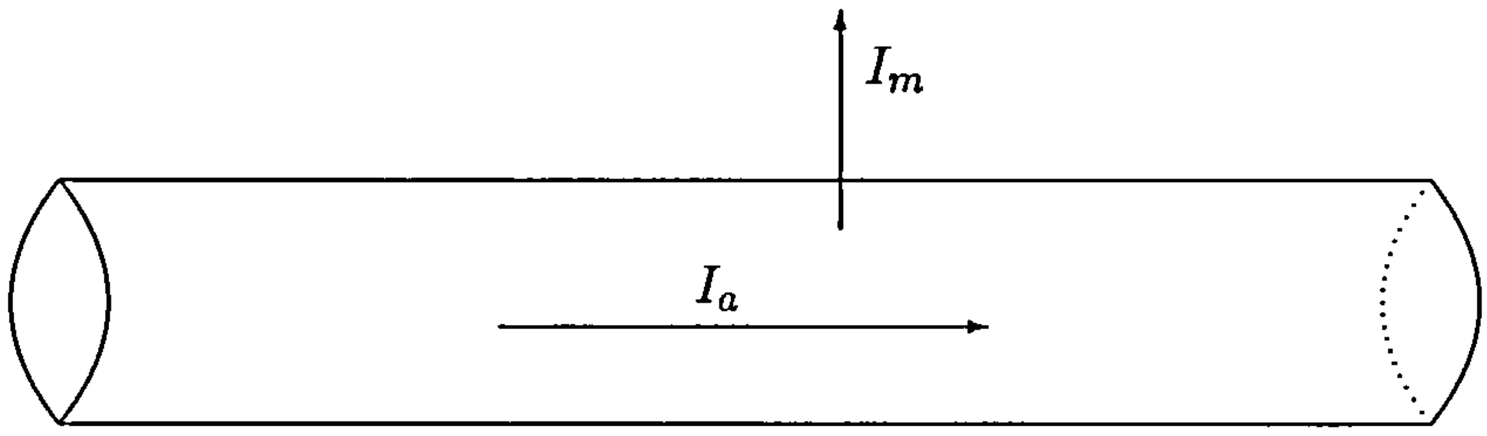

Figure 5.1: Cable model for one-dimensional propagation.

membrane current by I_m. The flow of current along the fibre will be proportional to the voltage gradient (assuming Ohm's law holds). Hence

$$\frac{\partial V}{\partial x} = -R_a I_a \tag{5.1}$$

where R_a is the resistance per unit length of fibre. As the axial current, I_a, flows along a fibre, some of it leaks across the surface membrane as membrane current, I_m. The membrane current in any region is therefore equal and opposite to the change in axial current across the region, i.e.

$$I_m = -\frac{\partial I_a}{\partial x} \tag{5.2}$$

Combining equations (5.1) and (5.2) gives us

$$I_m = \frac{\partial}{\partial x}\left(\frac{1}{R_a}\frac{\partial V}{\partial x}\right)$$

Thus the membrane current is proportional to the second derivative of the voltage. The total membrane current, I_m, includes both a capacity current, I_c, and an ionic current, I_i, (made up of Na^+, K^+, Ca^{2+} and other ions). i.e.

$$\begin{aligned} I_m &= I_c + I_i \\ &= C_m\frac{\partial V}{\partial t} + I_i \end{aligned}$$

where C_m is the membrane capacitance which we assume to be constant. We therefore get the following equation for the voltage propagation,

$$\frac{\partial}{\partial x}\left(\frac{1}{R_a}\frac{\partial V}{\partial x}\right) = C_m\frac{\partial V}{\partial t} + I_i$$

or

$$\frac{\partial V}{\partial t} = \frac{\partial}{\partial x}\left(D\frac{\partial V}{\partial x}\right) - \frac{1}{C_m}I_i$$

where D is the diffusion coefficient (with units of cm^2s^{-1}). The diffusion coefficient plays an important quantitative role and determines the spread of voltage and the conduction velocity. D has varying values in different parts of the heart and in different directions. (Electrical conductivity is greater along fibres (longitudinally) than across them (transversely)). A typical value of the diffusion coefficient longitudinally (for atrial tissue) is $D \approx 1cm^2s^{-1}$ although values given in literature vary considerably. (See [45]). For our purposes we will assume that the diffusion coefficient is constant everywhere and hence

$$\frac{\partial V}{\partial t} = D\frac{\partial^2 V}{\partial x^2} - \frac{1}{C_m}I_i \tag{5.3}$$

In our following analysis the ionic current, I_i, will be described by the currents I_1 and I_2 in the previous chapters. Note that due to the nonlinearity of the current equations the only way to obtain a solution to equation (5.3) is by numerical simulation.

5.2 Model Equations

In the single cell case, when the system is spatially uniform and there is no propagation, $\frac{\partial V}{\partial x} = 0$. There is no net current flow into or away from the cell and the membrane current $I_m = 0$. From equation 5.3 we then have

$$\frac{dV}{dt} = -\frac{I_i}{C_m}$$

In Chapters 3 and 4 (after scaling by a factor of $1/C_m$) we studied single cell models of this type. Recall that our equations are of the following form,

$$\begin{aligned}
\dot{V} &= I_1 - I_2 \\
\dot{I}_1/\epsilon_1 &= -(VI_1 + \delta)(I_1 - h_f(V)) + \alpha(\beta - I_2) \\
\dot{I}_2/\epsilon_2 &= (I_1 - I_2)(I_2 - h_g(V)) + \gamma(V + \bar{V})
\end{aligned}$$

In order to incorporate diffusion into these equations we need to recall the general form of equations from which they were derived (following the change of variables in the Noble model). This was as follows,

$$\begin{aligned} \dot{V} &= I_1 - I_2 \\ \dot{I}_1/\epsilon_1 &= f_1(V, I_1)\dot{V} + f_0(V, I_1) \\ \dot{I}_2/\epsilon_2 &= g_1(V, I_2)\dot{V} + g_0(V, I_2) \end{aligned}$$

Only one of the state variables, voltage, interacts diffusively and including this into these equations gives

$$\begin{aligned} \dot{V} &= D\nabla^2 V + I_1 - I_2 \\ \dot{I}_1/\epsilon_1 &= f_1(V, I_1)\dot{V} + f_0(V, I_1) \\ \dot{I}_2/\epsilon_2 &= g_1(V, I_2)\dot{V} + g_0(V, I_2) \end{aligned} \tag{5.4}$$

where D is the diffusion coefficient, ∇^2 is the diffusion operator, and the functions $f_1(V, I_1)$, $f_0(V, I_1)$, $g_1(V, I_2)$, $g_0(V, I_2)$ are nonlinear functions. It is important to note here that due to the V term appearing in the I_1 and I_2 equations the diffusion of the voltage affects the rate of change of the currents. Finally note that by rescaling length in (5.4) the diffusion coefficient, D, may be scaled to 1. We shall fix $D = 1$ for the remainder of this chapter and consider changes in the length scale.

5.3 One Spatial Dimension

We shall initially consider one spatial dimension. The diffusion operator ∇^2 becomes $\frac{\partial^2 V}{\partial x^2}$ and we have the following equation for voltage,

$$\dot{V} = \frac{\partial^2 V}{\partial x^2} + I_1 - I_2$$

5.3.1 Initial Discussion

In our numerical scheme for the one-dimensional domain we impose periodic boundary conditions. We use spectral time stepping for diffusion and second-order Adams-

Bashforth time stepping for the kinetics. Further details of the numerics may be found in Appendix A.3.

The effect of using periodic boundary conditions is to stimulate a new wave each time the action potential has crossed the spatial domain. This is analogous to studying a wave travelling around a ring of excitable tissue. As the length decreases, the equations are stimulated at a higher frequency. Therefore, at length scales shorter than the length of a free travelling wave, a new action potential is initiated before the previous one has fully recovered. This behaviour is an example of reentry in which the action potential pulse enters tissue that has already been excited by the previous wave. Reentry of an electrical wave over a one-dimensional path such as a ring can occur in actual myocardium due to the heterogeneous distribution of tissue. A wave travelling across the heart can begin (via a conduction block) to propagate around an inexcitable obstacle in the tissue (for example the aorta, a scar or a bundle of connective tissue). If the circulation time is large enough to permit repeated excitation the wave will follow a circular path around the obstacle. Indeed this type of anatomical reentry has been shown to be the mechanism underlying certain cardiac arrhythmias [13]. Anatomical reentry in cardiac tissue of this type dates back to 1914 when Mines [1] generated reentrant excitation in a ring of cardiac tissue taken from the heart of a dog. On stimulating one point of the ring, a circulating pulse was generated. More recent studies of this experiment have been carried out [14] and as the circumference of the ring is decreased, so that the tissue in the ring is excited before recovering fully from the previous action potential, changes in the behaviour of wave propagation are observed. In general, at short lengths, both the duration of the action potential and the speed of propagation decrease. If the length is decreased past a certain size so that the stimuli are too closely spaced in time, the behaviour becomes unstable and complex fluctuations in the action potential duration are observed. The tissue responds with an alternating sequence of short and long action potential durations and recovery times. This phenomenon is frequently referred to as alternan behaviour. Alternan behaviour has been observed numerically in partial differential equation models [11, 17, 18] and has recently been shown to result from a Hopf bifurcation [26] (see also [38]). For the 1962 Noble

model it is found that alternans occur when wave period becomes less than about $260ms$ and an example wave train is shown in figure 5.2.

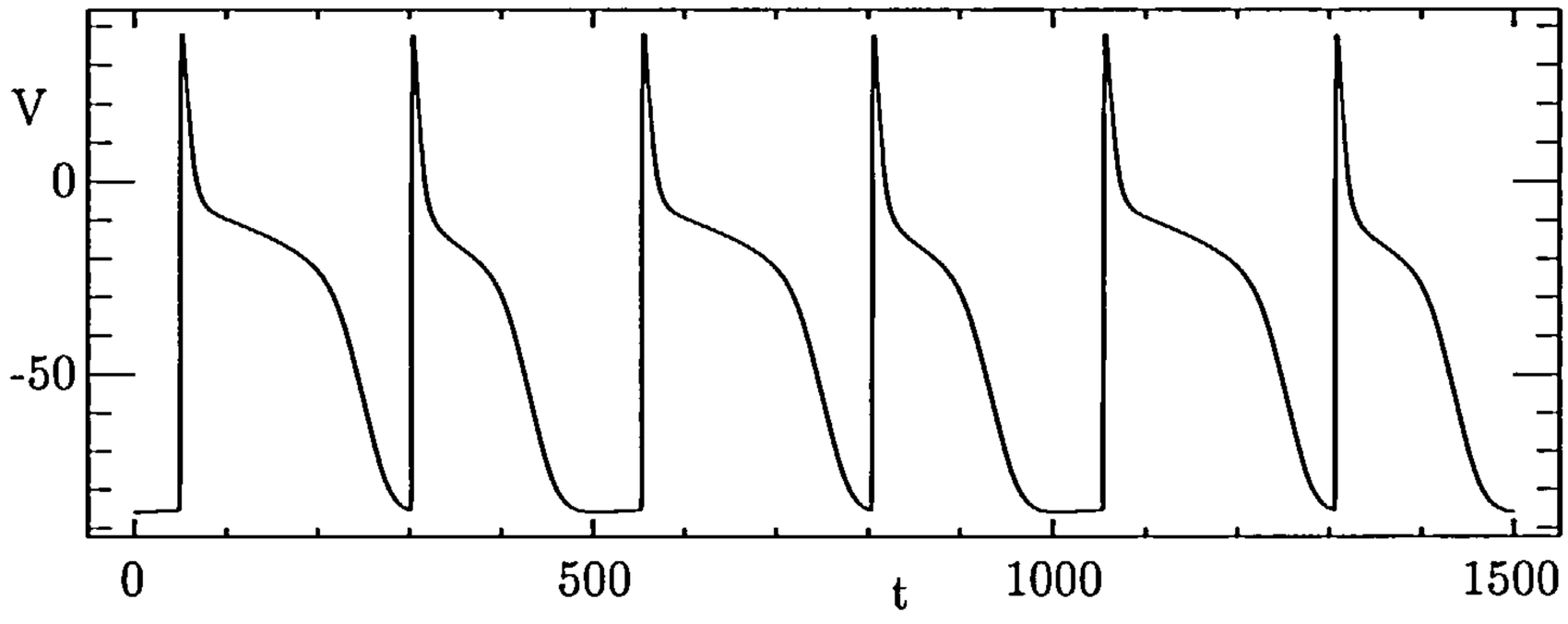

Figure 5.2: Alternan behaviour for the Noble model.

5.3.2 Restitution and Dispersion

Restitution and dispersion are two important quantitative measures of wave phenomena in excitable media.

Restitution is a relation between the diastolic interval (the time from the end of an action potential and the initiation of the next one) and the duration of the next action potential, both which are shown in figure 5.3. A short diastolic interval typically generates a short action potential and vice-versa.

Dispersion is a relation between the speed of the front end of an action potential (moving in space) at a certain location and the time since the back end of the previous action potential passed through the same location (the diastolic interval). Again these terms are shown in figure 5.3.

In cardiac tissue there is a strong dependence of the action potential duration on the diastolic interval and the restitution property is important. The size of an action potential propagating in the wake of a preceding action potential is shortened if recovery to equilibrium of the system has not been completed. This is due to the local ionic currents having not fully recovered. The closer the action potentials,

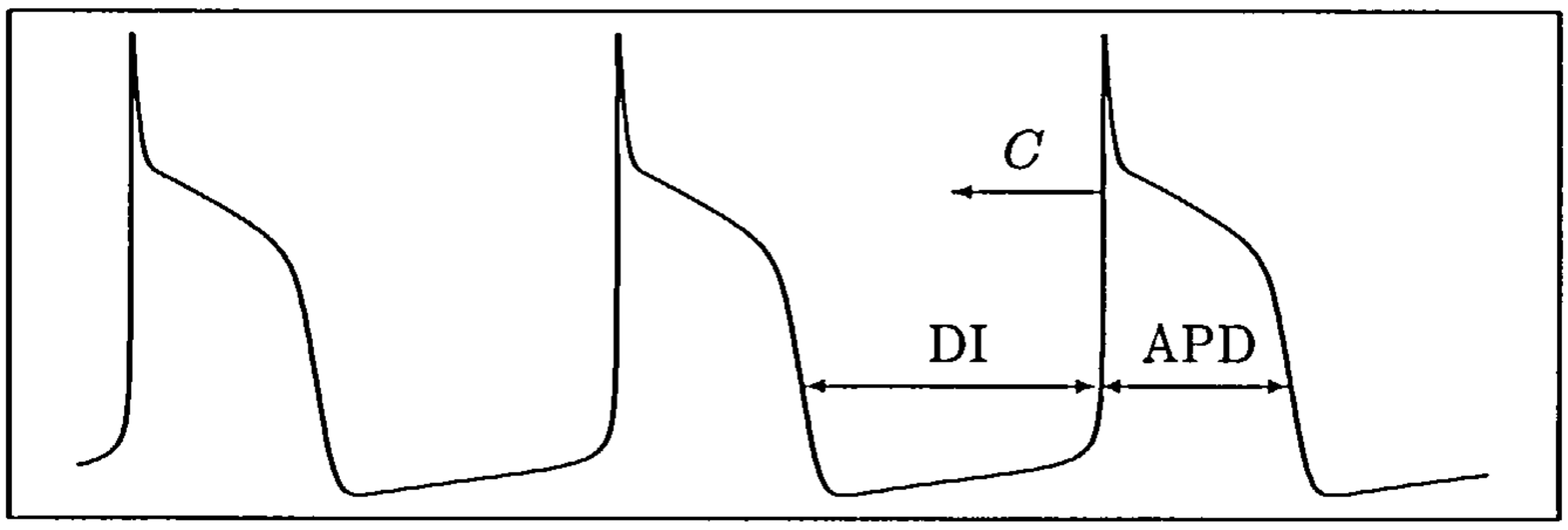

Figure 5.3: Time intervals involved in restitution and dispersion. The wave train is travelling from right to left across space and C is the speed of the action potential, APD is the action potential duration and DI is the diastolic interval.

the shorter the duration of the following action potential. If action potentials are stimulated too frequently then the system is not excitable and no action potential occurs. The refractory property of cardiac tissue is clearly important. The atria and ventricles need to be filled with blood before contraction occurs if the heart is to act as an efficient pump. Premature contraction will not pump blood in an effective way. The restitution property has been linked to alternan behaviour occurring in waves propagating in one-dimensional loops [7, 26] (mentioned above), and also to phenomena in higher dimensions (see later).

Unlike in other excitable media, dispersion is usually weak in cardiac tissue, and although the pulse speed decreases monotonically as the rate of stimulation increases, the speed of propagation is not very sensitive to the post-repolarisation state. When the diastolic interval falls below a certain size however, the pulse speed vanishes. In fact, in general, dispersion curves for excitable media have an upper (faster) stable branch and a lower unstable branch. They meet in a limit point giving this smallest diastolic interval that fails to produce an action potential. Premature stimulation at a diastolic interval less than this point will not initiate an action potential. This can prevent the propagation of the pulse and is known as a conduction block.

In the following analysis we use normalised restitution and dispersion curves. This

facilitates the comparison of dimensionless models (such as FitzHugh-Nagumo and the models presented in the previous two chapters) and physiological models (such as Noble). As the length of the domain decreases, the speed of propagation of the pulse, C, the action potential duration, APD, and the diastolic interval, DI, all decrease. We normalise the speed by the speed of a free travelling pulse, C_0, and the action potential duration and diastolic interval by the action potential duration of a free travelling pulse, APD_0.

The normalised restitution and dispersion relations for the FitzHugh-Nagumo model are shown in figure 5.4(a). It can be seen from figure 5.4(a) that, unlike cardiac tis-

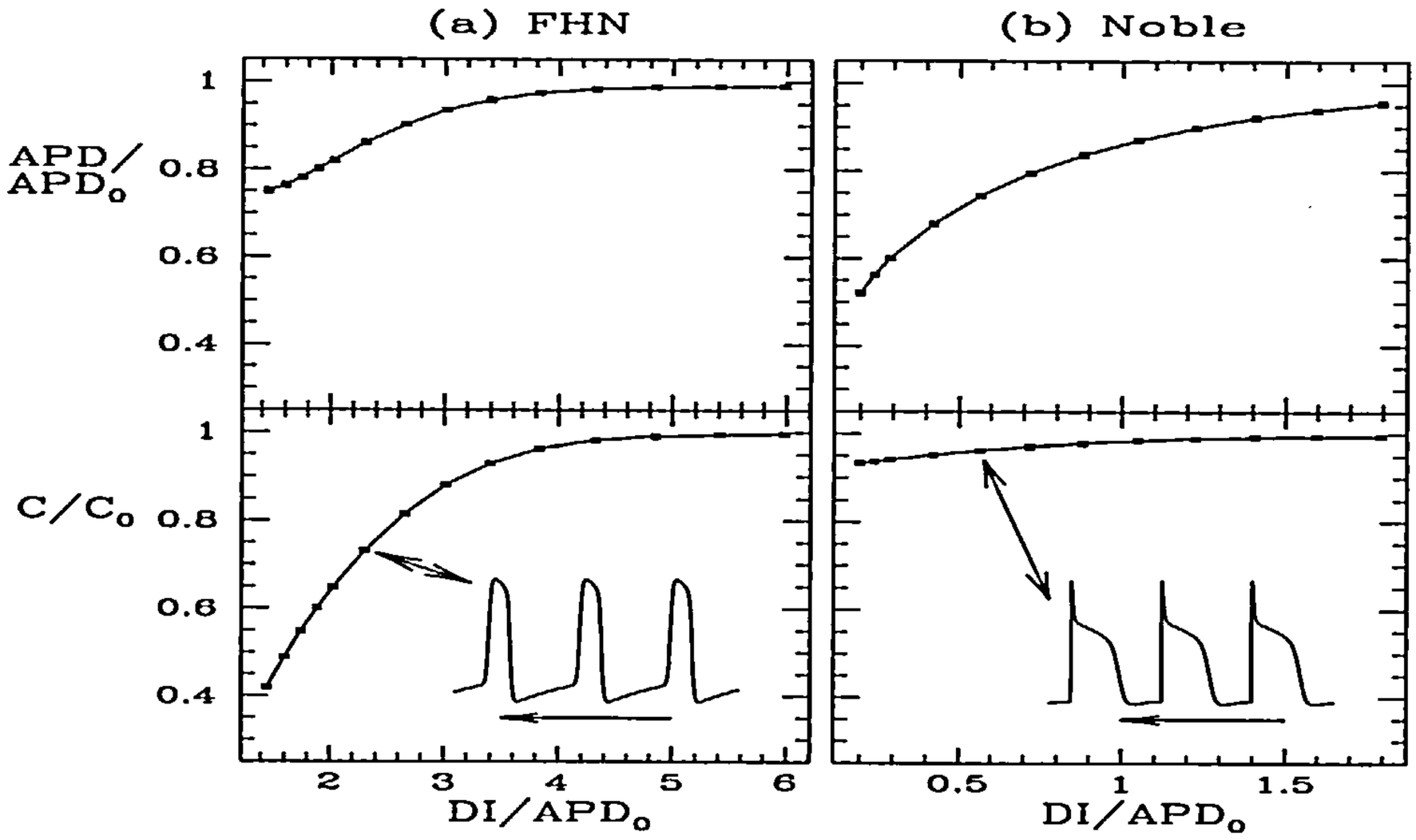

Figure 5.4: Normalised restitution and dispersion curves for (a) the FitzHugh-Nagumo (FHN) model and (b) the Noble model. Typical wave trains for both models are also shown with the direction of propagation indicated by an arrow. (a) The same parameters as in Section 2.6 are used ($a = 0.15$, $\epsilon = 0.002$ and $\gamma = 2.5$). Simulations were carried out with 128 grid points and a time step of 0.1. The action potential duration was measured when $V > 0.1$. (b) $\tilde{g}_{Na} = 0.132$ is used in simulations with 4096 grid points and a time step of 0.05. The action potential duration was measured when $V > -70$.

sue in which restitution is strong, the restitution property for the FitzHugh-Nagumo model is fairly weak with the action potential duration at the shortest length supporting waves around 75% of that of a free travelling wave. The dispersion property of the FitzHugh-Nagumo model, however, is strong. The speed of the wavefront at short lengths is around only 40% of the speed of a free travelling wave.

Ionic models, such as the 1962 Noble model, have more accurate restitution and dispersion relations. Normalised restitution and dispersion curves for the Noble model (in terms of currents) are shown in figure 5.4(b).* It can be seen that the restitution relation is stronger than that of the FitzHugh-Nagumo model. At short lengths the action potential duration is around half that of a free travelling wave. Furthermore, the weakness of dispersion is evident with the speed varying over a factor of around only 7% with changes in the diastolic interval.

We shall now investigate the restitution and dispersion properties of the models developed in the previous two chapters with an example of both a fast and slow response action potential.

5.3.3 Fast Response

We begin by looking at Model A from Chapter 3 that has dynamics closely matching those of the Noble model. Calculated restitution and dispersion curves are compared with those of Noble in figure 5.5. It can be seen that both the restitution and dispersion curves are of a similar shape and while the curves do not agree exactly, in particular the restitution curve (which is slightly steeper), there is a significant improvement over FitzHugh-Nagumo. In both, the restitution relation is strong whereas the dispersion relation is weak. The time series for similar points on the curves are also shown and we can see that the wave trains match closely.

*Note that for the Noble model we have set the diffusion coefficient to 1 for the purpose of analysing the normalised dispersion and restitution relations. The actual speeds of propagation (and the length scale) are therefore altered, although this does not affect the shape of the curves.

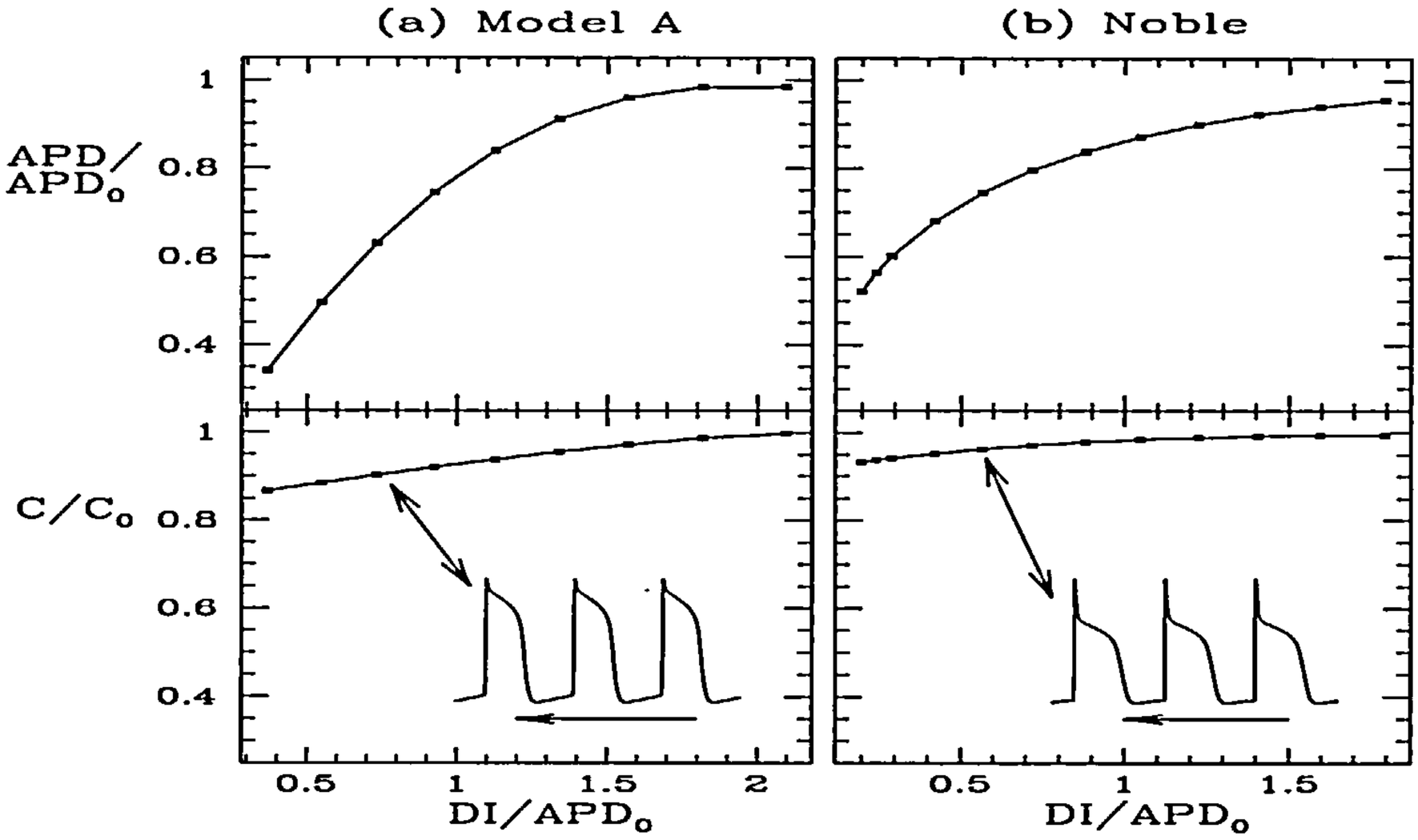

Figure 5.5: Normalised restitution and dispersion curves for (a) Model A (the polynomial model approximating Noble) and (b) the Noble model as in figure 5.4. For Model A, $h_f(V)$ and $h_g(V)$ are as in Chapter 3 with the parameters $c_f = 20$, $m = 3.14$, $\epsilon_1 = 0.0055$, $\epsilon_2 = 0.0175$, $c_g = 0.005$ and $\bar{V} = 75$. Simulations were carried out with 1024 grid points and a time step of 0.05. The action potential duration was measured when $V > -70$.

Discussion

Although the basic behaviour of the two models is similar a few differences were observed whilst running simulations.

Firstly, one effect of incorporating diffusion into Model A is to lessen the extent of the spike. This can be seen in the wave trains in figure 5.5. Although the Noble and Model A action potentials are essentially of the same shape, the voltage in Model A does not get as positive on the upstroke and the amplitude of the waves is slightly reduced. For example, in the wave train shown the voltage reaches a value of $V \approx +10$ compared to $V \approx +35$ in Noble. (Wave trains at different length scales have similar action potentials). The reason for this reduction in amplitude is that,

on adding diffusion, the rate of change of the fast inward current I_1 increases during the later stages of the upstroke (when $\frac{\partial^2 V}{\partial x^2}$ is large). Therefore it returns to lower values more quickly than in the single cell simulations.

Another difference between the behaviour for the Noble model and Model A, its approximation, is observed in the restitution relation. Whereas in the Noble model the actual duration of the action potentials varies over a factor of roughly 2, the action potential duration in Model A varies over a greater factor of around 10.[†] The action potentials at small lengths get very short in comparison with the action potential duration of a free travelling pulse. This effect is not apparent in the normalised restitution curve as the diastolic interval changes in a corresponding manner. That is, the ratio between the size of the diastolic interval and the action potential duration in Model A remains more constant than in the Noble model. To explain this behaviour we discuss the dynamical basis of the restitution relation. It appears from our investigations that it is the inward current I_2 that plays the dominant role. As the length of the domain is reduced, I_2 is more affected by the diffusion of voltage. During the upstroke, when $\dot{V}$ has the greatest effect on the current equations, I_2 attains higher values. This behaviour is also observed in simulations of the Noble equations on a one-dimensional ring and is shown for Model A in figure 5.6. As the length of the domain decreases, I_1 and I_2 cross at a higher value following the completion of the upstroke. Recall that this occurs when the voltage changes direction at its uppermost value. A consequence of this change is that, following the overshoot, the currents become close at a higher value. The trajectory thus remains on the plateau (where $\dot{V}$ is small) for a shorter period of time. Therefore, at smaller domain lengths, the plateau is shorter and the action potential duration is reduced. In the Noble model, this behaviour continues until the time spent on the plateau is roughly halved, after which action potentials cease to exist. However, in Model A the behaviour continues until the currents spend very small periods on the "plateau portion" of the phase portrait (as shown in the figure). Following further reductions in the length scale, the action potentials persist with the behaviour of I_2 increasing on the upstroke and decreasing during repolarisation

[†]In the restitution and dispersion curves action potentials down to around 30% are plotted.

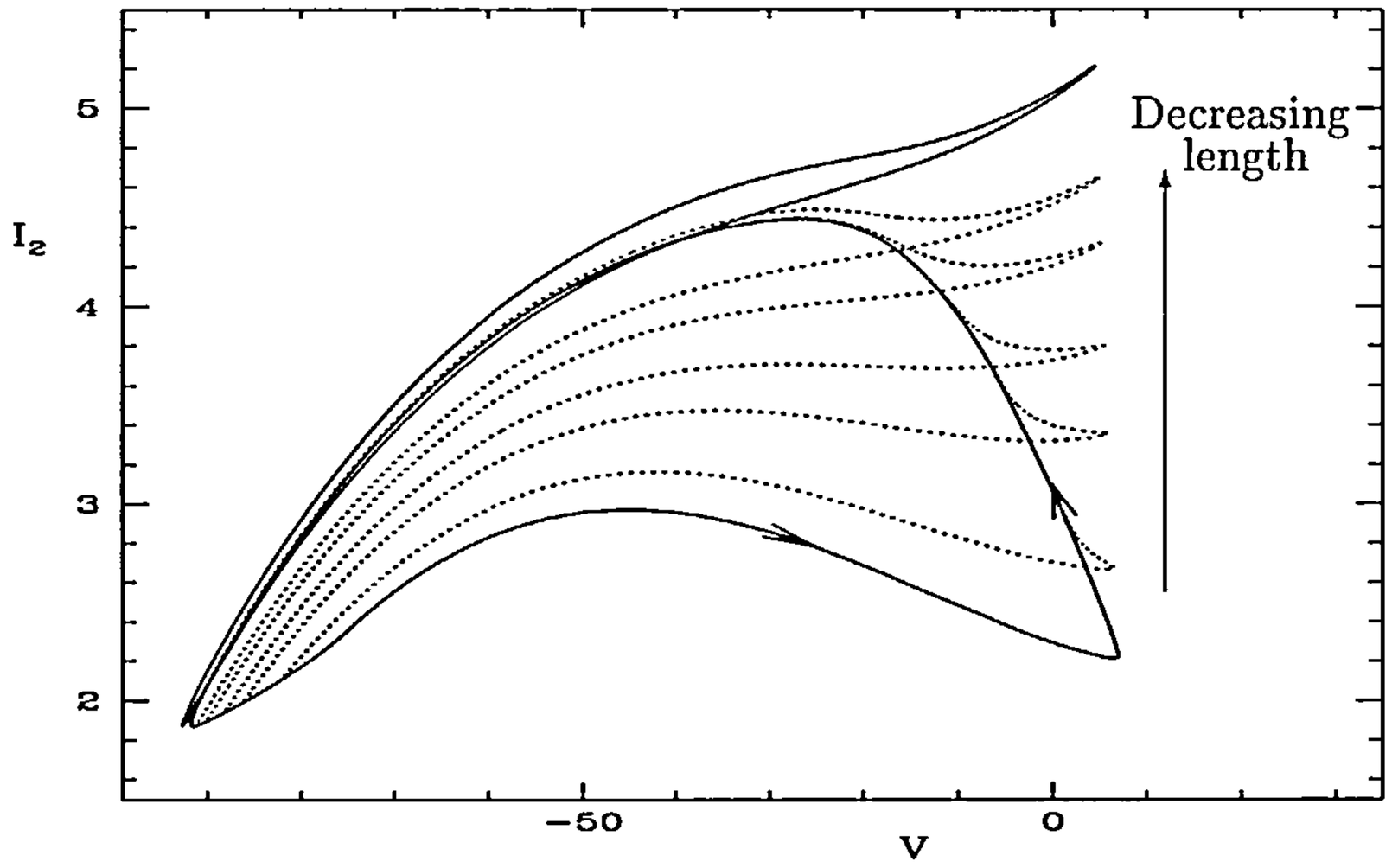

Figure 5.6: Behaviour of the outward current I_2 as the length scale is changed for Model A.

without spending any time on the plateau portion of the phase portrait (similar to the uppermost trajectory in figure 5.6). In fact it can be seen that, due to the higher value of I_2 on the upstroke, the quadratic component of the $\dot{I}_2$ equation plays a small part in the I_2 dynamics at small length scales.

Alternans

Recall from earlier in this section that when the period of stimulation in the Noble model becomes sufficiently low, alternan behaviour occurs (figure 5.2).

Although we did not observe a lower limit giving rise to this type of behaviour for Model A (due to very short action potential durations being possible as discussed above), alternans were frequently observed during our investigations upon changing the length scale or a parameter value. This behaviour would persist for several action potentials before steadily dying down to give a uniform travelling pulse. Model A is based on the dynamics of the Noble model (which exhibits alternans) and also seems to support alternan behaviour to some extent. A typical example of observed

alternan behaviour in a simulation of Model A is shown in figure 5.7.

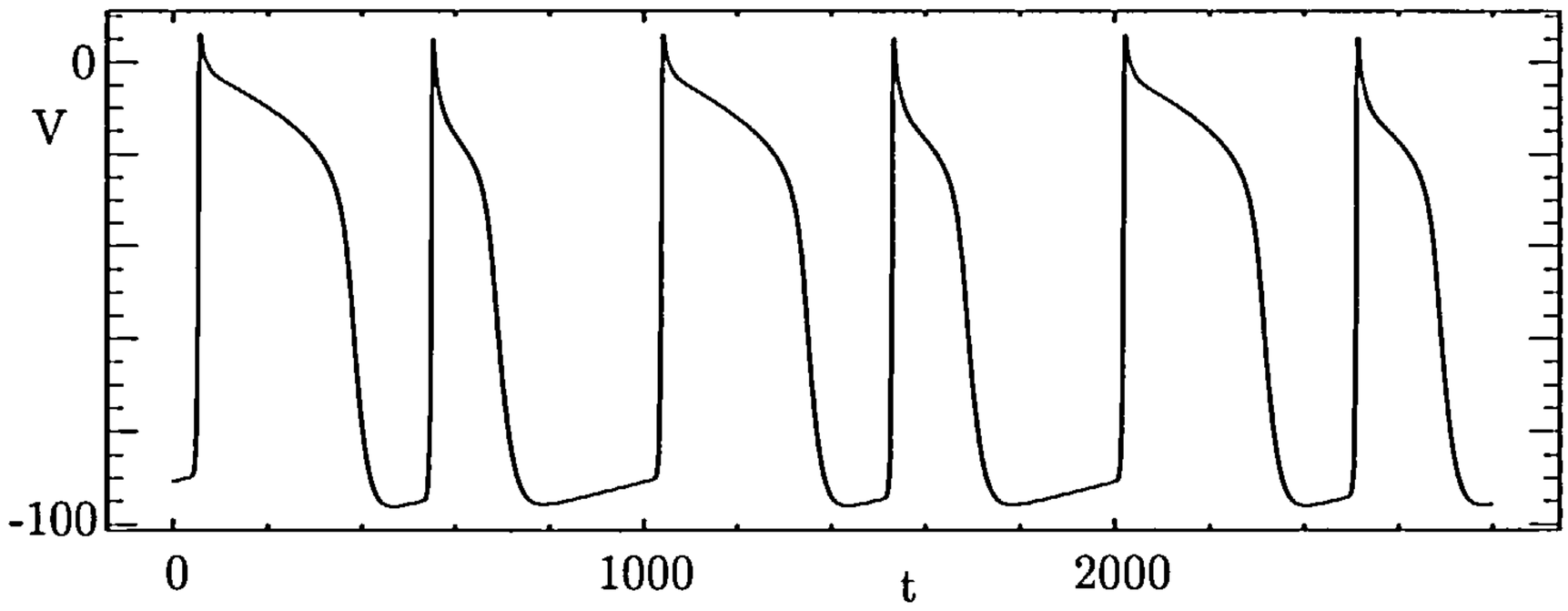

Figure 5.7: Alternan behaviour for Model A.

The observed trajectory of the inward and outward currents in the phase plane during alternans is as follows. The trajectory of I_1 remains relatively constant compared with that of I_2. During oscillations associated with alternan behaviour, the trajectory of I_2 during the upstroke rises and falls, varying between two particular trajectories of the types shown in figure 5.6. This behaviour is shown in figure 5.8 and also occurs for the Noble model during alternans. This observation suggests that the dynamics of the outward current I_2 plays an important role in alternan behaviour although at present we are not certain of the exact dependence or dynamical basis of this phenomena. It is worth noting here that in the (original) FitzHugh-Nagumo equations, and in some modified models improving restitution properties, (for example [40]), alternans are not observed. They can however be obtained by suitable modifications of the FitzHugh-Nagumo equations, as in [23], although the mathematical representation of the equations tend to be rather complicated.

5.3.4 Slow Response

We can also calculate restitution and dispersion relations for action potentials typical of the slow response (such as those shown in figure 4.6). For this we use the simple models discussed in the previous chapter. Example curves are shown in figure 5.9 together with those of the Noble model.

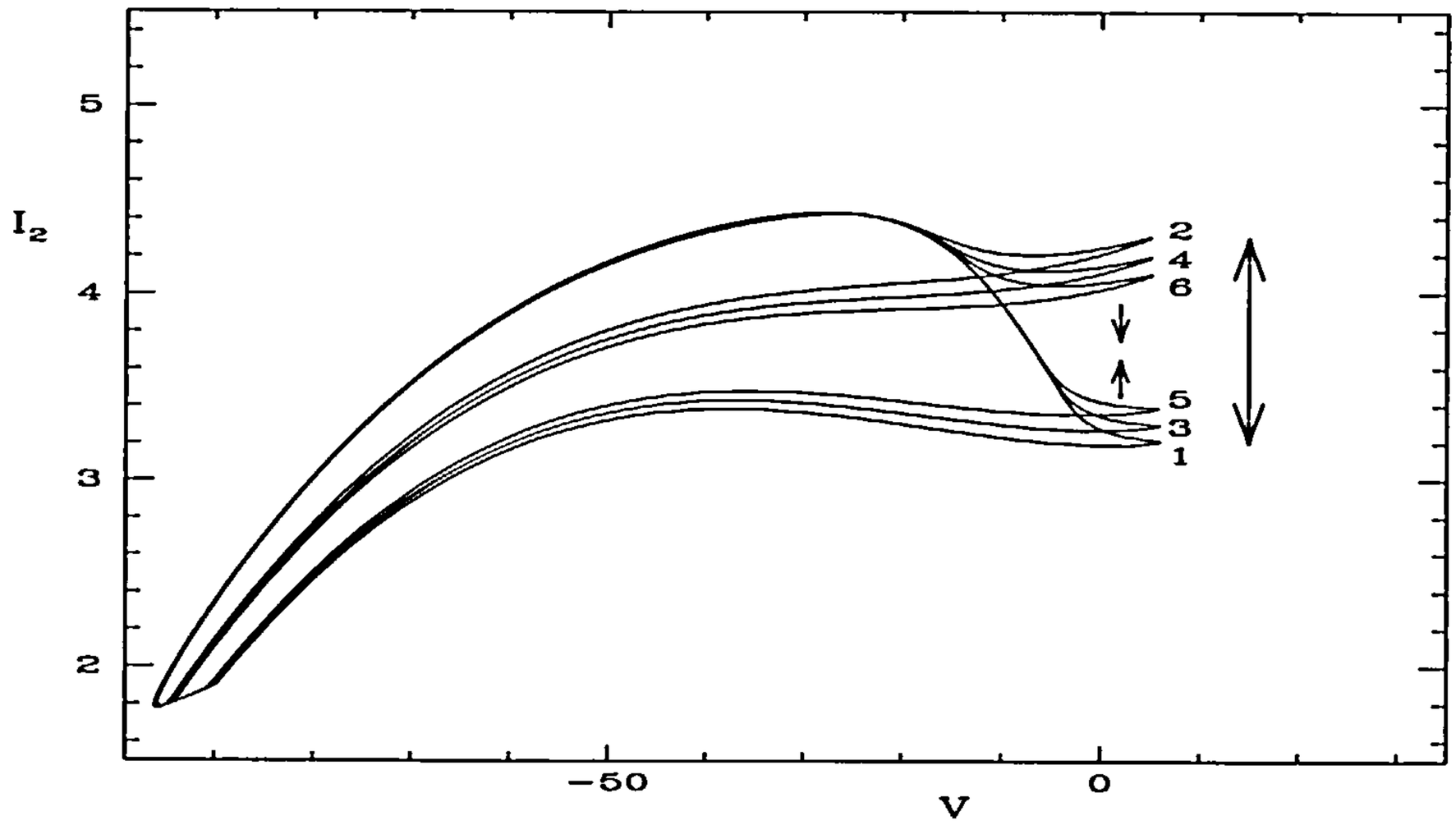

Figure 5.8: Behaviour of the current I_2 during alternans for Model A. The trajectory oscillates between high and low values of I_2 with the effect slowly dying down as time increases. i.e. the time direction of the trajectory is $1 \to 2 \to 3 \to \cdots$

Both the restitution and dispersion relations are similar with two slight differences. First, the restitution relation for the simple model is stronger than that of Noble with the size of the action potential duration reaching lower values. As in Model A, the action potentials get short as the domain length is reduced. The dispersion curve for this simple model is relatively flat, although the dispersion relation is not as weak as that for the Noble model. At short diastolic intervals the dispersion curve tails off as expected leading to conduction blocks.

The trajectory of the currents in the phase plane is similar to that in Model A with one main difference. Due to the different nullcline structure, V becomes more negative during repolarisation and I_2 remains at higher values. (In Model A, both V and I_2 returned to their usual steady state value following an action potential). The upstroke in the simple model at short length scales is therefore initiated at a more negative value of V and at a higher value of I_2. This behaviour is essentially

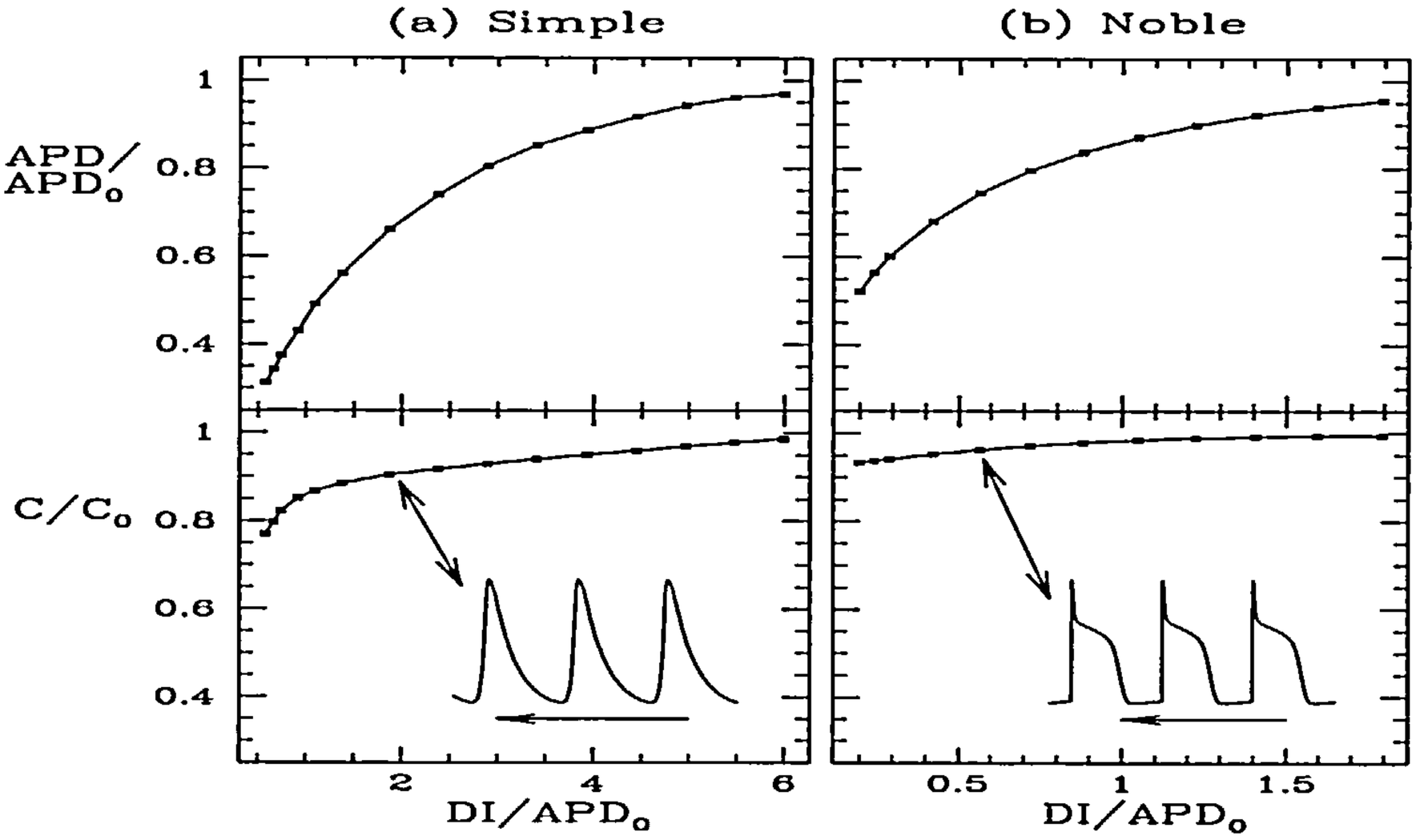

Figure 5.9: Normalised restitution and dispersion curves for (a) the simple model with $h_f(V) = -V/3$ and $h_g(V) = 6V$, and (b) the Noble model as in figure 5.4. The same parameters as in table 4.1 in Section 4.4 are used for the simple model. ($\alpha = 1$, $\beta = 1$, $\gamma = 0.5$, $\bar{V} = 3$ and $\epsilon = 0.015$). Simulations were carried out with 256 grid points and a time step of 0.02. The action potential duration is measured when $V > 2$.

due to the function $h_g(V)$ being linear rather than quadratic (slowing the decrease of I_2 during repolarisation), and the function $h_f(V)$ being linear rather than quartic (enabling the effect of diffusion to excite an action potential at a lower value of V).

The shortening of the action potential duration as the length of the domain decreases results from a similar mechanism to that of the fast response action potentials of Model A discussed above. At short length scales, I_2 attains higher values during the upstroke, the currents are further apart during the plateau phase, and hence the action potential duration is shorter.

The alternan behaviour seen in the fast response waves was not observed for this more basic model. This may be a result of the whole I_2 trajectory being raised

at short length scales rather than just at higher values of V but this needs further investigation.

5.4 Two Spatial Dimensions

Now let us consider two spatial dimensions. The diffusion operator ∇^2 becomes $\frac{\partial^2 V}{\partial x^2} + \frac{\partial^2 V}{\partial y^2}$ (recall that we are assuming an isotropic domain with diffusion coefficient $D = 1$) and we get the following equation for voltage,

$$\dot{V} = \left(\frac{\partial^2 V}{\partial x^2} + \frac{\partial^2 V}{\partial y^2} \right) + I_1 - I_2$$

5.4.1 Initial Discussion

The anatomy of the heart is three-dimensional although certain areas may be considered as two-dimensional. For example, the atria are thin walled and behave essentially as a two dimensional surface. The surface of the ventricles, which are thicker and more three-dimensional in nature, can also be considered as two-dimensional.

In two-dimensional excitable media there are three basic types of waves that are observed; plane, circular and spiral. Plane waves simply propagate across the two-dimensional surface travelling perpendicular to the wavefront. For example, the wave travelling across the atria during the normal heartbeat may be considered as a plane wave. Circular waves propagate out from the point of initiation in a target pattern. As the sinoatrial node fires a circular wave will travel outwards into the atrial muscle. The third type of wave, the spiral wave (also known as a vortex or reentrant wave), is a stable two-dimensional rotating pattern of excitation that is typical of any excitable medium. It is nonlinear and rotates about a core with constant angular velocity. The velocity of conduction at the wavefront of a spiral wave (in isotropic media) is dependent on its curvature as well as the time since the preceding wave (dispersion). The wavefront of a spiral wave will travel more slowly in the core, where the curvature is greater, than in the tail. Indeed the wavefront

will not propagate if the curvature is above a critical value and this influences the size of the spiral core.

This third basic wave type is thought to play an important role in irregular electrical activity of the heart (cardiac arrhythmias). There are two main types of cardiac arrhythmias depending on the location of the irregular activity; ventricular and atrial. Furthermore there are two main classes of arrhythmias; tachycardia and fibrillation. Atrial arrhythmias are not usually lethal and are often self-terminating. Ventricular arrhythmias, however, are clinically more serious and are often lethal. During tachycardia the heartbeat is excessively fast. Ventricular tachycardia results from excitation being initiated in one or both of the ventricles independent of the sinoatrial node (the natural pacemaker). Ventricular tachycardia can degenerate to the more lethal ventricular fibrillation. During ventricular fibrillation the electrical activity in the ventricles becomes turbulent and the beating is of a very high rate (typically greater than 500 beats/min.). The heart quivers, resulting in blood being shifted from one area of the heart to another rather than pumping it out into the body and lungs in an effective manner. Wiener and Rosenblueth described this behaviour (in [2]) with the following metaphor,

> "The ventricle looks like a quivering mass of worms"

If the heart is not defibrillated promptly death usually ensues.

Understanding how fibrillation occurs from a dynamical viewpoint has been a primary focus of research for many years across many disciplines [54, 55, 56, 58, 42, 43, 59]. Current knowledge suggests that the mechanism underlying the most dangerous cardiac arrhythmias (ventricular tachycardia and ventricular fibrillation) is the recirculation of excitation, or reentry. In two-dimensions, such as the atrial wall, reentry appears as a rotating spiral wave, whereas in the thicker ventrical wall it appears as a scroll wave (the three-dimensional version of a spiral wave). During reentry, the propagating wave of excitation travelling across the myocardium during the normal heartbeat begins to repeatedly reinvade the same area of tissue. This reentrant electrical activity, which can lead to reentrant tachycardia, is usually related to un-

derlying heart disease. Reentrant arrhythmias usually have a higher frequency than the sinoatrial node and will thus set the period of the heartbeat. This results in the faster heartbeat during tachycardia. The self-sustaining reentrant waves causing tachycardia are unstable and one possible mechanism which is currently believed to be responsible for the sudden transition from ventricular tachycardia to the more deadly fibrillation is the spontaneous breakup of the spiral wave. The breakup of the single spiral wave generates multiple spirals of electrical activity leading to turbulent wave behaviour and fibrillation. Different parts of the tissue are activated at different times and the coordination of the contraction of the heart is destroyed.

There is substantial experimental and theoretical evidence that spiral waves and reentrant excitation underly cardiac arrhythmias [54, 31, 33]. People have observed spiral reentrant waves in heart tissue during ventricular tachycardia by using voltage-sensitive dyes and video imaging [24, 25, 34]. Also, theoretical studies of excitable media based on electrophysiological models have provided supportive evidence of spiral waves and the occurrence of spiral wave breakup in cardiac tissue [21, 22, 44, 59].

Spiral waves may occur through heterogeneities in the anatomy of the heart but reentry does not require structural heterogeneities and can occur due to the intrinsic dynamics in a homogeneous medium. A homogeneous excitable medium described by a parabolic partial differential equation can support a spiral wave of excitation, in which the propagation of excitation causes the spiral to rotate. The behaviour of spiral waves in the plane can be both stationary, where the core remains fixed, or non-stationary, where the spiral tip meanders (i.e. the tip movement is not a circle but a closed or open sequence of loops). In heterogeneous tissue, such as that in the heart, spiral waves can also be anchored to an obstacle such as a tissue scar.

The understanding of reentrant propagation in the heart and its instabilities may lead to useful new proposals for treating or preventing deadly cardiac arrhythmias. However, the mechanisms involved are not yet fully understood and may be a result of numerous factors including spatial heterogeneities, restitution properties [29], alternans [28, 30], and the meander of the spiral wave tip [22, 27]. Despite progress in

this area, the mechanism of fibrillation and the underlying dynamical behaviour still remains unclear. Electrophysiological models are often too complicated to analyse from a dynamical systems perspective and numerical simulations on the large spatial domains needed for spiral wave behaviour in two or more dimensions are not practical. Consequently, the FitzHugh-Nagumo equations, which support spirals and are quick to simulate, are still frequently used in the study of reentry rather than more physiologically realistic equations.

5.4.2 Two-dimensional Investigations

We now investigate the behaviour of our model in two dimensions. To simulate waves in two dimensions we use an adaptation of EZ-Spiral [60]. The numerical scheme we use is first order explicit and nine-point Laplacians are implemented for the diffusion operator. Further details of this time-stepping scheme may be found in Appendix A.4.

We shall check that our models support spiral waves and shall concentrate on the simple model used in the previous chapter to obtain restitution and dispersion curves for the slow response action potential type. That is, $h_f(V) = -V/3$, $h_g(V) = 6V$, $\alpha = 1$, $\beta = 1$, $\gamma = 0.5$, $\bar{V} = 3$ and $\epsilon = 0.015$.

To initiate a spiral wave we need spatially non-uniform states. There are numerous ways to proceed, some of which are outlined below.

1. Cross field stimulation. First take a plane wave travelling across the domain, say from bottom to top. If a second plane wave is then initiated in a direction perpendicular to the first, for example from right to left, then the interaction between the two will result in a single spiral wave. This results from the fact that colliding waves in excitable media annihilate each other.

2. Premature stimulation. If the tail end of a propagating (plane) wave is stimulated before the medium has fully recovered then a conduction block in one direction (towards the passing wave) will prevent propagation in that direction and the result will be a pair of spiral waves.

3. In a manner similar to the previous case, if a half plane wave stimulus rather than just a point stimulus is applied in the wake of a passing wave the conduction block will lead to a single spiral wave.

4. Another method for obtaining spiral waves is to take a plane wave travelling across the medium, say from the bottom to top and instantaneously reset the left half of the domain to rest. This will result in a single spiral wave.

5. Spatial inhomogeneities. Spiral waves can also result from spatial inhomogeneities in the domain.

We have generated spiral waves from all but the last of these methods for our simple model and the initiation of a spiral wave from the fourth is shown diagrammatically in figure 5.10

It is therefore seen that our model supports spiral waves. Note also that the relatively slow repolarisation of our model (compared to the upstroke) is evident from the plots. That is, the size of the intermediate states (between excited and resting points), shown in black, is greater in the wake of the wave than immediately before one.

The restitution property discussed previously has a significant effect on the dynamics of the spiral wave. We can see from figure 5.10 that for our model, the size of the action potential of the plane wave is greater than that of the spiral. This is a result of the restitution property. During a spiral wave, the wave repeatedly reenters areas of the domain that have previously been excited. Recall that the restitution property results in a shortening of the action potential duration if the domain has not fully recovered from the previous excitation. Our model has a strong restitution property and thus the shortening of the action potential during a spiral is observed. The weak restitution property of the FitzHugh-Nagumo model means that the action potential is not substantially shortened during a spiral wave.

The behaviour of individual points of the two-dimensional domain is shown in figure 5.11. We can see that during a spiral wave (plots (b) and (c)), points in the domain are repeatedly excited by the reentrant activity. Recall from one-dimensional

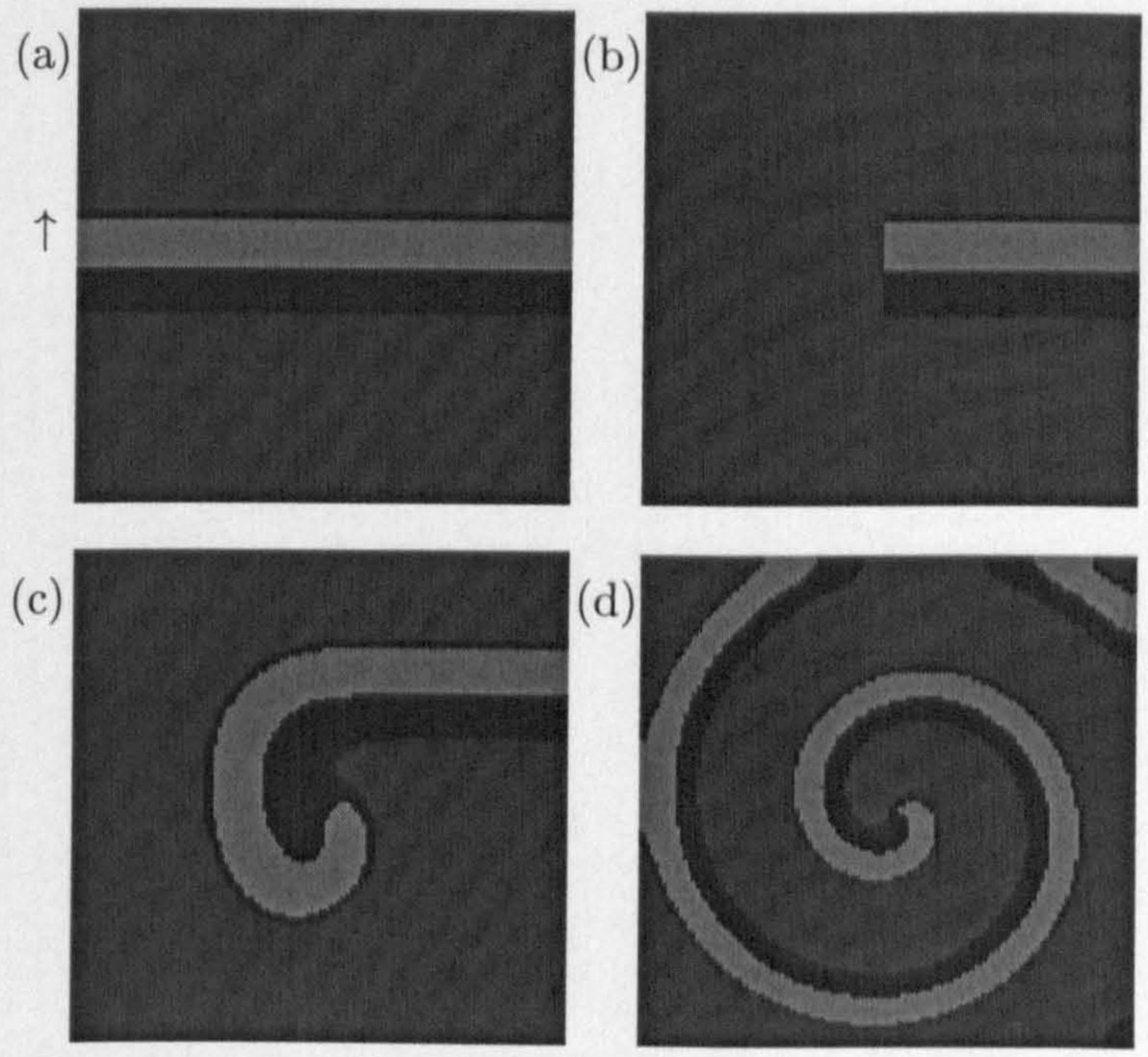

Figure 5.10: Initiation of a spiral wave for the simple model. The voltage V is plotted with excited regions shown in light grey, resting regions in dark grey and the interface in black. The length of the side of the spatial domain is 40 and 121 grid points are used in each direction. (a) We first initiate a plane wave travelling across the domain from bottom to top. (b) When the plane wave gets approximately half way we instantaneously reset the left hand side of the domain to rest. (c) The end of the plane wave then diffuses into the resting part of the domain initiating a spiral wave. (d) As the simulation continues we get a single anti-clockwise spiral wave.

simulations in the previous section that, for this model, the voltage V at small length scales (and hence high stimulation frequencies) becomes more negative. This is observed in points out on the spiral arm (plot (b)). However, note that for points close to the centre (core) of the spiral wave, the amplitude of the action potential is reduced (plot (c)). We can also see that the action potential duration of points during plane wave behaviour is slightly greater than that during spiral wave behaviour when the domain is not fully recovered from the passing of the previous action potential. However, the effect is smaller than that observed in figure 5.10. This difference is due to the combined effect of the restitution property shortening the action poten-

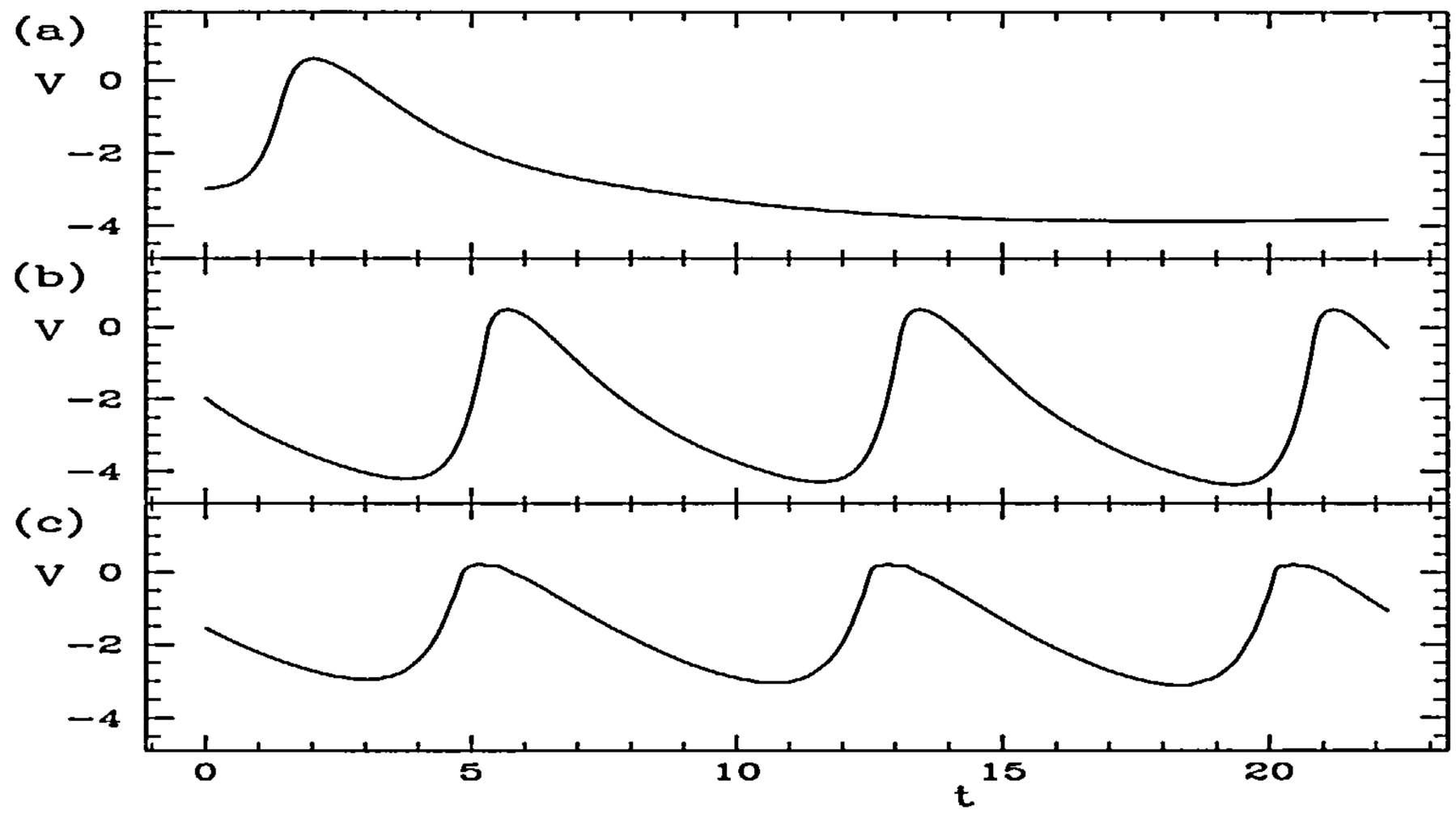

Figure 5.11: Time series for points in the domain. (a) A plane wave traversing the domain. (b) A point towards the edge of the spiral wave. (c) A point towards the centre of the spiral wave.

tial duration and the speed of propagation of the spiral wave being reduced. As mentioned earlier, the speed of propagation in two-dimensional excitable media decreases with increased curvature. Therefore the speed of propagation of the spiral wave is less than that of a plane wave and the effect in the centre is stronger than in the spiral arm. Finally note that the frequency for all points during a spiral wave remains the same.

In our simulations of this slow response action potential model we did not observe meandering of the spiral tip on varying parameters. The core of the spiral wave remained fixed at a particular location in the domain about which the spiral wave rotated. Furthermore, as in our one-dimensional investigations of this simple model, alternan behaviour was not observed in the two-dimensional domain.

Chapter 6

Conclusions

The aim of this work was to derive a new mathematical approach to modelling the dynamics of cardiac action potentials. We were looking to obtain model equations that are simple and easy to analyse and yet have a more physiologically realistic basis than other simple models used for computations of waves in extended media.

We began by investigating the 1962 Noble equations for the Purkinje fibres which, although incorrect on an ionic level, are relatively simple and generate good action potentials. Furthermore, important quantitative properties such as restitution are more accurate than in simple mathematical models. In Chapter 3 we carried out the first detailed analysis of the Noble phase plane from the perspective of the overall inward and outward currents. This enabled us to obtain an idea of their dynamical behaviour during the course of an action potential and to isolate some key features underlying this behaviour, such as the mechanism for excitability involving the fast inward current. By using ideas resulting from this analysis we constructed a mathematical model that has the same key phase plane features. The model has three physically meaningful variables; the membrane voltage, the inward current, and the outward current, and the equations are expressed in terms of relatively simple polynomial functions. Due to the similar mathematical structure of the nullclines, the dynamics of the currents resulting from simulations is extremely close to that of the Noble model. We believe that the phase plane dynamics of this model is closer to that of the real system than many other simple mathematical models currently used in the study of cardiac tissue such as FitzHugh-Nagumo and

its modifications. In particular, the new idea of excitability, resulting from the rapid increase of the inward current, matches well both experimental behaviour and that of recent ionic models. Recall that in fast response cardiac action potentials the upstroke is caused by a rapid influx of sodium ions, giving a large increase in the inward sodium current. The FitzHugh-Nagumo equations do not contain information about this fast current. The fundamental features of our model are simple and equations with a more basic structure can be used to give the same dynamical behaviour. We have investigated examples of these and shown that the simplified equations can be used to generate a variety of different action potentials. On varying the functions and parameters involved, waves of both the fast and slow response type can be obtained. The behaviour of such waves can be changed from excitable to oscillatory (via Hopf bifurcations) and other properties such as the sharpness of the upstroke, the wave amplitude, and the plateau length can be altered.

In Chapter 3 we chose particular functional forms for our model that gave an extremely close match to the Noble model. Ionic models such as Noble are continuously changing as new experimental results are obtained and equations describing cardiac tissue are constantly being refined to incorporate these new discoveries. We believe that by varying the functions and parameters involved in the general approach that we have carried out for the Noble model it should be possible to match action potentials of our model to those of more recent and accurate ionic models.

We see no reason why more variables cannot be implemented into our modelling approach. Different variables could be used to describe individual currents rather than the overall inward and outward currents that we have concentrated on in this work. In particular, the inward current we used in Model A is responsible for both the fast upstroke of the action potential and the plateau phase. In cardiac cells these phases are generated by two separate currents; a fast sodium current and a slower calcium current respectively. The overall inward current in Model A could therefore be split into two components, one generating the fast upstroke and one generating the plateau. This approach would sacrifice the three-dimensional phase plane structure that we have concentrated on but would remove the need for the

quartic structure used for the inward current.

On including a spatial dependence in our model and studying the equations on a one-dimensional ring, we analysed important dynamical properties such as restitution and dispersion. We found that, with respect to cardiac tissue, the restitution and dispersion relations of our model were a considerable improvement over those of the FitzHugh-Nagumo equations. Due to the simple form of our equations, we were able to briefly analyse the dynamical basis of restitution from a phase plane point of view. The behaviour of our model was the same as the Noble model with the shortening of the action potentials at short length scales resulting from the inward and outward currents remaining close (during the plateau) for a shorter period of time. We did however observe a few important differences. The biggest of these was that our model supported action potentials at shorter lengths with the action potential duration decreasing to lower values. Also, we did not observe a transition to alternans as the stimulation frequency was decreased. However, unlike some other simple mathematical models of cardiac tissue which exhibit no alternan behaviour, "transient" alternans were frequently observed during simulations of our fast response model and they probably exist at some parameter values. We were able to obtain an idea of the dynamical behaviour of alternans for our model in terms of the phase plane and it was found to match closely that of the Noble model. However, the underlying dynamical mechanism still remains poorly understood and needs to be investigated further. Whether components that govern alternan behaviour can be isolated in our equations is uncertain but we suspect that for the particular models studied here it is the dynamics of the slow outward current that plays the dominant role.

Finally, we briefly investigated two-dimensional simulations and found that the simple form of our model supports spiral wave activity. The slower wave back of the action potential remained and the restitution property resulted in the shortening of the action potential duration during a spiral wave. During simulations in two dimensions we did not observe meandering of the spiral wave tip. In fact the core of the spiral wave appears to remain fixed at a particular location in the domain.

Recall that meander, together with alternan behaviour, may be an important factor in spiral wave breakup. This in turn is thought to play an important role in the transition from ventricular tachycardia to the more lethal ventricular fibrillation.

In general, we believe that the development of action potential models throughout this work provides some valuable insight into the underlying dynamical behaviour of more complex physiological models. The simplicity of the models not only enables the behaviour of action potentials to be studied from a dynamical systems viewpoint (important properties such as restitution and alternation can be studied in the phase plane) but means that simulations are quick to run. Our main hope is that these, or similar equations, provide a basis for future large scale simulations of waves that are physiologically meaningful.

Appendix A

Numerics

A.1 Description of Equations

The equations that we are concerned with are shown below.

$$\begin{aligned}
\frac{\partial V(\underline{\mathbf{x}},t)}{\partial t} &= f_0\Big(V(\underline{\mathbf{x}},t), I_1(\underline{\mathbf{x}},t), I_2(\underline{\mathbf{x}},t)\Big) + D\nabla^2 V(\underline{\mathbf{x}},t) \\
\frac{\partial I_1(\underline{\mathbf{x}},t)}{\partial t} &= f_1\left(V(\underline{\mathbf{x}},t), I_1(\underline{\mathbf{x}},t), I_2(\underline{\mathbf{x}},t), \frac{\partial V(\underline{\mathbf{x}},t)}{\partial t}\right) \\
\frac{\partial I_2(\underline{\mathbf{x}},t)}{\partial t} &= f_2\left(V(\underline{\mathbf{x}},t), I_1(\underline{\mathbf{x}},t), I_2(\underline{\mathbf{x}},t), \frac{\partial V(\underline{\mathbf{x}},t)}{\partial t}\right)
\end{aligned}$$

There are three variables, each depending on both space and time; the voltage V, and the inward and outward currents I_1 and I_2. ∇^2 represents the diffusion operator, D the diffusion coefficient, and f_i, $i = 0, \ldots, 2$, are nonlinear functions. This is a system of three differential equations, the first being a parabolic partial differential equation (PDE). Note that $\frac{\partial V(\underline{\mathbf{x}},t)}{\partial t}$ appears in the functions f_1 and f_2. The method we use for solving these equations depends upon the spatial dimension of the domain. For the one-dimensional case (where $\nabla^2 V = \frac{\partial^2 V}{\partial x^2} = \partial_{xx} V$) we use both finite difference and spectral methods. The (nonlinear) functions f_i are time stepped explicitly (by either Forward Euler or second-order Adams-Bashforth). The linear diffusion term is time stepped explicitly or implicitly (Backwards Euler or Crank-Nicolson) for no-flux (Neumann) boundary conditions, and explicitly or by using a Spectral

Method (Collocation Weighted Residual Method) for periodic boundary conditions. For the two-dimensional case (where $\nabla^2 V = \frac{\partial^2 V}{\partial x^2} + \frac{\partial^2 V}{\partial y^2} = \partial_{xx} V + \partial_{yy} V$) we only use finite differences and all terms are time stepped explicitly using Forward Euler. The Laplacian is evaluated using the nine-point formula.

A.2 Notation

Solving the PDE involves discretising both the spatial and temporal domains by a uniform lattice. It is then possible to express terms such as $\frac{\partial V(\underline{\mathbf{x}},t)}{\partial t}$ and $\frac{\partial^2 V(\underline{\mathbf{x}},t)}{\partial x^2}$ numerically.

For example in the one-dimensional case, if the length of the domain is L we divide it up into N equally spaced grid points, creating $N-1$ equal intervals of size $h = L/(N-1)$. Similarly, if the time of the simulation is T and we are simulating for M time steps, then each time step will be of size $\Delta t = T/M$. We shall use V_i^n to represent the value of the variable V at the i^{th} spatial point and the n^{th} time step. i.e. $V_i^n = V(ih, n\Delta t)$.

For the two-dimensional case we use a regular square grid with sides of length L. We divide both the x and y directions into N equally spaced grid points so that the intervals in both directions are given by $h = L/(N-1)$. A similar notation to the one-dimensional case is used and $V_{i,j}^n = V(ih, jh, n\Delta t)$.

A.3 One Spatial Dimension

A.3.1 Explicit Time Stepping

The equation that is non-trivial to time step due to the diffusion term is the voltage equation.

$$\frac{\partial V(x,t)}{\partial t} = f_0(V(x,t), I_1(x,t), I_2(x,t)) + D\frac{\partial^2 V(x,t)}{\partial x^2}$$

Upon discretising both space (using the three-point formula for $\partial_{xx}V$) and time (using forward differences for $\partial_t V$) we get the following equation for the point V_i at the time step n. We shall use f_i^n to represent $f_0(V_i^n, I1_i^n, I2_i^n)$.

$$\frac{V_i^{n+1} - V_i^n}{\Delta t} + O(\Delta t) = f_i^n + D\left(\frac{V_{i+1}^n - 2V_i^n + V_{i-1}^n}{h^2}\right) + O(h^2)$$

Recall that Δt is the size of the time step and h is the (spatial) interval size. Rearranging this equation gives the following formula for the value of V_i at a time step $(n+1)$ in terms of the value of V_i's at a time step n.

$$V_i^{n+1} = V_i^n + \Delta t f_i^n + \frac{\Delta t}{h^2} D(V_{i+1}^n - 2V_i^n + V_{i-1}^n) + \Delta t O(h^2 + \Delta t)$$

We shall omit the error term from now onwards but note that after M time steps we get an error of the order $M\Delta t O(h^2 + \Delta t) = TO(h^2 + \Delta t)$. i.e. the time stepping is second order in space and first order in time. The equation above only holds for "internal" points. At the (spatial) boundaries the scheme has to be altered slightly as shown below. With periodic boundary conditions we use

$$V_0^{n+1} = V_0^n + \Delta t f_0^n + \frac{\Delta t}{h^2} D(V_1^n - 2V_0^n + V_{N-1}^n)$$

$$V_{N-1}^{n+1} = V_{N-1}^n + \Delta t f_{N-1}^n + \frac{\Delta t}{h^2} D(V_0^n - 2V_{N-1}^n + V_{N-2}^n)$$

and with no-flux boundary conditions we use

$$V_0^{n+1} = V_0^n + \Delta t f_0^n + \frac{\Delta t}{h^2} D(2V_1^n - 2V_0^n)$$

$$V_{N-1}^{n+1} = V_{N-1}^n + \Delta t f_{N-1}^n + \frac{\Delta t}{h^2} D(2V_{N-2}^n - 2V_{N-1}^n)$$

Note that both these boundary conditions also have errors that are second order in space. These equations may be re-written in the slightly neater form below which gives a formula for calculating all values of V at a time step $(n+1)$ in terms of the values of V at a time step n.

$$V^{n+1} = \Delta t f^n + (I + D\mathrm{B})V^n$$

where $f^n = f_0(V^n, I_1^n, I_2^n)$ and

$$\mathbf{B} = \begin{pmatrix} -2r & 2r & & & \\ \ddots & \ddots & \ddots & & \\ & r & -2r & r & \\ & & \ddots & \ddots & \ddots \\ & & & 2r & -2r \end{pmatrix} \text{ or } \begin{pmatrix} -2r & r & & & r \\ \ddots & \ddots & \ddots & & \\ & r & -2r & r & \\ & & \ddots & \ddots & \ddots \\ r & & & r & -2r \end{pmatrix}$$

for no-flux and periodic boundary conditions respectively. Here $r = \frac{\Delta t}{h^2}$ and all other matrix terms are zero. For the variables I_1 and I_2 (which do not diffuse) a simple Forward Euler time stepping scheme is used. The only slight difficulty is that $\partial_t V$ must be calculated first as f_1 and f_2 depend on it. If we are given initial conditions for the three variables at each point in the domain then the above time stepping scheme is simple to implement into a program.

A.3.2 Implicit and Spectral Time Stepping

Recall the equation for voltage.

$$\frac{\partial V(x,t)}{\partial t} = f_0(V(x,t), I_1(x,t), I_2(x,t)) + D\frac{\partial^2 V(x,t)}{\partial x^2}$$

To obtain a more accurate time stepping scheme (second order in time) we can take the average of the finite difference approximations for diffusion at the time steps n and $(n+1)$ (Crank-Nicolson) and use second order Adams-Bashforth (an explicit multi-step method) for the kinetics giving the following formula,

$$\frac{V_i^{n+1} - V_i^n}{\Delta t} = \frac{1}{2}(3f_i^n - f_i^{n-1}) + O(\Delta t^2)$$
$$+\frac{D}{2}\left(\frac{V_{i+1}^{n+1} - 2V_i^{n+1} + V_{i-1}^{n+1}}{h^2} + \frac{V_{i+1}^n - 2V_i^n + V_{i-1}^n}{h^2}\right) + O(h^2 + \Delta t^2)$$

Rearranging to collect the terms at the $(n+1)^{th}$ time step on the left hand side and terms at the n^{th} time step (or less) on the right hand side gives

$$-\frac{Dr}{2}V_{i+1}^{n+1} + (1+Dr)V_i^{n+1} - \frac{Dr}{2}V_{i-1}^{n+1} =$$
$$\frac{\Delta t}{2}(3f_i^n - f_i^{n-1}) + \frac{Dr}{2}V_{i+1}^n + (1-Dr)V_i^n + \frac{Dr}{2}V_{i-1}^n + \Delta t O(h^2 + \Delta t^2)$$

where $r = \frac{\Delta t}{h^2}$ as before. Again we shall omit the error term from now on but will note that the scheme is second order in both space and time. The boundary conditions will have a similar (numerical) form to those in the explicit time stepping scheme discussed above. Including these boundary conditions, the above equation can be re-written in the slightly neater form below which gives a formula for calculating all values of V at a time step $(n+1)$ in terms of previous time steps.

$$\left(I - \frac{D}{2}\mathbf{B}\right) V^{n+1} = \frac{\Delta t}{2}(3f^n - f^{n-1}) + \left(I + \frac{D}{2}\mathbf{B}\right) V^n = r^n \qquad \text{(A.1)}$$

where

$$\mathbf{B} = \begin{pmatrix} -2r & 2r & & & \\ \ddots & \ddots & \ddots & & \\ & r & -2r & r & \\ & & \ddots & \ddots & \ddots \\ & & & 2r & -2r \end{pmatrix} \text{ or } \begin{pmatrix} -2r & r & & & r \\ \ddots & \ddots & \ddots & & \\ & r & -2r & r & \\ & & \ddots & \ddots & \ddots \\ r & & & r & -2r \end{pmatrix}$$

depending on the boundary conditions. Therefore

$$V^{n+1} = \left(I - \frac{D}{2}\mathbf{B}\right)^{-1} \left[\frac{\Delta t}{2}(3f^n - f^{n-1}) + \left(I + \frac{D}{2}\mathbf{B}\right) V^n\right]$$

which is second order accurate in both space and time. Before proceeding further we shall introduce a useful "trick" to simplify the above time stepping scheme. Recall equation (A.1).

$$\left(I - \frac{D}{2}\mathbf{B}\right) V^{n+1} = \frac{\Delta t}{2}(3f^n - f^{n-1}) + \left(I + \frac{D}{2}\mathbf{B}\right) V^n = r^n$$

Now

$$\begin{aligned} r^n &= \frac{\Delta t}{2}(3f^n - f^{n-1}) + 2V^n - \left(I - \frac{D}{2}\mathbf{B}\right) V^n \\ &= \frac{\Delta t}{2}(3f^n - f^{n-1}) + 2V^n - r^{n-1} \end{aligned}$$

Therefore the time-stepping scheme for simulations, making use of stored values (denoted by s), will be

$$\begin{aligned} r^n &= \frac{3}{2}\Delta t f^n + 2V^n - s^{n-1} \\ s^n &= \frac{\Delta t}{2} f^n + r^n \\ V^{n+1} &= \left(I - \frac{D}{2}\mathbf{B}\right)^{-1} r^n \end{aligned}$$

with the first time step as

$$\begin{aligned} r^0 &= \Delta t f^0 + \left(I + \frac{D}{2}\mathbf{B}\right) V^0 \\ s^0 &= \frac{\Delta t}{2} f^0 + r^0 \\ V^1 &= \left(I - \frac{D}{2}\mathbf{B}\right)^{-1} r^0 \end{aligned}$$

Implicit Time Stepping

The Backwards Euler part of the above equation is

$$\left(I - \frac{D}{2}\mathbf{B}\right)^{-1}$$

As shown above, if the boundary conditions are no-flux then the matrix $\mathbf{B}$, and hence $(I - \frac{D}{2}\mathbf{B})$, is tridiagonal. It can therefore be inverted relatively easily using a standard numerical routine such as the LAPACK routine "dgtsv".* This will lead to implicit time stepping of second order in both space and time.

Spectral Methods

However, recall that if the boundary conditions are periodic then the matrix $\mathbf{B}$ (and hence $(I - \frac{D}{2}\mathbf{B})$) is no-longer tridiagonal and non-trivial to invert. A good way to solve this problem is to use spectral methods for periodic boundary conditions and to make use of fast fourier transforms (FFTs). We shall not go into the details of spectral methods and the reader is advised to refer to [49] for a detailed discussion. In the Collocation (Pseudospectral) Weighted Residual method with periodic boundary conditions (i.e. $V(x + L, t) = V(x, t)$), V is approximated using fourier transforms as follows,

$$V^N(x_m, t) = \frac{1}{N} \sum_{n=0}^{N/2} a_n(t) e^{-ik_n x_m}$$

where $k_n = \frac{2\pi n}{L}$ and $x_m = \frac{mL}{N}$. (Note that the superscript of V now denotes the number of grid points and not the time step). The $a_n(t)$ are complex and the x_m

* "dgtsv" is a Fortran 77 subroutine for inverting a tridiagonal matrix by Gaussian elimination with partial pivoting.

are the discretised points of the spatial domain. $(0 \leq m \leq N)$. In this method the coefficients a_n are time stepped in spectral space rather than the variables at the grid points. An advantage of this is that in spectral space the derivative operators are diagonal and easy to invert. It also results in greater accuracy $(O(e^{-N^2}))$ than finite difference methods (for example $O(N^{-2})$ for second-order finite difference). Furthermore, the boundary conditions are "naturally" imposed. V is transformed to spectral space by

$$a_n = \sum_{m=0}^{N-1} V_m e^{ik_n x_m} = \sum_{m=0}^{N-1} V_m e^{\frac{i2\pi nm}{N}}$$

where $V_m = V(x_m)$. In practice this is done by a fast fourier transform. On passing into spectral space our (Backwards Euler) operator will be transformed as follows,

$$(I - \frac{\Delta t}{2} D\partial_{xx})^{-1} \longrightarrow (I + \frac{\Delta t}{2} Dk_n^2)^{-1} = \frac{1}{1 + \frac{\Delta t}{2} Dk_n^2} = c_{k_n}$$

Hence in spectral space we multiply each mode (which are complex) by c_{k_n}.

$$a_n(t + \Delta t) = c_{k_n} a_n(t)$$

Once this is done we can transform back to physical space through an inverse fourier transform and proceed to the next time step. The variables I_1 and I_2 (which do not diffuse) are time stepped using second-order Adams-Bashforth and again $\partial_t V$ needs to be calculated first.

A.4 Two Spatial Dimensions

For two-dimensional simulations we make use of the program EZ-Spiral [60], a C program for studying the dynamics of spiral waves in (isotropic) excitable media. The original version of EZ-Spiral uses model equations of the FitzHugh-Nagumo type (for details see [16]). We have therefore used a modification of the program to enable our three variable models to be simulated.

The equation for voltage in two dimensions is

$$\frac{\partial V(x,y,t)}{\partial t} = f_0(V(x,y,t), I_1(x,y,t), I_2(x,y,t)) + D\left(\frac{\partial^2 V(x,y,t)}{\partial x^2} + \frac{\partial^2 V(x,y,t)}{\partial y^2}\right)$$

In the original version of EZ-Spiral the simple form of the model equations (the f_i's) enables an efficient implicit scheme to be used to time step the kinetics. For our models this method is not suitable and we concentrate on a first order explicit scheme. On discretising time using Forward Euler we obtain the following equation for the grid point $V_{i,j}$ at the time step n,

$$\frac{V_{i,j}^{n+1} - V_{i,j}^{n}}{\Delta t} + O(\Delta t) = f_{i,j}^{n} + D\left(\frac{\partial^2 V_{i,j}^{n}}{\partial x^2} + \frac{\partial^2 V_{i,j}^{n}}{\partial y^2}\right)$$

Here $f_{i,j}^{n} = f_0(V_{i,j}^{n}, {I_1}_{i,j}^{n}, {I_2}_{i,j}^{n})$. This is first order in time and rearranging to put the terms at the $(n+1)^{th}$ time step on one side of the equation gives

$$V_{i,j}^{n+1} = V_{i,j}^{n} + \Delta t f_{i,j}^{n} + \Delta t D\left(\frac{\partial^2 V_{i,j}^{n}}{\partial x^2} + \frac{\partial^2 V_{i,j}^{n}}{\partial y^2}\right)$$

where we have omitted the error term.

Now let us concentrate on the spatial derivatives (diffusion terms). If the three-point formula is used for both $\partial_{xx}V$ and $\partial_{yy}V$ we get the five-point Laplacian formula for the two-dimensional diffusion operator. That is,

$$\frac{\partial^2 V_{i,j}^{n}}{\partial x^2} + \frac{\partial^2 V_{i,j}^{n}}{\partial y^2} = \frac{1}{h^2}(V_{i+1,j}^{n} + V_{i-1,j}^{n} + V_{i,j+1}^{n} + V_{i,j-1}^{n} - 4V_{i,j}^{n}) + O(h^2)$$

which is second order in space. This can be represented diagrammatically by a computational molecule as shown in figure A.1. With appropriate boundary conditions the above equation may be used to represent the diffusion operator on a regular two-dimensional lattice. EZ-Spiral gives the option of using the nine-point formula for the Laplacian as well as the five-point formula. The nine-point Laplacian formula [53] uses the following second difference on the discretised domain for the point $V_{i,j}^{n}$,

$$\begin{aligned}\frac{\partial^2 V_{i,j}^{n}}{\partial x^2} + \frac{\partial^2 V_{i,j}^{n}}{\partial y^2} &= \frac{2}{3}\left(\frac{V_{i,j+1}^{n} + V_{i,j-1}^{n} + V_{i+1,j}^{n} + V_{i-1,j}^{n} - 4V_{i,j}^{n}}{h^2}\right) \\ &\quad + \frac{1}{3}\left(\frac{V_{i+1,j+1}^{n} + V_{i+1,j-1}^{n} + V_{i-1,j+1}^{n} + V_{i-1,j-1}^{n} - 4V_{i,j}^{n}}{(\sqrt{2}h)^2}\right) \\ &= \frac{1}{6h^2}\sum_{r,s=-1}^{1} A_{r,s} V_{i+r,j+s}^{n} + O(h^2)\end{aligned}$$

$$\nabla^2 V_{i,j} = \frac{1}{h^2}\left\{ \quad \right\} + O(h^2)$$

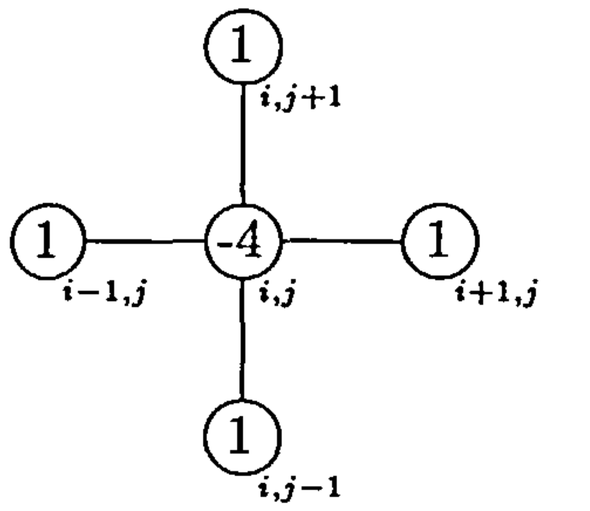

Figure A.1: Computational molecule for the five-point Laplacian formula.

where $A_{0,0} = -20$, $A_{r,s} = 4$ for the four nearest neighbours, and $A_{r,s} = 1$ for the four diagonal next nearest neighbours. The computational molecule is shown in figure A.2.

$$\nabla^2 V_{i,j} = \frac{1}{6h^2}\left\{ \quad \right\} + O(h^2)$$

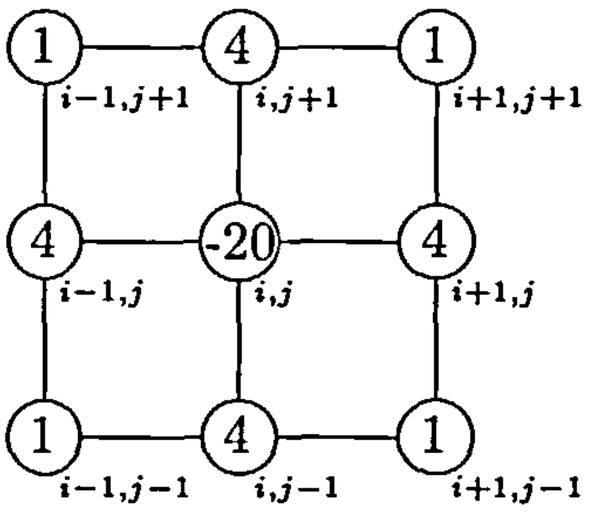

Figure A.2: Computational molecule for the nine-point Laplacian formula.

The nine-point formula for the Laplacian is second order in space and maintains rotational symmetry to leading order. We use this formula in our simulations as the difference in execution time is small compared with the accuracy gained.

We concentrate on no-flux boundary conditions in our two-dimensional simulations (although EZ-Spiral also enables periodic boundary conditions to be used). An example computational molecule of the no-flux boundary condition for a point on the both the edge and corner of the (square) domain is shown in figure A.3.

V, I_1, and I_2 are time stepped using Forward Euler and if we are given the values of V, I_1, and I_2 at the time $t = \Delta tn$ we may use the above equations to find the values at a time $t = \Delta t(n+1)$. The time stepping scheme can then be used to simulate

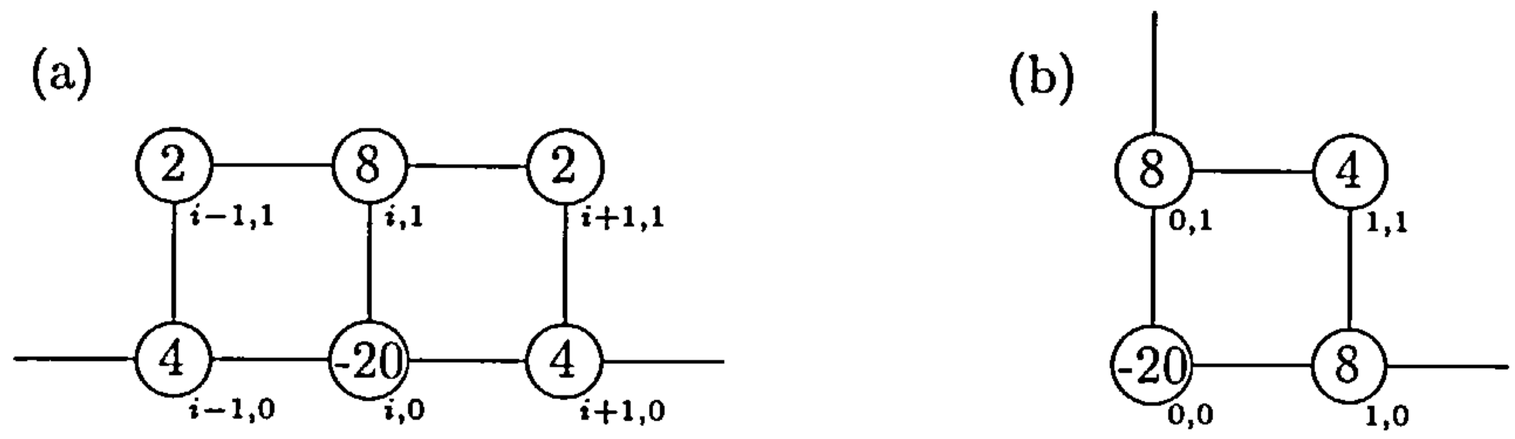

Figure A.3: Computational molecules for no-flux boundary conditions using the nine-point Laplacian formula. (a) A point on the edge of the domain (with $j = 0$). (b) A point on the corner of the domain (with $i = j = 0$).

our equations on the two-dimensional domain.

Bibliography

[1] G. R. Mines, *On Circulating Excitation on Heart Muscles and their Possible Relation to Tachycardia and Fibrillation*, Trans. R. Soc. Can. 4, 43 (1914).

[2] N. Wiener and N. Rosenbluth, *The Mathematical Formulation of the Problem of Conduction of Impulses in a Network of Connected Excitable Elements, Specifically in Cardiac Muscle*, Arch. Inst. Card. Mex., **16**, 205 (1946).

[3] A. L. Hodgkin and A. F. Huxley, *A Quantitative Description of Membrane Current and its Application to Conduction and Excitation in Nerve*, J. Physiol. **116**, 449 (1952); **116**, 473 (1952); **116**, 497 (1952); **117**, 500 (1952).

[4] R. FitzHugh, *Impulses and Physiological States in Theoretical Models of Nerve Membrane*, Biophys. J. **1**, 445 (1961).

[5] J. S. Nagumo, S. Arimoto and S. Yoshizawa, *An Active Pulse Transmission Line Simulating Nerve Axon*, Proc. IRE. **50**, 2061 (1962).

[6] D. Noble, *A Modification of the Hodgkin-Huxley Equations Applicable to Purkinje Fibre Action and Pace-Maker Potentials*, J. Physiol. **160**, 317 (1962).

[7] J. B. Nolasco and R. W. Dahlen, *A Graphic Method for the Study of Alternation in Cardiac Action Potentials*, J. Appl. Physiol. **25**(2), 191 (1968).

[8] R. E. McAllister, D. Noble and R. W. Tsien, *Reconstruction of the Electrical Activity of Cardiac Purkinje Fibres*, J. Physiol. **251**, 1 (1975).

[9] G. W. Beeler and H. Reuter, *Reconstruction of the Action Potential of Ventricular Myocardial Fibres*, J. Physiol. **268**, 177 (1977).

[10] F. J. L. Van Capelle and D. Durrer, *Computer Simulation of Arrhythmias in a Network of Coupled Excitable Elements*, Circ. Res. **47**, 454 (1980)

[11] M. R. Guevara, G. Ward, A. Shrier and L. Glass, *Electrical Alternans and Period-Doubling Bifurcations*, In: Computers in Cardiology, Silver Spring, IEEE Computer Society, 167 (1984).

[12] D. DiFrancesco and D. Noble, *A Model of Cardiac Electrical Activity Incorporating Ionic Pumps and Concentration Changes*, Phil. Trans. R. Soc. B **307**, 353 (1985).

[13] L. H. Frame, R. L. Page and B. F. Hoffman, *Atrial Reentry Around an Anatomical Barrier with a Partially Refractory Excitable Gap: A Canine Model of Atrial Flutter*, Circ. Res. **58**, 495 (1986).

[14] L. H. Frame and M. B. Simson, *Oscillations of Conduction, Action Potential Duration, and Refractoriness*, Circulation **78**, 1277 (1988).

[15] Y. E. Earm and D. Noble, *A Model of the Single Atrial Cell: Relation Between Calcium Current and Calcium Release*, Proc. R. Soc. B **240**, 97 (1990).

[16] D. Barkley, M. Kness and L. S. Tuckerman, *Spiral-wave Dynamics in a Simple Model of Excitable Media: The Transition from Simple to Compound Rotation*, Phys. Rev. A **42**(4), 2489 (1990).

[17] W. Quan and Y. Rudy, *Unidirectional Block and Reentry of Cardiac Excitation: A Model Study*, Circ. Res. **66**, 367 (1990).

[18] T. J. Lewis and M. R. Guevara, *Chaotic Dynamics in an Ionic Model of the Propagated Cardiac Action Potential*, J. Theor. Biol. **146**, 407 (1990).

[19] A. T. Winfree, *Varieties of Spiral Wave Behaviour: An Experimentalist's Approach to the Theory of Excitable Media*, Chaos 1(3) 303, (1991).

[20] Ch. Luo and Y. Rudy, *A Model of the Ventricular Cardiac Action Potential: Depolarization, Repolarization, and their Interaction*, Circ. Res. **68**, 1501 (1991).

[21] A. V. Panfilov and A. V. Holden, *Spatiotemporal Irregularity in a Two-dimensional Model of Cardiac Tissue*, Int. J. Bifurcation Chaos **1**(1), 219 (1991).

[22] M. Courtemanche and A. T. Winfree, *Reentrant Rotating Waves in a Beeler-Reuter Based Model of Two-dimensional Cardiac Electrical Activity* Int. J. Bifurcation Chaos **1**(2), 431 (1991).

[23] B. Y. Kogan, W. J. Karplus, B. S. Billett, A. T. Pang, H. S. Karagueuzian, and S. S. Khan, *The Simplified FitzHugh-Nagumo Model with Action Potential Duration Restitution: Effects on 2D Wave Propagation*, Physica D **50**, 327 (1991).

[24] J. M. Davidenko, A. M. Pertsov, R. Salomonsz, W. T. Baxter and J. Jalife, *Stationary and Drifting Spiral Waves of Excitation in Isolated Cardiac Muscle*, Nature **355**, 349 (1992).

[25] A. M. Pertsov, J. M. Davidenko, R. Salomonsz, W. T. Baxter and J. Jalife, *Spiral Waves of Excitation Underlie Reentrant Activity in Isolated Cardiac Muscle*, Circ. Res. **72**, 631 (1993).

[26] M. Courtemanche, L. Glass and J. P. Keener, *Instabilities of a Propagating Pulse in a Ring of Excitable Media*, Phys. Rev. Lett. **70**(14), 2182 (1993).

[27] M. Bär and M. Eiswirth, *Turbulence Due to Spiral Breakup in a Continuous Excitable Medium*, Phys. Rev. E **48**(3), 1635 (1993).

[28] A. Karma, *Spiral Breakup in Model Equations of Action Potential Propagation in Cardiac Tissue*, Phys. Rev. Lett. **71**(7), 1103 (1993).

[29] A. V. Panfilov and P. Hogeweg, *Spiral Breakup in a Modified FitzHugh-Nagumo model*, Phys. Lett. A **176**, 295, (1993).

[30] A. Karma, *Electrical Alternans and Spiral Wave Breakup in Cardiac Tissue*, Chaos **4**(3), 461 (1994).

[31] A. T. Winfree, *Electrical Turbulence in 3-Dimensional Heart Muscle*, Science **266**(5187), 1003 (1994).

[32] C. Luo and Y. Rudy, *A Dynamic Model of the Ventricular Cardiac Action Potential: I. Simulation of Ionic Currents and Concentration Changes*, Circ. Res. **74**, 1071 (1994).

[33] A. V. Panfilov and P. Hogeweg, *Mechanisms of Cardiac Fibrillation*, Science **270**(5239), 1223 (1995).

[34] R. A. Gray, J. Jalife, A. V. Panfilov, W. T. Baxter, C. Cabo, J. M. Davidenko and A. M. Pertsov, *Non-stationary Vortex-like Reentry as a Mechanism of Polymorphic Ventricular Tachycardia in the Isolated Rabbit Heart*, Circ. **91**, 2454 (1995).

[35] B. Y. Kogan, W. J. Karplus and M. G. Karpoukhin, *The Third-order Action Potential Model for Computer Simulation of Electrical Wave Propagation in Cardiac Tissue*, In Proceedings of the Third International Conference on Computers in Biomedicine (1995).

[36] D. Noble, *The Development of Mathematical Models of the Heart*, Chaos, Solitons and Fractals **5**(3), 321 (1995).

[37] A. V. Panfilov and J. P. Keener, *Reentry in an Anatomical Model of the Heart*, Chaos, Solitons and Fractals **5**(3), 681 (1995).

[38] T. R. Chay, *Bifurcations in Heart Rhythms*, Int. J. Bifurcation Chaos **5**(6), 1439 (1995).

[39] A. V. Panfilov and J. P. Keener, *Reentry in Three-Dimensional FitzHugh-Nagumo Medium with Rotational Anisotropy*, Physica D **48**, 545 (1995).

[40] R. R. Aliev and A. V. Panfilov, *A Simple Two-variable Model of Cardiac Excitation*, Chaos, Solitons and Fractals **7**(3), 293 (1996).

[41] A. V. Holden, M. J. Poole and J. V. Tucker, *An Algorithmic Model of the Mammalian Heart: Propagation, Vulnerability, Reentry and Fibrillation*, Int. J. Bifurcation Chaos **6**(9), 1623 (1996).

[42] L. Glass, *Dynamics of Cardiac Arrhythmias*, Physics Today **49**(8) Part 1, 40 (1996).

[43] R. A. Gray and J. Jalife, *Spiral Waves and the Heart*, Int. J. Bifurcation Chaos **6**(3), 415 (1996).

[44] M. Courtemanche, *Complex Spiral Wave Dynamics in a Spatially Distributed Ionic Model of Cardiac Electrical Activity*, Chaos **6**(4), 579 (1996).

[45] A. T. Winfree, *Heart Muscle as a Reaction-Diffusion Medium: The Roles of Electric Potential Diffusion, Activation Front Curvature, and Anisotropy*, Int. J. Bifurcation Chaos **7**(3), 487 (1997).

[46] G. Whitteridge, *William Harvey and the Circulation of the Blood*, MacDonald, London (1971).

[47] J. Jack, D. Noble and R. W. Tsien, *Electric Current Flow in Excitable Cells*, Oxford University Press (1975).

[48] D. Noble, *The Initiation of the Heartbeat*, Oxford University Press, Second Edition (1979).

[49] D. Gottlieb and S. A. Orszag, *Numerical Analysis of Spectral Methods: Theory and Applications*, SIAM-CBMS, Philadelphia (1984).

[50] E. Doedel, *AUTO: A Software for Continuation Problems in Ordinary Differential Equations with Applications*, Technical Report in Applied Mathematics, California Institute of Technology.

[51] E. Doedel, H. B. Keller and J. P. Kernevez, *Numerical Analysis and Control of Bifurcation Problems (I). Bifurcation in finite dimensions*, Int. J. Bifurcation Chaos **1**, 493 (1991).

[52] E. Doedel, H. B. Keller and J. P. Kernevez, *Numerical Analysis and Control of Bifurcation Problems (II). Bifurcation in infinite dimensions*, Int. J. Bifurcation Chaos **1**, 745 (1991).

[53] *Handbook of Mathematical Sciences*, Chemical Rubber, Boca Raton, Sixth Edition (1987).

[54] A. T. Winfree, *When Time Breaks Down*, Princeton University Press, Princeton (1987).

[55] V. S. Zykov, *Simulation of Wave Processes in Excitable Media*, Manchester University Press, New York (1987).

[56] L. Glass, P. Hunter and A. McCulloch, *Theory of Heart*, Springer-Verlag (1991).

[57] R. M. Berne and M. N. Levy, *Cardiovascular Physiology*, Mosby Inc., St. Louis, Sixth Edition (1992).

[58] D. P. Zipes and J. Jalife, *Cardiac Electrophysiology: From Cell to Bedside*, W. B. Saunders, Philadelphia, Second Edition (1995).

[59] A. V. Panfilov and A. V. Holden, *Computational Biology of the Heart*, John Wiley & Sons (1997).

[60] D. Barkley, *EZ-Spiral, A Code for Simulating Spiral Waves*, Version 2 (1997).

[61] D. Noble, *Oxsoft HEART*, Oxsoft HEART Manual, Version 3.4, Oxsoft, Oxford (1994).